A general method for studying autocrine signaling and its impact on cancer cell growth

by

Somponnat Sampattavanich
B.S. Biomedical Engineering
Johns Hopkins University, 2005
S.M. Electrical Engineering
Massachusetts Institute of Technology, 2007

SUBMITTED TO THE HARVARD-MIT DIVISION OF HEALTH SCIENCES AND TECHNOLOGY IN PARTIAL FULFILLMENT OF THE REQUIREMENTS FOR THE DEGREE OF

DOCTOR OF PHILOSOPHY IN ELECTRICAL AND MEDICAL ENGINEERING
AT THE
MASSACHUSETTS INSTITUTE OF TECHNOLOGY

June 2011

Signature of Author_____
Harvard-MIT Division of Health Sciences and Technology
April 14, 2011

Certified by_____
Joel Voldman
Associate Professor of Electrical Engineering and Computer Science
Thesis Supervisor

Accepted by _____
Ram Sasisekharan
PhD/Director, Harvard-MIT Division of Health Sciences and Technology
Edward Hood Taplin Professor of Health Sciences & Technology and Biological Engineering

A general method for studying autocrine signaling and its impact on cancer cell growth

by

Somponnat Sampattavanich

Submitted to the Harvard-MIT Division of Health Sciences and Technology
on April 15, 2011 in Partial Fulfillment of the Requirements for the
Degree of Doctor of Philosophy in Electrical and Medical Engineering

Abstract

Autocrine signaling plays essential roles in providing self-sustaining growth signals to cancer cells. Since the introduction of the autocrine hypothesis in 1980s, the contribution of autocrine signaling in cancer medicine has been limited to cancer tissues with adequately characterized mitogenic pathways. Its closed-loop nature and complex interplay with other environmental cues prevents the experimental study of unknown autocrine loops, requiring specific perturbing agents to inhibit the underlying ligand/receptor interactions. Recent studies reported the ability of drug-resistant cancer cells to acquire mitogenic signals from previously neglected autocrine loops, causing tumor recurrence. Methods that can evaluate autocrine-loop dependency in more diverse cancer tissues will help identify other means that autocrine signaling employs to maintain cancer growth.

This thesis presents the use of cell-patterning methods as a tool for modulating intrinsically generated diffusive signaling cues. Such technology enables the investigation of autocrine loops without the need for specific therapeutics or prior knowledge of underlying ligand/receptor pairs. To achieve this goal, the first aim of this thesis is to determine characteristics of autocrine signaling that pertain to modulation of intercellular spacing, using existing investigation methods. In addition to demonstrating the limitation of conventional methods in examining unknown autocrine loops, we showed that changes of intercellular spacing in randomly plated culture cannot specifically modulate autocrine activity, due to the concurrent changes of other environmental cues.

The second aim of this thesis is to establish engineering tools for 1) ensuring modification of only autocrine loops with the modulated cell arrangement and 2) providing prediction of autocrine activity changes with varying intercellular spacing. We illustrated cell-patterning approaches for introducing spatial regularity to standard cell culture. We then developed a stochastic model to predict changes of ligand/receptor binding with varying cell arrangement designs. We determined the spatial requirement for autocrine activity to transition from the isolated to the communicative mode. The model also helps determine cell-patterning designs that can potentially maintain uniform impacts of non-diffusive signaling cues while enabling specific modulation of autocrine signaling.

In the last aim of this thesis, we evaluated the ability of regularly-shaped cell arrays to demonstrate the impact of autocrine signaling in supporting cancer growth. In comparison to randomly-plated culture, the cell-patterning platform exhibited growth change with altering intercellular spacing that better corresponds with the predicted and measured changes of autocrine ligand capture. With increasing global cell density, we also showed that regularly-shaped cell arrays acquire more uniform distribution of local cell density, while the randomly-plated cells exhibit distinct changes of local cell density. We present in this thesis the first method for the modulation of combined autocrine activity while ensuring minimal concurrent alteration of non-diffusive cues without the need of specific perturbing agents.

Thesis supervisor: Joel Voldman
Title: Associate Professor of Electrical Engineering and Computer Science, MIT
Thesis chair: William M. Deen
Title: Professor of Chemical Engineering, MIT
Thesis committee member: Peter K. Sorger
Title: Professor of Systems Biology, HMS and Professor of Biological Engineering, MIT
Thesis committee member: Douglas A. Lauffenburger
Title: Professor of Biological Engineering, MIT

Acknowledgment

This thesis would not have been completed without substantial supports from many individuals at MIT and Harvard. First, I would like to thank my research adviser, Prof.Joel Voldman for giving me the opportunity to join his research group and for his continual supports during my career at MIT. I also would like to thank all members of my thesis committee. Prof.Peter Sorger has offered me opportunities to work closely with his students and postdocs. Without resources from his laboratory, I would not be able to perform many biological studies in this thesis. Prof.William Deen has given me very helpful guidance on the development of mathematical modeling in this thesis. Finally, I would like to thank Prof.Douglas Lauffenburger for sharing his insights that are essential for my general understanding of autocrine systems.

I am also very grateful to the generosity of my colleagues and collaborators. First, I am very lucky to be working with Mario Niepel, a research fellow in Peter's research group. Without prior experience in System Biology, Mario has taught me how to design and conduct various experiments. Our scientific conversation on cancer biology contributes significantly to my current passion in this field. I also work closely with Michael Vahey, a former graduate student in Joel's, in a number of projects. I really appreciate his insights and helps in developing mathematical models that considerably help my understanding of the complex biological systems like autocrine loops. Brian Taff and Salil Desai, both former graduate students in Joel's group, work with me on the S-DEP project. Both of them were my big brothers in the lab and have taught me various lessons on how to survive in grad school. Jamie Sprangler, my undergrad friend from Hopkins and now a graduate student in Prof.Wittrup's group, kindly taught me how to grow hybridoma and purify monoclonal antibody 225, a vital tool for various studies in this thesis. Bjorn Millard, a grad student in Peter's group, has helped me on high-throughput imaging. His software, ImageRail, is clearly a work of perfection and provided me a simple yet powerful tool to study signaling cascades. Laura Kleiman also shared many scientific conversations with me that help my understanding of signal transduction via the ErbB-family receptors.

I must also acknowledge other helps from my various friends around MIT. Joseph Kovacs, my former officemate, has shared many scientific conversations with me. His encouragement in having me do outdoor sports also has saved me from getting burned out from lab work a number of times. Lily Kim and Adam Rosenthal, both HST students and among the pioneer members of the Voldman group, had provided me many advises and share my early passion in embryonic stem cells. Laralynne Przybyla and Katarina Blagovic have offered me helps in various biological assays. To other past and present members of the Voldman group, I would like to thank all of them for creating a supportive research group and a fun place to work.

I would also like to thank the following centers at MIT and Harvard: CDP center for giving me opportunities to share ideas and meet with various scientists, MTL staffs for providing guidance and support for my microfabrication, RLE staffs for their helps in creating wonderful research center.

Finally, I am very thankful for the supports from my family. Even though they are all in Thailand, I won't be able to survive the stressful and tough time at MIT without their encouragement. Last, I would like to thank my girlfriend, Nattaporn Ariyatanasuporn. Although we have been physically apart while I am in gradschool, her caring and support had got me through many down times.

Table of Contents

Commonly Used Symbols and Notations **10**
Chapter 1: Introduction **11**
1.1 Significance 11
1.2 The canonical signaling cascade of cell growth in normal and cancer cells 11
1.3 Other signaling cues that affect cell growth 13
1.4 Autocrine signaling and its clinical implications on the autonomous cancer growth 14
As targets of novel cancer therapeutics 15
As prognostic factors of cancers 17
As mechanisms of acquired resistance to cancer therapeutics 17
1.5 Existing methods for examining autocrine loops 18
Screening for autocrine impacts on phenotypic regulation 18
Identifying prospective autocrine loops 18
Validating the presence and phenotypic impacts of specific autocrine loops 19
1.6 Cell patterning technology as enabling tools for investigating cue-response relationship 19
1.7 Scope of this study 21
Chapter 2: Important characteristics of autocrine systems: **23**
A case study in A431 epidermoid carcinoma cell line 23
2.1 Introduction 23
2.2 Results 24
The EGFR autocrine loop and its function in A431 cells 24
The underlying intracellular signaling cascades of A431 growth 26
The hidden intricacy of the medium conditioning assay 28
Varying accumulation of EGFR Ligands in conditioned media at different plating densities 29
Roles of the ErbB3 receptor in A431 cells 30
Autocrine ligands initiate unique temporal changes of ERK phosphorylation 31
Changes of mitogenic signaling activation with altering plating densities 32
2.3 Discussion 34
2.4 Summary 35
2.5 Material and methods 35
Appendix A: Purification of murine monoclonal antibody 225 from hybridoma supernatant 37
Chapter 3: Technologies for configuring the spatial arrangement of cells **40**
3.1 Introduction 40
3.2 Results 41
Optimizing stencil cell patterning for biological studies 41

Construction of heterotypic cell patterns with s-DEP 45
Cell adhesion and motility on S-DEP chip 49
Investigation of cell motion within cell monolayer using S-DEP 51
3.3 Discussion 52
3.4 Summary 53
3.5 Materials and methods 53
Chapter 4: Mathematical modeling of autocrine ligand binding with varying cell arrangement 56
4.1 Introduction 56
4.2 Theory 57
4.3 Results 64
Ligand accumulation and capturing with varying cell arrangement 64
Temporal changes of ligand/receptor complex formation with altering cell arrangement 66
Relationship between cell densities and its impact on ligand/receptor interaction 67
Interactive impacts of cell arrangement and ligand/receptor productions on ligand propagation 69
Roles of cell arrangement on the impact of ligand/receptor affinity on ligand propagation range 70
4.4 Discussion 71
4.5 Summary 72
Chapter 5: Uniformly-shaped array as a method for determining direct autocrine impacts 74
5.1 Introduction 74
5.2 Results 75
Randomly-plated cell culture as inaccurate platform for exhibiting autocrine activity 75
Impacts of cell-cell contacts on growth of randomly-plated A431 cells 78
Changes of autocrine ligand capturing with the altered plating densities 81
Arrays of uniformly-shaped cell patches reveal impacts of autocrine signaling on A431 growth 82
Mathematical prediction of autocrine ligand capture for varying cell-positioning configuration 86
5.3 Discussion 88
5.4 Summary 91
5.5 Materials and methods 91
Chapter 6: Conclusions 93
6.1 Thesis contributions 93
Development of a novel general method for examining impacts of autocrine signaling 93
Demonstration of unique autocrine-signaling characteristics 93
Development of cell-patterning technologies that can be easily integrated with biological studies 94
Description of cell arrangement impacts on intercellular communication in autocrine systems 94
6.2 Future directions and possible challenges 94
Changes of phenotypes and signal activation with varying cell-patterning designs 94

The prediction of cancer prognosis with autocrine activity index 96
Dissecting the role of autocrine signaling as the underlying cause of cell-to-cell variability..... 97
A microfluidics-based technology for faster measurement of combined autocrine activity..... 98
Extending the developed stochastic model for autocrine systems with two ligands 99
Bibliography 102

Figures and Tables

Figure 1-1 EGFR Signaling pathway 12
Figure 1-2 Common approaches to interrupt autocrine loops 15
Figure 1-3 Cell-patterning approaches for investigating cue-response relationship 20
Figure 2-1 Validation of the EGFR autocrine loop in A431 cells 25
Figure 2-2 Intracellular mitogenic signaling cascades of A431 cells 27
Figure 2-3 Growth-promoting and signal-activating effects of A431-conditioned media 28
Figure 2-4 Accumulation of secreted EGFR ligands at varying initial plating densities 30
Figure 2-5 Role of the ErbB3 receptor in A431 cells 31
Figure 2-6 Unique temporal changes of ERK phosphorylation from autocrine signaling 32
Figure 2-7 Changes of ERK and AKT phosphorylation with varying cell plating densities 33
Figure 3-1 Stencil cell patterning and its common complications 42
Figure 3-2 Stencil-defined cell arrays of different cell types 43
Figure 3-3 Different stencil designs for use with 6-well and 96-well plates 44
Figure 3-4 Patterning stripes with conventional stencil and DEP forcing 45
Figure 3-5 Comparison of s-DEP to existing cell-patterning technologies 46
Figure 3-6 Implementation of s-DEP cell-patterning device 47
Figure 3-7 S-DEP Patterning 48
Figure 3-8 Topography of the s-DEP chip 49
Figure 3-9 Attachment and motion of A431 cells on the s-DEP chip 50
Figure 3-10 Time-lapsed study of striated cell patches 51
Figure 3-11 Fabrication of stencil and S-DEP chip 54
Figure 3-12 Simulation of cell positioning for different electrode designs 55
Figure 4-1 Examining impacts of cell arrangement with cell arrays 58
Figure 4-2 Boundary homogenization of cell-surface 59
Figure 4-3 Calculation of ligand survival probability 60
Figure 4-4 Changes of ligand capturing with varying cell plating densities 65
Figure 4-5 Temporal change of complex formation for different cell-positioning geometry 66
Figure 4-6 Predicted complex formation at 72 hours for varying cell arrangement geometry 67
Figure 4-7 Change of autocrine ligand capturing with varying ligand/receptor production ratios 69
Figure 4-8 Changes of autocrine ligand capturing with varying ligand/receptor affinity 70
Figure 5-1 Growth change with the alteration of initial plating density of randomly-plated cells 76
Figure 5-2 Experimental measurement of local cell density 77
Figure 5-3 Growth change with varying local density 78
Figure 5-4 Effects of contact-mediated signaling on the density-growth relationship 79
Figure 5-5 Density-dependent growth change with double neutralizing antibodies 80
Figure 5-6 Accumulation of secreted EGFR ligands at varying initial plating densities 82
Figure 5-7 Stencil cell patterning 83
Figure 5-8 The design of uniformly-shaped cell arrays 84

Figure 5-9 Density-dependent growth change of regularly-spaced cell arrays....85
Figure 5-10 Neighbor count distribution of randomly-plated and patterned cell patches....86
Figure 5-11 Stochastic simulation of paracrine exchange of secreted ligands....87
Figure 5-12 Predicted complex formation with changes of cell-patterning configuration....88
Figure 5-13 Phenotypic changes with altering intercellular spacing of different autocrine loops....90
Figure 6-1 Changes of ERK phosphorylation with altering local and global cell densities....95
Figure 6-2 Experimental validation of differences between isolated and communication modes....96
Figure 6-3 Proposed cell patterning design for studying cell-to-cell variability....97
Figure 6-4 Proposed design of microfluidic device to measure combined autocrine activity....99

Table 1....73

Commonly Used Symbols and Notations

Parameter	Definition	Units
σ	Cell-covered area fraction	(unitless)
r_{patch}	Radius of cell patch	m
n_{patch}	Number of cells per patch	cells·patch^{-1}
R_{c-c}	Centroid-to-centroid spacing between patches	m
κ_{eff}	Effective trapping rate (paracrine trajectories)	m·s^{-1}
κ_{patch}	Patch trapping rate (autocrine trajectories)	m·s^{-1}
D	Ligand diffusion coefficient in medium	m^2·s^{-1}
R_{total}	Total number of receptors per cell	molecules·cell^{-1}
r_{total}	Molar area density of total receptor	moles m^{-2}
N_A	Avogadro's number	molecules·mole^{-1}
A_{patch}	Patch area	m^2
A_{cell}	Cell area	m^2
h	Thickness of cultivating fluid	m
Q_{cell}	Total ligand secretion rate per cell	molecules·cell^{-1}
q	Total ligand secretion flux	mole·m^{-2}·s^{-1}
s	Total receptor production flux	mole·m^{-2}·s^{-1}
L	Ligand concentration in supernatant	mole·m^{-3}
C	Surface concentration of bound receptor	mole·m^{-2}
k_{off}	Dissociation rate constant	s^{-1}
k_{on}	Association rate constant	mole^{-1}·m^{-3}·s^{-1}
k_e	Internalization rate of bound receptors	s^{-1}
K_M	Michaelis–Menten constant	mole·m^{-3}
Da	Damköhler number	(unitless)
υ	Probability of internalization	(unitless)

Chapter 1

Introduction

1.1 Significance

Cancer continues to be one of the most deadly diseases, the second leading cause of death that affects one in two men and one in three women in the US (Jemal, Siegel et al. 2010). It is now understood that cancer is only a group of genetic diseases at the cellular level that give rise to uncontrolled growth and invasion of transformed cells. Because of the unique characteristics and the different sites of origin, each cancer type should ideally be treated by a specifically tailored approach. Currently, chemotherapy and radiation are the two major classes of noninvasive treatment that are commonly used for all cancers. These approaches aim at killing fast dividing cells by inducing DNA damage or inhibit DNA synthesis but unfortunately lack an ability to distinguish cancer cells from the normal ones. As a result, these conventional approaches often cause severe side-effects and exhibit variable outcomes in different patients. Regardless of their adverse limitations, cytotoxic therapeutics continue to extend and save more lives. With decades of cancer research and investment in genomics, we now understand the precise molecular etiology of many cancers. More novel cancer therapeutics have been developed to inhibit specific molecular targets, and these drugs have shown improved treatment efficacy with minimal side effects. Despite their progresses, recent studies report chances of tumor recurrence after long-term treatment with targeted cancer therapeutics (Nguyen, Kobayashi et al. 2009; Rexer, Engelman et al. 2009). To understand the mechanism of the emerging drug resistance and to expand regimens for cancer treatment, further research is needed to identify how a specific molecular pathway may also interact with other existing but untargeted pathways. Additionally, an *in vitro* cultivation method that can better mimic the tumor microenvironment will provide a more reliable platform for drug testing.

This thesis explores the role of a unique mode of chemical signaling commonly known as autocrine signaling on the autonomous growth of cancer cells and its potential involvement in resistance and heterogeneous sensitivity to targeted cancer therapeutics. Autocrine signaling is a mechanism used by some cancer tissues to self-supply their needs of exogenous mitogens (Sporn and Roberts 1985). Regardless of its critical role on cancer growth and its early discovery in 1980s (Sporn and Todaro 1980), most drugs that were designed to target autocrine loops exhibited therapeutic benefits only to very specific cancer tissues and often suffer from the development of resistance after long-term usage (Henson, Johnston et al. 2007; Nguyen, Kobayashi et al. 2009; Glisson 2010). The hurdle is believed to lie in the unique characteristics of autocrine signaling, namely its complex feedback-control loop, its limited spatial propagation, and its complex but poorly characterized interplay with other signaling cues and unknown autocrine loops. This thesis examines the nature of autocrine signaling and its interactions with other environmental cues in the regulation of cancer growth. Our ultimate goal is to provide a general method for quantifying the direct impact of autocrine signaling in regulating an interested phenotype without needing perturbing drugs to inhibit specific autocrine loops. This technique will provide a screening platform for identifying novel autocrine loops in more cancer types and serve as a more physiologically relevant *in vitro* model for testing cancer therapeutics.

1.2 The canonical signaling cascade of cell growth in normal and cancer cells

Cell proliferation is a complex biological process that is controlled by multi-layered, cross-connected signaling cascades. To initiate cell division, cells must acquire appropriate mitogens or growth factors to get through the G_1 restriction point, after which cells do not require growth factors to proceed through the cell cycle. The mitogenic signaling cascade begins when these growth factors are bound to the corresponding receptors on cell surface, causing conformational changes of receptors that then transduce mitogenic signals into the cell. Within the cell, signal propagation is conducted through biochemical reactions among multiple signaling molecules. While there are multiple types of growth factors, the epidermal growth factor receptor (EGFR) pathway is an important paradigm of the mitogenic signaling

cascade and contains the most targets of current cancer therapeutics. EGFR is a member of the ErbB-receptor family that are composed of 4 receptors and 11 cognate ligands (Hynes and MacDonald 2009). Members of EGFR ligands alone include epidermal growth factor (EGF), transforming growth factor-alpha (TGF-α), amphiregulin (AR), heparin-binding EGF (HB-EGF) betacellulin, epiregulin and epigen (Harris, Chung et al. 2003). All of these ligands are first transcribed as transmembrane-anchored proteins. Some ligands such as EGF and TGF-α require a proteolytic cleavage at the N-terminus by ADAM-family metalloproteases to be released as mature, soluble forms. Other ligands such as HB-EGF and AR may bind to EGFR and activate downstream signaling without ligand pre-processing via juxtacrine signaling (Dong, Opresko et al. 2005). The EGFR Pathway can activate three major intracellular signaling cascades, including the MAP kinase pathway, the PI3K/AKT pathway and the STAT pathway. After being activated by series of phosphorylation reaction, these kinases will eventually translocate into the nucleus, activate transcription factors and initiate synthesis of various gene targets. For example, the phosphorylated MAPK can induce the expressions of c-fos, c-jun, Fra-1, Fra-2 and JunB (Chang and Karin 2001).

In normal cells, all steps along the mitogenic signaling cascade are reversible and under tight controls of negative regulators. The phosphorylation of kinases such as Raf and MAPK is strictly regulated by phosphatases, enzymes that can remove phosphate groups from these proteins. In the case of transcription factors, mRNA transcripts usually have short half lives, due to their incorporation of instability motifs. Systematically, the expression of downstream gene targets may also modulate the abundance of upstream signaling molecules, creating complex feedback control loops that secure the integrity of the mitogenic signaling cascade. The autonomous growth of cancer cells occurs when these

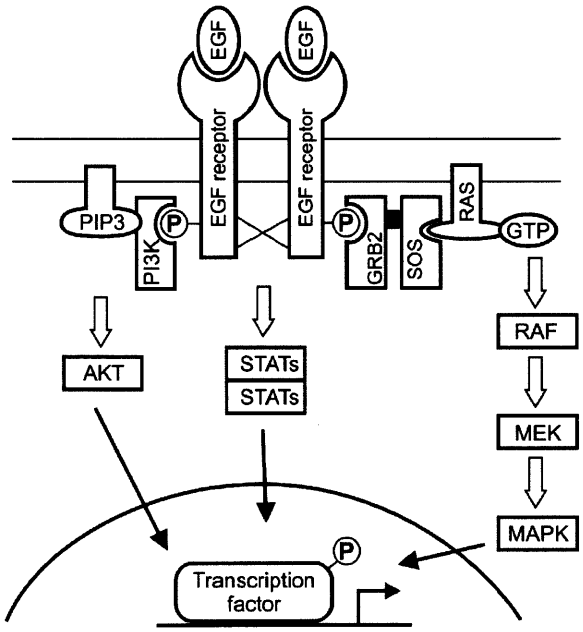

Figure 1-1 EGFR Signaling pathway
ErbB Pathway has 4 receptors and 11 ligands that can bind to one another via both homo- and heterodimerization. EGFR can bind to six different ligands. Upon binding of EGFR and its cognate ligands, the receptors dimerize and autophosphorylate one another, allowing intracellular adapter molecules to interact with their phosphorylated sites. Via series of cytosolic interactions of downstream signaling molecules, the mitogenic signal gets amplified and eventually gets delivered into the nucleus to activate its gene targets.

balances of signal transduction are destroyed. Such process mostly occurs due to mutation of molecules along the signaling cascade and can be summarized into two major types: 1) oncogenes for mutation that causes elevated activity or more abundance of gene products and 2) tumor suppressor genes for mutation

that leads to a loss of gene function. In the case of deregulated cell growth, most of the genetic lesions are oncogenes. Point mutation or deletion in the coding sequence can lead to structural changes of the signaling molecules that may inhibit their ability to propagate signals. A good example is the commonly observed point mutation in the RAS protein that causes disruption of GTPase activity in RAS molecule and its inability to return to inactive conformation. Oncogenic mutation may not affect the structure of signaling molecules but instead cause changes in the expression level of the normal gene products, also known as proto-oncogenes. The gaining copy number of the EGFR gene is commonly observed in both epithelial malignancies (carcinomas) as well as cancers of glandular tissues (adenocarcinomas). Overexpression of wild-type HER2 is also commonly observed in breast cancers (Birner, Oberhuber et al. 2001). Finally, aberrant expression or novel function of oncogenes could emerge from gene insertions or chromosomal translocations. An excellent example of these oncogenes is the reciprocal translocation of the Philadelphia chromosome that gives rise to the overproduction of fusion protein BCR-ABL that eventually causes outgrowth of hematopoietic cells in chronic myelogenous leukemia (CML) (Druker 2002). All of the previously discussed mutations are current targets for novel cancer therapeutics. Ras mutations are observed in over 20% of all tumors and targeted therapeutics are being developed to either reduce the expression of Raf protein, its downstream effectors, or interfere with RAS post-translational process (Downward 2003). Small molecules such as Iressa and Tarceva or the antibody-based drugs like Erbitux have been shown to exhibit improved anti-tumor effects in cancer cells with overexpressed EGFR. Imatinib is an example of the most successful cancer drugs, enabling remission in over 96% of patients with early-stage CML (Druker 2002).

1.3 Other signaling cues that affect cell growth

While it is straightforward to presume from our previous discussion that cell growth is only regulated by mitogen-mediated signaling cascades, studies have shown that the control of cell growth is much more convoluted and also influenced by other non-mitogen signaling cues. We will discuss below how the interaction of cells to extracellular matrices (ECMs), the direct cell-cell contacts, and the non-mitogen diffusive signaling ligands may also interact with the canonical mitogenic signaling cascade to modulate cell growth.

The interaction between cells and ECMs was found to influence cell growth both via direct molecular cross-talk with the mitogenic signaling cascade and via indirect localization of growth factors. First, the integrin signaling cascade was found to support the progression of cells through the G_1 phase of cell cycle by helping to sustain the mitogen-mediated ERK phosphorylation (Roovers and Assoian 2000). Studies showed that induction of MAPK gene targets may require different duration of ERK activity (Cook, Aziz et al. 1999). For example, when lysophosphatidic acid (LPA) was used to stimulate a transient MAPK activation in Rat-1 fibroblasts, the initiated expression of c-Fos was found to be transient while those of c-Jun, JunB and Fra-1 were more temporally sustained. In suspended fibroblasts, growth factors can only induce transient ERK activity and require the activation of integrin signaling to ensure the progression through G1 phase (Roovers, Davey et al. 1999). The integrin signaling can be activated either via the interaction of cells to fibronectin directly or other molecules such as the anti-integrin antibody. While the molecular connection between integrins and the mitogenic signaling cascade is still a subject of current research, recent studies showed that integrin binding can augment the mitogenic signaling via the receptor tyrosine kinase (RTK) pathway, by promoting signal transduction through the Raf/MEK/ERK cascade or facilitating ERK trafficking into nucleus (Juliano, Reddig et al. 2004). Indirectly, ECMs can instead serve as a storage depot of growth factors and their related enzymes. The ECM-growth factor interactions were first recognized by the observation that the basic fibroblast growth factor (bFGF) required interactions to membrane-anchored heparin sulfate proteoglycan to generate tight binding to its native receptor (Klagsbrun and Baird 1991; Yayon, Klagsbrun et al. 1991). Such growth factor reservoir may may be regulated by the release of appropriate cleavage enzymes, possibly creating growth factor gradient under tight regulation by cells (Hynes 2009).

Another major non-canonical regulator of cell growth is the signaling though cell adhesion molecules (CAMs) and juxtacrine growth factors. Direct cell-cell contacts were found to implicate cell growth as both positive and negative regulators. Contact-dependent growth inhibition is a common attribute in epithelial cells and its functional loss often implicates tumorigenic transformation in most cancer tissues (Hanahan and Weinberg 2000). The ability of cancer cells to growth independently of contact-mediated signaling has been shown to correlate with increased invasiveness of cancers (Cavallaro and Christofori 2004). E-cadherin is a member of CAMs that plays a critical role on contact inhibition. E-cadherin inhibits cell growth by increasing the expression of cyclin-dependent kinase inhibitor $p27^{kip1}$, a process that relies on mitogenic activation through EGFR signaling cascade (St Croix, Sheehan et al. 1998). The molecular connection between E-cadherin and EGFR is still controversial but has been shown to involve the interactions of E-cadherin to β-catenin (Perrais, Chen et al. 2007) and/or NF2/Merlin (Curto, Cole et al. 2007). In some cancer tissues, direct cell-cell contacts can also promote cell growth via juxtacrine growth factors. In human glioma, the most common brain tumor, juxtacrine signaling via the Notch/Delta pathway was found to promote proliferation (Zhang, Zheng et al. 2008). Notch receptors and most common ligands were detected in most human astrogliomas. Constitutive overexpression of notch-intracellular domain was found to promote cell growth and colony-forming activity of glioma cell lines. In addition to the Notch/Delta interaction, some premature ErbB-family ligands such as HB-EGF (Raab, Kover et al. 1996) and Amphiregulin (Lysiak, Johnson et al. 1995; Inui, Higashiyama et al. 1997) can interact with ErbB receptors through juxtacrine signaling. Due to their membrane-anchored nature, these transmembranous growth factors can form complex structures with other proteins such as CD9. The clustering of membrane anchored growth factors with junctional proteins was observed to play a critical role in promoting juxtacrine activity (Inui, Higashiyama et al. 1997) and enable cross-interaction of mitogenic signaling cascade to other cytoskeletal molecules such as integrins, α-catenin and vinculin (Goishi, Higashiyama et al. 1995; Nakamura, Iwamoto et al. 1995).

Lastly, non-mitogen diffusible factors can also influence cell growth. Cytokines, interleukins and hormones have been illustrated to affect growth via their molecular interactions with the canonical mitogenic signaling cascade, a process known as transactivation. At the cellular levels, these soluble ligands can be exposed to cells via various chemical signaling mechanisms including autocrine, paracrine and endocrine signaling. Many of these soluble ligands promote signal transduction through the G-protein coupled receptors (GPCRs). It was found that the GPCR pathway can cross-interact with the EGFR signaling pathway by modulating the activity of ADAM-family metalloprotease in cleaving EGFR ligands (Fischer, Hart et al. 2003; Schafer, Marg et al. 2004). For example, interleukin (IL)-8, which signals through a GPCR, can promote growth of non-small cell lung cancer cells in a dose-dependent manner but its effect could be inhibited by addition of either EGFR tyrosine kinase inhibitor, anti-EGFR antibody or metalloproteinase inhibitor (Luppi, Longo et al. 2007). The EGFR ligands that underlie this ligand-dependent transactivation were found to be cell-specific. The role of HB-EGF on EGFR transactivation was observed in lung epithelial cells and rat cardiomyocytes although the accumulation of mature ligand may not be detected in the covering fluid due to its strong affinity to heparan sulphate proteoglycan matrix (Prenzel, Zwick et al. 1999; Yan, Shirakabe et al. 2002; Fischer, Hart et al. 2003). Amphiregulin was also shown to be released by head and neck squamous cell carcinoma after stimulation with LPA and carbachol radicals (Gschwind, Hart et al. 2003) or after exposure with cigarette smoke that can stimulate ADAM17 function due to the generated oxygen radicals (Lemjabbar, Li et al. 2003). Finally, TGF-α is involved in EGFR transactivation by carbachol in colonic epithelial cells (McCole, Keely et al. 2002). These indirect mitogenic transactivation processes complicate the regulation of cell growth by other diffusive signaling cues.

1.4 Autocrine signaling and its clinical implications on the autonomous cancer growth

Autocrine signaling is an unusual mode of chemical signaling which occurs when cells secrete soluble ligands that can bind to corresponding receptors on their own cell surface. While autocrine signaling is also involved in many physiological processes (Duprez, Lenoir et al. 1985; Vallesi, Giuli et al. 1995; Piepkorn, Pittelkow et al. 1998; Wasserman and Freeman 1998), it has been illustrated as a major

mechanism that allows cancer cells to sustain their growth without needing exogenous supply of growth factors (Sporn and Todaro 1980; Sporn and Roberts 1985). Multiple mechanisms can lead to the emerging autocrine activity in cancer cells. Aberrant expression of oncogenes is an uncommon process to acquire a novel autocrine loop but can best illustrate the role of autocrine signaling on tumorigenic transformation. The viral src-family oncogene was found to relieve the requirement of myelomonocytic growth factor (cMGF) for maintaining growth of the transformed chicken myeloblasts (Adkins, Leutz et al. 1984). Upon cultivation with anti-serum against cMGF, growth of the transformed cells was inhibited, validating the secretion of an autocrine ligand after infection with the src oncogene and its similar mitogenic acitivity as cMCF. While viral infections (via Epstein-Barr virus, hepatitis B virus, hepatitis C virus, human T-cell lymphotropic virus type I, immunodeficiency virus type I and several human papillomavirus types) have been illustrated to account for almost 15% of all human malignancies (Boccardo and Villa 2007), the role of viral oncogene in establishing growth-promoting autocrine loops has never been described in naturally occurring human cancers. More often, autocrine loops that have been identified in cancer tissues originate from the modulated expression of pre-existing, human ligands or receptors that causes constitutive activation of the mitogenic signaling cascade. Because numerous autocrine loops have been identified, it will be most useful to examine these autocrine loops based on their unique clinical contributions.

As targets of novel cancer therapeutics

Because of its critical role in producing intrinsic supply of mitogens for cancer cells, autocrine signaling has been one of the most commonly targeted pathways in developing cancer therapeutics. Two distinct molecular approaches have been developed to interrupt autocrine loops, receptor-targeted or ligand-targeted therapeutics. We will review here existing drugs that could successfully inhibit autocrine activity in each category and discuss their strengths and limitations (Figure 1-2).

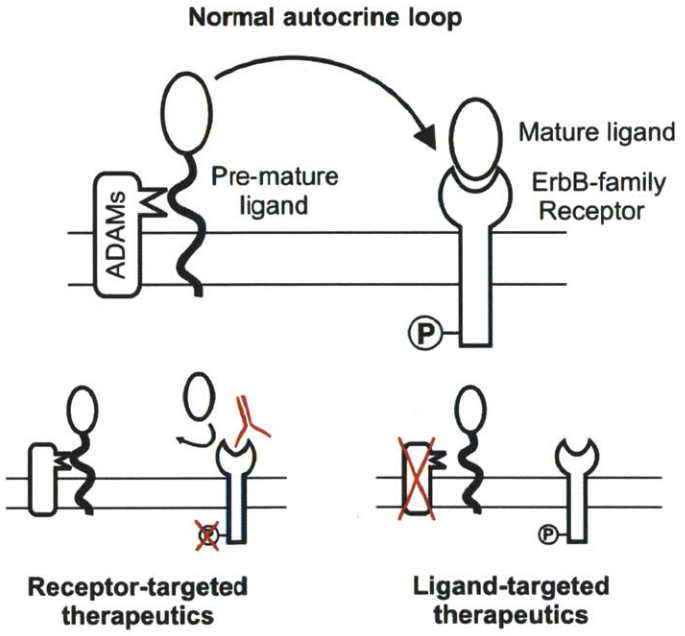

Figure 1-2 Common approaches to interrupt autocrine loops
For many autocrine loops, the transmembranous pre-mature ligands first need to be enzymatically cleaved to form their mature diffusible forms. The mature ligand can then diffuse into the surrounding liquid and may get recaptured by the originally secreting cell or by adjacent cells. Two major approaches can be conducted to inhibit autocrine loops. Receptor-targeting therapeutics inhibits interaction between receptors and their cognate ligands. Novel drugs are now designed to target the pre-processing of ligand, blocking the activity of ligand cleavage enzymes.

The oldest approach to disrupt autocrine loops is to target the underlying autocrine receptors. Two classes of clinically approved therapeutics are available to perform this task. Receptor-neutralizing antibodies were developed first to specifically interrupt interactions between receptors and their cognate ligands while low-molecular-weight agents were designed to inhibit the receptor signaling ability. Various drugs have been developed to target EGFR. The murine monoclonal antibody 225 and its chimeric human:murine derivative Cetuximab were the first antibody-based therapeutics that can successfully prevent EGFR interactions to TGF-α, one of its most commonly observed cognate ligands in cancer tissues (Mendelsohn 1997; Mendelsohn and Baselga 2003). The anti-proliferative function of receptor-blocking antibodies was shown to be caused by the increasing expression of cyclin-dependent kinase inhibitor $p27^{kip-1}$ that in turn caused cell arrest in G_1 phase (Peng, Fan et al. 1996; Fan, Shang et al. 1997; Kiyota, Shintani et al. 2002). On the other hand, the small-molecule, ATP-competitive inhibitors can permeate through cell membrane and were specifically screened to bind strongly to EGFR tyrosine kinase domain and to inhibit its enzymatic activity. These small-molecule inhibitors may act on a single receptor (e.g. gefitinib and erotinib for EGFR) or multiple receptors at once (e.g. CI-1033 and lapatinib for pan ErbB-family receptors). Unique treatment characteristics have been observed from these two classes of therapeutics. In addition to blocking ligand-receptor binding, anti-receptor antibodies were observed to promote receptor internalization and downregulation, processes which can further limit tumor growth (Fan, Lu et al. 1994; Spangler, Neil et al. 2010). Kinase inhibitors, on the contrary, can act on both homodimers and heterodimers of targeted receptors (Moasser, Basso et al. 2001; Anido, Matar et al. 2003). Some of these small-molecule inhibitors could even inhibit kinase activity of mutated receptors that lacked the extracellular domain (Lal, Glazer et al. 2002). Interestingly, Cetuximab and Gefitinib showed antiproliferative effects mainly in cancer tissues that acquire overexpressed EGFR (Fan, Lu et al. 1994; Matar, Rojo et al. 2004). Cetuximab also exhibited synergistic growth-inhibiting effects in combination with conventional chemotherapeutic agents (Fan, Baselga et al. 1993; Thienelt, Bunn et al. 2005). The mechanisms which underlie these commonly-observed treatment characteristics require further investigation on how the EGFR targeted autocrine loop may cooperate with other signaling cues and/or other unidentified autocrine loops to sustain cancer growth.

More recently, a novel approach to perturb autocrine loops has been developed by inhibiting the pre-processing of autocrine ligands. Many autocrine ligands are originally synthesized as transmembranous proteins and must be proteolytically cleaved to generate their mature, diffusible forms. In the case of ErbB-family autocrine loops, the ADAM-family (a disintegrin and metalloprotease) proteins are responsible for shedding of ErbB ligands. In particular, ADAM17 participated in the maturation of TGF-α, heparin-binding EGF-like growth factor (HB-EGF), amphiregulin and epiregulin whereas ADAM10 was found to be the most potent sheddase of EGF and beta-cellulin (Blobel 2005; Maretzky, Reiss et al. 2005). Regardless of their apparent specificity, gain-of-function studies showed that many of these ADAM proteins still maintained redundancy in their ligand-cleavage activity (Horiuchi, Le Gall et al. 2007). Two major classes of therapeutics can inhibit the enzymatic activity of ADAM proteins. First, the broad-spectrum metalloproteinase inhibitors (MPIs) were originally designed to restrain cancer invasiveness but can also inhibit enzymatic activity of the ErbB ligand sheddases (Dong, Opresko et al. 1999). Despite their efficacy in cell lines and animal studies, clinical trials of these MPIs do not illustrate distinct therapeutic benefits, instead causing severe side-effects such as musculoskeletal pain and inflammation (Coussens, Fingleton et al. 2002). For the past few years, specific inhibitors of ligand sheddases have then been developed. The orally bioavailable, small-molecule inhibitor INCB3619 is an example of small molecules that can selectively inhibit function of the ADAM proteases (Zhou, Peyton et al. 2006; Fridman, Caulder et al. 2007). This inhibitor can prevent cleavage of many ErbB ligands including heregulin, TGF-α, HB-EGF, amphiregulin as well as EGF (Liu, Fridman et al. 2006). Experiments with lung cancer cell line showed that INCB3619 can interrupt the heregulin-ErbB3 autocrine loop. Interestingly, early investigation of first-generation sheddase-specific inhibitors reported the development of musculoskeletal side effects (Brown 2000; Coussens, Fingleton et al. 2002). Whether or

not this new inhibitor would follow the unsuccessful path of its broad-spectrum predecessors still requires further clinical investigation.

As prognostic factors of cancers

Although the current focus in cancer research is to develop novel targeted therapeutics, early detection of tumors still remains as the most critical determinant of cancer prognosis. Clinical studies have showed that information about the abundance of autocrine-related biomolecules could assist physicians in choosing appropriate therapeutics and predicting drug sensitivity. mRNA or protein expression profiles from dissected tumors are the most commonly used diagnostic tool to measure activity of a predicted autocrine loop. In general, tumors that have been identified to acquire co-expression of ligands as well as their corresponding receptors often exhibit poorer prognosis. For example, co-expression of TGF-alpha and EGFR of the dissected axillary lymph nodes correlates well with reduced survival in breast cancer patients (Umekita, Ohi et al. 2000). In addition to this general trend, types of autocrine ligands or receptors can also implicate cancer prognosis. High expression of epiregulin was found to confer more invasiveness of non-small cell lung cancers (NSCLCs) with mutated EGFR (Zhang, Iwanaga et al. 2008). However, NSCLCs with overexpressed wild-type EGFR exhibited improved sensitivity to EGFR-targeted therapies with the overexpression of Amphiregulin (Yonesaka, Zejnullahu et al. 2008). Regardless of the correlations between these biomarkers and cancer prognosis, there are still limitations to using autocrine-related biomarkers as true prognostic factors. First, the measurement of mRNA or protein expression can greatly vary among the different clinical institutions. Standardized measurement methods must first be developed in order to allow reliable comparison of these autocrine-signaling-related biomarkers. Second, existing techniques for measuring RNA and protein expression levels are bulk assays. An averaged measurement from pooled cells may not provide adequate sensitivity to identify rare, unique cells with novel autocrine loops. Finally, it is important to keep in mind that many of the observed correlations between autocrine-related biomarkers and cancer prognosis are tissue-specific and even controversial in some cancer types. It is essential that we first identify mechanistic links between such biomarkers and the cancer etiology before using these correlations to exclude patients from receiving any specific treatment.

As mechanisms of acquired resistance to cancer therapeutics

Regardless of its improved therapeutic efficacy, increasing bodies of evidences have revealed that patients who took targeted cancer therapeutics often suffer from cancer recurrence or development of drug resistance. Recent studies reported the emerging role of untargeted autocrine loops as mechanism for cancer to avoid the drug effect. Because the ErbB-family signaling cascade is the most pursued therapeutic targets, we will discuss two distinct sources of emerging autocrine activity in cancers using examples from this pathway.

First, cancer cells can acquire novel autocrine activity by the altered expression of ligands and receptors of the same receptor family. EGFR is the most commonly detected ErbB-family receptor and can bind to six different ErbB ligands while ErbB3 is found less often and can interact to only one ligand, heregulin (Normanno, Bianco et al. 2003). A recent study showed that the heregulin-ErbB3 autocrine loop existed in some lung cancer cells and may serve as an alternative mitogenic signaling cascade for gefitinib-resistant non-small-cell lung cancers (NSCLC) (Zhou, Peyton et al. 2006). To arrive at this conclusion, the investigators first experimented with lung cancer cell lines with EGFR mutations that could not by themselves secrete heregulin. With supplementation of heregulin, the cell lines with no EGFR amplification were observed to have reduced drug sensitivity to Gefitinib but no change to their AKT phosphorylation. Such effects were not observed in cell lines with amplified EGFR expression, suggesting the role of ErbB3 to transduce mitogenic signaling cascade via AKT when the activation of EGFR pathway is inhibited. A549 cells are human lung adenocarcinoma epithelial cells and that were observed to acquire functioning heregulin-ErbB3 autocrine loop. To inhibit AKT phosphorylation in A549 cells, both EGFR and ErbB2 must be knocked down simultaneously, implying the critical roles of ErbB2/ErbB3 heterodimerization to activate AKT phosphorylation. This study shows how swapping of ligand-receptor pair within the same receptor family may provide an alternative mitogenic signaling to promote cancer

growth, substantiating the importance of cancer therapeutics that can target multiple ErbB-family receptors at once.

Cancer cells can also acquire novel autocrine activity from the interaction of ligands and receptors of different receptor families. A recent study by Guix *et al.* (Guix, Faber et al. 2008) demonstrated how the insulin-like growth factor (IGF) autocrine loop could bypass mitogenic signaling through the EGFR signaling pathway during treatment of EGFR-targeting therapeutics. Investigators created an *in vitro* model of gefitinib-resistant cells (GR cells) by treating epidermoid carcinoma A431 cells with increasing doses of gefitinib and continually selecting for surviving cells. After having developed GR cells, the investigators then determined the sensitivity of various signaling molecules to Gefitinib treatment. While the phosphorylation of EGFR, ErbB3 and ERK significantly decreased with Gefitinib addition, AKT phosphorylation was found to be unaffected. The investigators then showed that AKT phosphorylation in GR cells were instead activated via the insulin-like growth factor receptor type I (IGF-IR) pathway. The decrease in IGF-binding protein type 3 (IGFBP-3), a negative regulator of IGF-IR signaling cascade, was found to be the underlying cause of increasing IGF-IR signaling activity. By adding anti-IGF-IR antibodies, gefitinib sensitivity of AKT phosphorylation could be rescued, confirming the presence and the critical roles of IGF autocrine loop in activating AKT phosphorylation in GR cells. Such emerging activity of unknown autocrine loops will be a major challenge for cancer treatment with targeted therapeutics. Preventing resistance of cancer therapeutics through this mechanism may require a novel diagnostic tool that can detect changes of the combined autocrine activity in cancer cells.

1.5 Existing methods for examining autocrine loops

The previously-discussed contribution of autocrine signaling in cancer medicine emphasizes the need for novel experimental tools to examine autocrine signaling and its interactions with other signaling cues in regulating cancer growth. In this section, we will explore the available techniques to screen, identify and validate functions of autocrine loops.

Screening for autocrine impacts on phenotypic regulation

Two commonly used techniques for screening the autocrine signaling contribution on phenotypic control are: 1) the alteration of initial plating density and 2) the medium conditioning assay. The two techniques were first demonstrated since 1966 when Rubin noticed the change in growth rate of chick embryo cells after plating the cells at different seeding density (Rubin 1966). Growth of cells that were plated at low density could however be promoted by cultivation these cells in medium that was pre-conditioned with the same cell type for at least 24 hours. Heating of such conditioned medium was found to inactivate its growth-promoting activity. Although it has been shown later that Rubin's 'conditioning factor' were composed of both growth factor and cell adhesion-promoting factors, the developed techniques were commonly adopted ever since, especially for illustrating effects of autocrine signaling. It is important that these two techniques are utilized together because each of techniques alone could not validate presence of autocrine signaling. Cell-cell contacts can exhibit the similar density-dependent phenotypes with varying physical contacts (Burke 1983; Tada, Sasada et al. 1999). Some autocrine ligands are too spatially localized to cell surface and may not accumulate at high quantity in the conditioned medium unless their interactions with receptors are initially blocked (Dempsey and Coffey 1994). To validate presence of an autocrine loop, a more specific technique is still necessary.

Identifying prospective autocrine loops

When autocrine phenomenon has been speculated in a new biological system, we can narrow the pool of prospective ligand-receptor pairs using bioinformatics approaches. Specifically, one can obtain the mRNA expression profile from the interested cell sample. Using the database of experimentally known ligand-receptor signaling partners, ligand-receptor pairs with the most significant correlation of gene expression could be determined. The details on such bioinformatics algorithms lie beyond the scope of this study but can be referred elsewhere (Graeber and Eisenberg 2001; Rana and Insel 2005; Castellano, Reid et al. 2006; Ben-Shlomo, Rauch et al. 2007). Regardless of the promising ability of these searching

tools to screen off unrelated targets, it is important to emphasize the necessity in validating whether the identified candidates are biologically functioning autocrine loops. Post-translational processes play a major role in receptor trafficking and can change receptor availability from the predicted gene expression profile. The enzymatic cleavage to generate functioning, mature ligands can also cause uncorrelated expression levels between mRNA and protein, resulting in incorrect searching algorithm or rejection of significant autocrine loops.

Validating the presence and phenotypic impacts of specific autocrine loops

The gold standard to verify the presence of an autocrine loop requires pharmacological agents that can specifically inhibit binding of autocrine ligands to their corresponding receptors. To exclude false-positive interaction via intracrine signaling, we must use agents that can prevent ligand-receptor interactions from the extracellular domain of the cells to illustrate secretion of diffusible ligands. At present these agents are monoclonal antibodies that are raised against either autocrine ligands or corresponding receptors (Lauffenburger, Oehrtman et al. 1998). One can then illustrate the presence of a specific autocrine loop by demonstrating changes of the autocrine ligand accumulation in the surrounding fluid or modified activity of downstream signaling molecules when cells are co-cultivated with these antibodies (DeWitt, Dong et al. 2001; Joslin, Opresko et al. 2007). Despite their numerous contributions in the past, receptor-blocking antibodies are available only for very limited autocrine loops.

Existing methods for studying autocrine loops are limited to techniques with poor specificity to autocrine signaling or those that require perturbation of specific ligand-receptor pairs. In order to detect changes of the combined autocrine activity in cancers, we need a novel diagnostic method that allows the evaluation of autocrine signaling impact in promoting cancer growth without the need to perturb specific autocrine loops.

1.6 Cell patterning technology as enabling tools for investigating cue-response relationship

Cell patterning technologies are methods that have been developed to localize or shape cells into the desired configuration. Two major cell patterning approaches have been developed. The first approach relies on chemical modification of the substrate surface. The substrate must contain areas where cells can adhere (adhesive region) as well as the region that prevents cell attachment (non-adhesive region). To create adhesive region, extracellular matrices (ECMs) such as collagen, fibronectin, laminin, and gelatin can be directly adsorbed onto the substrate or covalently attached to intermediate molecules. A technique called microstamping is used to deliver adhesive molecules onto the substrate with the desired shape and positions (Mrksich, Dike et al. 1997). The rest of the substrate can then be coated with cell-repelling materials including various types of carbohydrates (Morra and Cassineli 1999; Luk, Kato et al. 2000; Nelson and Chen 2002), proteins (Ostuni, Kane et al. 2000) and synthetic polymers (Chen, Mrksich et al. 1997; Thomas, Lhoest et al. 1999; Liu, Jastromb et al. 2002). The second cell-patterning approach is to prevent cells from attaching to the substrate by physical means. One may use physical barriers such as stencils (Folch, Jo et al. 2000; Ostuni, Kane et al. 2000) or microwells (Rettig and Folch 2005) to passively constrain cells into the desired areas. Alternatively, we can actively push or pull cells to form the desired shapes using physical forces such as optical tweezers (Ashkin, Dziedzic et al. 1986; Grier 2003) or dielectrophoretic forces (Rosenthal and Voldman 2005; Taff and Voldman 2005). Selection of cell patterning methods depends on applications, cell cultivation substrates and the number of cells to be patterned.

The relationship between the governing environmental cues and the ultimate cell responses has long been a popular research topic in cell biology because of its critical implications to all areas of cutting-edge medicine including the ability to pre-program stem cells into specific cell fates, the discovery of novel cancer therapeutics, or the development of artificial organs. Regardless of its significance, past studies of cue-response relationship have been limited to models with simple non-physiologically relevant cues due to the inability to dissect complex interplays of multiple environmental cues in conventional cell culture. Using the previously discussed cell-patterning technology, a few recent studies have exemplified

approaches to study phenotypic regulation via a specific regulator while maintaining uniform impacts of other signaling cues.

First, the complex interactive roles between cell-cell contacts and cell spreading on the growth of endothelial and smooth muscle cells were revealed using 2D spatially defined cell culture (Nelson and Chen 2002). By localizing cells as multiple cell spots with varying patch area and varying number of cells per patch, investigators found that the impact of cell spreading could mask the positive influence of cell-cell contact in promoting cell growth. Specifically, round cells with more physical contacts were observed

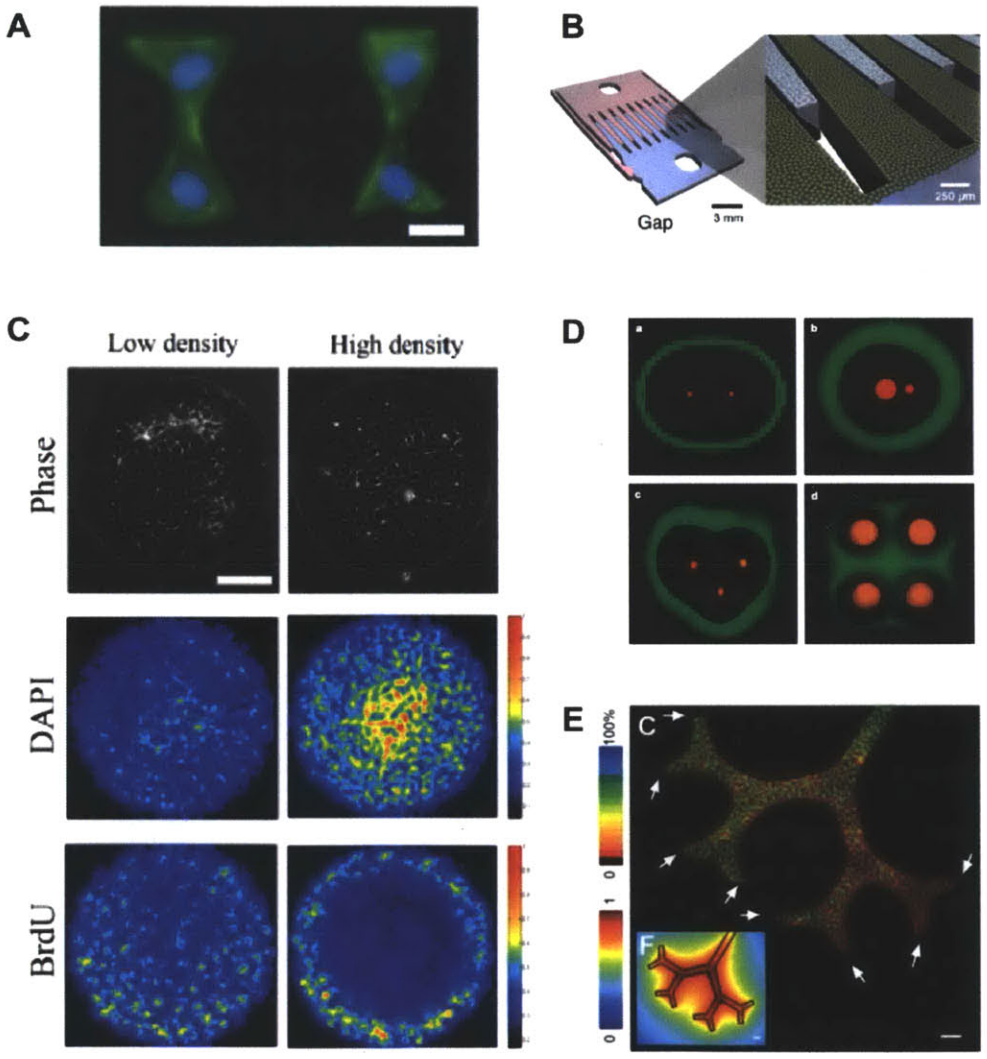

Figure 1-3 Cell-patterning approaches for investigating cue-response relationship
A) The bowtie-shaped, agarose-carved wells for studying interplay between cell-cell contacts and cell spreading (Nelson and Chen 2002). B) Micromachined reconfigurable cell culture substrate for studying temporal dynamic of cell-cell contacts and paracrine signaling (Hui and Bhatia 2007). C) Simple 2D cell patterning for studying contact inhibition of mammary epithelial cells (Kim, Kushiro et al. 2009). D) Complex cell arrangement on agar to study paracrine signaling of genetically engineered bacterial cells (Basu, Gerchman et al. 2005). E) Complex 3D collagen-embed cell patterning to study the effect of autocrine ligand TGF-β to inhibit mammary branching morphogenesis (Nelson, Vanduijn et al. 2006).

to exhibit less growth than spreading, isolated single cells. To study the true contribution of contact-mediated signaling independently of cell spreading, the investigators compared growth of cells with varying cell-cell contacts but similar spreading using the cleverly-designed bowtie-shaped, agarose-carved well (Figure 1-3A). Cells with contacts exhibited higher growth than those without any contact. Additionally, Inhibition of PI3K signaling, but not the diffusive paracrine signaling, could eliminate the elevated growth of bowtie-shaped double cells with contacts, suggesting the connection between PI3K signaling pathway and the contact-mediated signaling in promoting the growth of endothelial and smooth muscle cells.

The connection between cell-cell contacts and soluble ligands is another complex cue interaction that is difficult to determine true effect of each individual input. Using microfabricated technology, the complex interactions between stromal fibroblasts and hepatocytes in maintaining hepatocellular phenotypes have been resolved (Hui and Bhatia 2007). It is known that fibroblasts can promote the maintenance of hepatocytes during *in vitro* cultivation via both paracrine interactions and direct cell-cell contacts. Using the reconfigurable micromachined silicon substrate (Figure 1-3B), investigators could examine the dynamic temporal effects of cell-cell contacts. Direct contacts with stromal fibroblasts were found to play a critical role on hepatocyte phenotype only within the first few hours of cell cultivation *in vitro*, after which paracrine signaling of stroma-secreted ligands was sufficient to maintain the hepatocellular phenotype.

In the cancer research community, the use of cell patterning to study cue-response relationship is still at its beginning. A recent investigation by Kim *et al.* (Kim, Kushiro et al. 2009) illustrated the use of cell patterning to dissect complex interplay between growth-factor mediated mitogenic signaling and contact-dependent growth inhibition in mammary epithelial cells. It was observed that growth-promoting roles of soluble ligands can dominate negative influence of direct cell-cell contacts when the concentration of growth factors exceeded a specific threshold. Using cell patterning (Figure 1-3C), the investigators could modulate the density of cells within an individual cell patch and found that the growth factor threshold increases with the increasing level of direct cell-cell contacts. Because of the common phenotypes between mammary epithelial cells and breast cancers, this study illustrates an approach to study how contact-mediated signaling plays a role on cancer growth.

Unlike other signaling cues, diffusive signaling cues have been least explored with cell patterning technology, especially for mammalian cell culture in liquid-covered media. In agar-based cell culturing system, two prior studies have illustrated examination of diffusible signaling cues using spatially-patterned cell constructs. First, Basu *et al.* (Basu, Gerchman et al. 2005) used the arrangement of cell positioning to study the dynamics of paracrine interactions between genetically engineered bacterial cells. To enable the reconstruction of ligand propagation, investigators engineered the 'receiver' bacterial cells to produce different colors and intensity of fluorescent reporter proteins when receiving different dose of lactone, the secreted message, from 'sender' cells. By arranging the geometry between the two cell types, intrinsic properties of this paracrine interaction can be examined (Figure 1-3D). Nelson *et al.* also demonstrated the use of microfabricated three-dimensional cell constructs to study the role of autocrine factor, TGF-β, in inhibiting mammary branching morphogenesis (Nelson, Vanduijn et al. 2006). The microfabricated collagen tubes were designed to mimic the physiological mammary tubules (Figure 1-3E). By embedding mammary epithelial cells within these microfabricated tubes that were positioned into different shapes, the investigators managed to demonstrate the anti-branching effect of TGF-β. These two studies illustrate how the spatiotemporal dynamics of diffusive signaling can be examined by altering the spatial arrangement of cell culture. By pre-defining cell positions on the substrate, the distribution of secreted ligands can be calculated, allowing the determination of cue-response relationship from the resulted cell response. The remaining challenge is how we can convert the previously discussed examples of diffusive signaling study in solid agar to that in liquid growth media, an environment where diffusive signaling can be easily perturbed by thermally-driven convection.

1.7 Scope of this study

The recently discovery of autocrine signaling contribution in causing cancer therapeutic resistance emphasizes the need for technologies that can monitor combined autocrine activity in more cancer types. Existing screening tools of autocrine activity are affected by the complex phenotypic regulation in the randomly plated cell culture. With the availability of cell-patterning technology, precise localization of adherent cells on tissue culture substrate can now be easily performed. We thus hypothesize that the cultivation of cells as uniformly-shaped cell arrays may provide an approach to specifically modulate activity of autocrine signaling while maintaining minimal impacts of other environmental cues. By altering the array spacing while maintaining the equivalent shape of cell clusters across the whole substrate, paracrine exchanges of autocrine ligands between the patterned cell patches should be modulated without perturbing other environmental cues. Since this technique does not require the use of specific inhibitors, the developed platform should be able to measure the combined autocrine activity in more tissue types.

In Chapter 2, we first explore common characteristics of autocrine signaling. Using A431 epidermoid carcinoma cell line as our model, we evaluated the performance of conventional screening techniques in exhibiting activity of autocrine signaling in promoting cell growth. We then investigated the closed-looped nature of autocrine signaling by quantifying the amount of secreted autocrine ligands with and without autocrine loop perturbation. To study the tentative interactions of autocrine signaling with other signaling cues, we monitored how the mitogenic signal activation would vary as a function of relative cell positioning and cell cultivation time. The identified change of mitogenic signal activation provides fundamental understanding of the autocrine signaling for our development of cell-patterning platform for exhibiting combined autocrine activity.

In Chapter 3, two unique methods for localizing cells on two-dimensional substrate are described. We first illustrated the use of stencils to pattern cells with the desired shape and positioning as well as describing its limitation. In combination with dielectrophoretic forcing, we then discussed the development of the stencil-delineated electroactive patterning (S-DEP). S-DEP enables microfabrication of heterotypic patterns-within-patterns. We then illustrated the use of ECM coating to reduce cell motility bias on the S-DEP chip. With both stencils and S-DEP, we can fabricate cells into any shape at any pre-defined positions on the substrate, a tool necessary for developing our autocrine screening platform.

In Chapter 4, we discuss mathematical simulations for predicting changes of ligand capture with altering designs of cell arrangement. Using stochastic modeling approach, we first investigated how changes in cell shape and array spacing would affect the paracrine exchange of autocrine ligands between the patterned cell clusters. Two critical modes of diffusive interactions were identified and confirmed by determining their analytical solutions of complex formation. We then explored the relationship of cell arrangement with the intrinsic properties of autocrine loops in governing ligand/receptor binding. The developed model helps us understand how cell-patterning geometries may affect changes of autocrine signaling activity.

Finally, in Chapter 5, we illustrate how the growth-promoting activity of the combined autocrine loops in A431 cells can be evaluated using regularly-spaced, cell-patterning platform. Changes of cell proliferation were compared between the patterned cells and the conventional randomly-seeded culture. We illustrated the ability of cell-patterning platform to better maintain impacts of non-diffusive signaling cues while allowing the modulation of autocrine signaling by simple alteration of cell-patterning designs. This study validates the use of the developed cell-patterning platform as a more general tool to determine the dependency of cancer growth on autocrine loops.

Chapter 2

Important characteristics of autocrine systems: A case study in A431 epidermoid carcinoma cell line

In this chapter, we explore characteristics of autocrine loops using currently available investigation methods. Some of these characteristics, such as change of cellular phenotypes from either conditioned medium or alteration of cell plating densities, are the more familiar features of autocrine systems but often complicated by the impacts of other environmental cues. Other characteristics, such as the acquisition of multiple autocrine loops within the same cell type, are currently less appreciated but have been shown recently to play critical roles in the development of cancer therapeutic resistance. We will be demonstrating these properties using autocrine loops in cancer cells although the illustrated properties of autocrine loops in this chapter should be applicable to most autocrine systems in any organisms and tissue types.

2.1 Introduction

Interactions between neighboring cells are major attributes of multicellular evolution. While protein families that are involved in cell signaling and cell adhesion have been shown to predate the origin of animals (King, Hittinger et al. 2003), the diversification of cell signaling modes to the currently known state mainly occurred during the development of metazoans (Pires-daSilva and Sommer 2003; King 2004). Juxtacrine signaling evolved with the primary requirement for stable cell adhesion during transition to multicellularity (Hynes and Zhao 2000). Paracrine signaling enabled the enlargement of organisms by allowing intercellular interactions beyond physically touching cells (Stoka 1999). Endocrine signaling emerges in higher eukaryotes where the body of organisms becomes compartmentalized, requiring central vasculature to transport signaling molecules across the different organs. It is therefore intuitive to infer from these cell signaling mechanisms that the complexity of intercellular interactions should correspond with the spatial requirement that each signaling mode is attempting to satisfy.

Unlike other chemical signaling modes where intercellular communication occurs between two separate cells with a defined propagation path, autocrine signaling has been shown to operate at flexible length scales and also permit an individual cell to capture and respond to its self-secreted ligands. Because of its unusual signaling topology and its initial discovery in cancer cells (Sporn and Todaro 1980), autocrine signaling has long been misperceived as a dysregulated cell-signaling mechanism. The first recognized characteristic of autocrine loops is the co-expression of diffusive ligands and the corresponding receptors (Markowitz, Molkentin et al. 1990; Yamanaka, Friess et al. 1993). After, it turned out that this unique mode of chemical signaling also participates in various physiological processes, mainly functioning to establish positive feedback control loops that help sustain signal activation or establish spatially defined signali activation for cell specification (Freeman 2000). In humans, autocrine loops are involved in the proliferation of immune cells (Boussiotis, Nadler et al. 1994) and mammary epithelial cells (Li, Plowman et al. 1992) and also underlie the tissue repair process (Piepkorn, Pittelkow et al. 1998). Despite advanced functions of autocrine signaling, this complex signaling mode also exists in primitive organisms. The ciliate *Euplotes raikovi* was found to secrete pheromones that can interact with its self-expressed receptors, inducing growth in juvenile organisms (Vallesi, Giuli et al. 1995). The ubiquitous presence of autocrine signaling in various tissue types and a variety of organisms implies its unique functional benefits over other cell signaling modes that may provide positive selection pressures for the acquiring cells.

To explore some of these distinct characteristics of autocrine signaling, we examine in this chapter properties of the ErbB-family autocrine loops in cancer cells. We chose to work with this biological system because of its well-defined dynamics and our ability to examine this system *in vitro* using cell lines (Wiley, Shvartsman et al. 2003). The A431 epidermoid carcinoma cells were selected as our study model because of their thoroughly characterized presence of the TGF-α/EGFR autocrine loop (Derynck, Goeddel

et al. 1987; Van de Vijver, Kumar et al. 1991; Thornley and Jones 1992). We begin our exploration by first demonstrating the validation of the EGFR autocrine loop in A431 cells using conventional investigation methods. We determine the underlying signaling cascades of A431 cell growth and use this analysis to examine efficacy of the medium conditioning assay for investigating impacts of autocrine loops. By measuring the concentration of EGFR ligands, we show that conditioned media may not contain some important autocrine ligands because of the spatially-limited propagating nature of these ligands. We show that the observed growth promotion of conditioned medium may actually arise due to accumulation of other ligands such as Amphiregulin. Using ErbB3-blocking antibodies, we demonstrate the significant role of the ErbB3 receptor in promoting growth and activating both ERK and AKT phosphorylation in A431 cells. These results substantiate the possible presence of multiple autocrine loops in a single biological system, either by the secretion of multiple ligands or by the production of multiple receptors. We then examine the distinct patterns of mitogenic signaling activation between autocrine signaling and exogenously supplied ligands and also investigate its variation with cell plating densities. Both characteristics provide important implications in using autocrine systems as a more physically relevant model for testing cancer drugs *in vitro*.

2.2 Results

The EGFR autocrine loop and its function in A431 cells

We begin our analysis by first validating the presence of autocrine loops in A431 cells using existing experimental methods. A commonly used assay to screen for autocrine phenomena is the medium conditioning assay. Specifically, media that were used to cultivate cells with autocrine loops is believed to accumulate the secreted diffusive ligands. If such conditioned medium (CM) can promote phenotypes of the fresh-batch cells, the cells are often assumed to obtain autocrine loops. This technique has been developed since 1966 when the chick embryo cells were observed to exhibit varying growth rates when cultivated at different plating densities. When culturing the cells in CM, the experimenters showed that growth of sparsely plated cells can be rescued (Rubin 1966; Rein and Rubin 1968). Since then, this technique has been widely used as a screening method for autocrine activity in various cell types (Mittal and Voldman ; Pouliot and Burgess 2000; Ellison, Munden et al. 2009). To assess the presence of autocrine loops in A431 cells, we generated CM by cultivating A431 cells in serum-free medium for 24 hours. A fresh batch of A431 cells at varying plating densities were then cultured with the prepared CM, either at 100% or 50% (mixed equally with fresh serum-free medium). By determining the increase in cell number for the different cultivating conditions and varying initial seeding density, we illustrated the ability of CM to promote A431 cell growth (Figure 2-1A). While serum-free medium does not exhibit any growth promotion between day1-3, both 50% and 100% CM were observed to promote A431 cell growth; their effects also increase with elevated seeding density. While both CM give rise to a general increase in cell growth during day 3-5, fold growth instead decreases with increasing seeding density, implying the saturating cell growth at higher cell seeding density. Overall, the result demonstrates the ability of A431 cells to self-produce diffusive factors that can self-support their own proliferation.

In addition to using CM, we further exhibit the effect of accumulated growth-promoting factors by altering the medium replenishing frequency. By altering the frequency to change media, the amount of accumulated ligands in the supernatant must therefore varies. We tested this hypothesis by comparing A431 growth in different medium conditions with two different medium replenishing frequencies, either every day or every three days. Changes in cell counts between day 3 and day 6 were obtained to compare the growth promoting activity of different cultivating conditions (Figure 2-1B). Cells in serum-free medium (NS) with every-three-day replenishing frequency exhibited higher growth change than those with everyday medium replenishment ($p = 0.017$ with paired t-test). In addition, we found that cells at high plating densities with every-three-day medium replenishment also exhibit higher growth than sparsely-plated cells ($0.6\text{-}1.3\times1{,}000$ cells/cm^2 vs $5\text{-}10\times1000$ cells/cm^2, $p=0.06$). With everyday medium changing, cell growth in NS was instead found to be comparable at all plating densities ($p=0.25$). Interestingly, the 50%CM was observed to exhibit different growth promoting activity between the everyday and every-

three-day medium replenishment (p=0.038 with paired t-test). The previous results confirm our postulation that medium changing can critically affect the accumulation of secreted factors in autocrine systems.

Regardless of our affirmative detection of autocrine loops in A431 using both assays, the gold standard for validating the presence of specific autocrine loops is to use autocrine-loop-specific

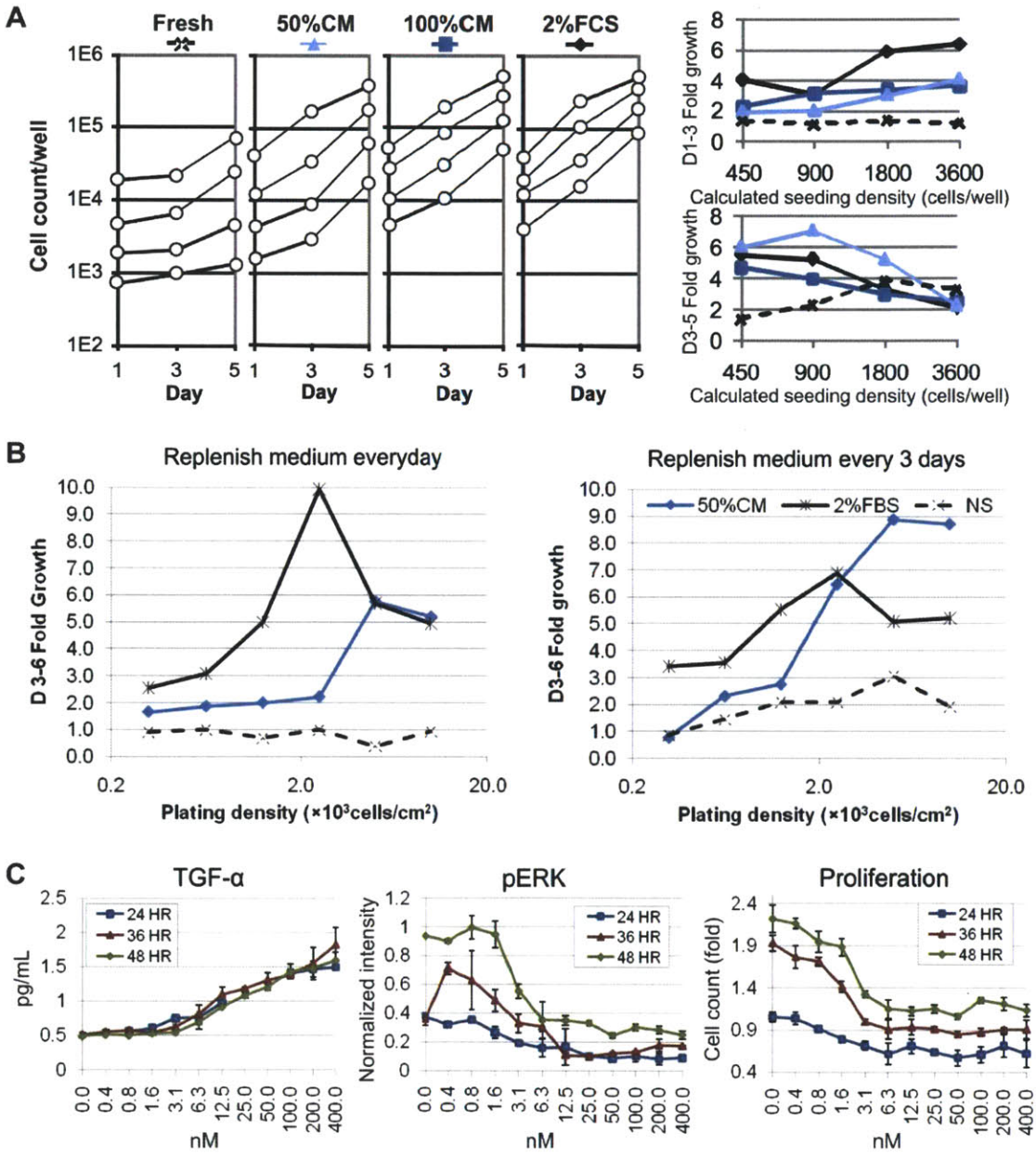

Figure 2-1 Validation of the EGFR autocrine loop in A431 cells

A) Total cell counts of A431 cells at different seeding densities in different cultivating conditions. Plots on the right illustrate the corresponding fold growth between day 1-3 and day 3-5. B) Growth change of A431 cells between day 3 and day 6 in different media with different medium-replenishing frequency. C) Changes of TGF-α accumulation, ERK phosphorylation and growth with varying doses of mAb225 at different time points after serum starvation. Error bars represent standard deviations from two biological replicates.

perturbation agents such as the receptor-blocking antibodies. If the cellular phenotype is modulated when we inhibit ligand/receptor interactions that underlie the tested autocrine loop, it is certain that cells must be able to acquire such ligands intrinsically. Because the antibody can only approach receptors from the extracellular space, this approach also distinguishes the impacts of autocrine signaling from intracrine signaling (Van de Vijver, Kumar et al. 1991). We attempted to validate the presence of the EGFR autocrine loop in A431 cells by co-cultivating the cells with varying doses of the murine monoclonal antibody 225 (mAb225) that has been shown to physically occlude binding of EGFR to its cognate ligands (Li, Schmitz et al. 2005). If the EGFR autocrine loop is in fact present, we expect to observe changes of all downstream biological processes. In the case of A431 cells, we measured the accumulation of TGF-α in the covering fluid to determine whether mAb225 can in fact compete with EGFR ligands in binding to EGFR. The phosphorylation of ERK1/2 is also determined because it is one of the major signaling molecules downstream of EGFR. We then determined changes in cell number because growth is the ultimate response of the EGFR autocrine loop (Figure 2-1C). With increasing concentration of mAb225, we observed increasing concentration of TGF-α in the covering medium. Both ERK phosphorylation and cell growth decrease with the elevated doses of mAb225. Interestingly, we found that A431 growth still persists even with the maximum dose of mAb225 (400 nM), as shown by the significant increase in cell counts between 24-48 hours. The observed incomplete growth inhibition by mAb225 should not arise from experimental artifacts because we also observed the corresponding increase in ERK phosphorylation with increasing incubation time. The refractory growth of A431 cells instead implies the presence of other growth promoting mechanisms, possibly via non-EGFR autocrine loops. These results validate the presence of the TGF-α/EGFR autocrine loop and its impact in promoting growth of A431 cells during serum-free cultivation.

The underlying intracellular signaling cascades of A431 growth

In order to further examine the presence of other autocrine loops, we decided to first determine the intracellular signaling pathways that underlie A431 cell growth during serum-free cultivation. Based on prior literatures of the ErbB-family receptors and their roles in cancer cells (Singh and Harris 2005; Hynes and MacDonald 2009), we validated the functions of two signaling pathways, the Ras/Raf/MAPK pathway and the PI3K/AKT pathway. In addition to our previous detection of ERK phosphorylation in A431 cells, both mitogenic pathways have been illustrated to underlie growth in various cancer tissues (Chen, Schoeberl et al. 2009). To investigate each individual signaling cascade, we quantified the phosphorylation of its major signaling target and monitored growth change when cells were co-cultivated with pathway-specific, small-molecule inhibitors. PD325901 was used to inhibit MEK phosphorylation while ZSTK474 was chosen to inhibit PI3K phosphorylation. We first determined the appropriate doses of both inhibitors to fully reduce the phosphorylation of each kinase (Figure 2-2A). We found that adding the MEK inhibitor (MEKi) and the PI3K inhibitor (PI3Ki) each at the final concentration of 5 μM adequately inhibit ERK1/2 and AKT phosphorylation, respectively (AKT phosphorylation signal is intrinsically small, giving rise to the noisy IC50 curves). We then determined how A431 cell growth would change with the addition of these inhibitors. Using the WST-1metabolic activity assay, we measured the metabolic rates of A431 cells with varying doses of MEKi and PI3Ki (Figure 2-2B). Changes of total cell counts were also determined for cells that were co-cultivated either with each inhibitor individually or with both inhibitors combined (5 μM each) (Figure 2-2C&D). Based on both proliferation assays, we found that adding MEKi or PI3Ki alone only causes cells to be cytostatic while simultaneous inhibition of both pathways causes cell death. The cytotoxic effect of the combined inhibitors is unlikely caused by the dose-dependent side-effect because the addition of PI3Ki at its maximal dose of 25 μM still exhibit higher metabolic rate than when we add both inhibitors, each at only 5 μM (Figure 2-2B). These results substantiate that the synergistic roles of Ras/Raf/MAPK and PI3K/AKT pathways in promoting both growth and survival of A431 cells during serum-free cultivation, and that these two pathways are the primary growth-regulating pathways in these cells.

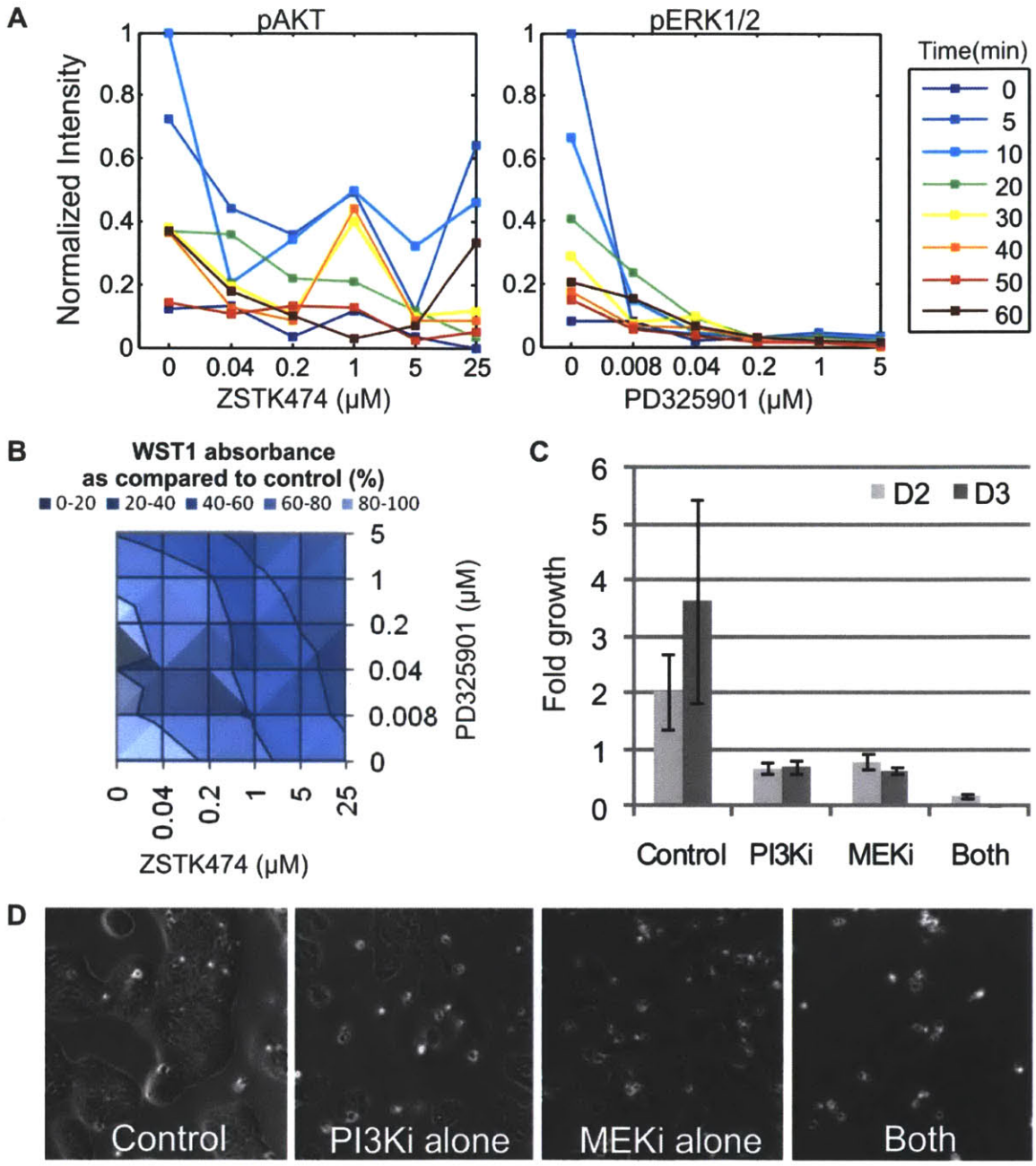

Figure 2-2 Intracellular mitogenic signaling cascades of A431 cells

A) Phosphorylation of AKT and ERK1/2 with varying does of ZSTK474 and PD325901, respectively. PD325901 and ZSTK474 were used to inhibit the phosphorylation of MEK and PI3K respectively. Measurements were performed at different time points after the addition of EGF at 200 ng/ml. B) Measurement of metabolic rates with WST-1 assay for varying combinatorial doses of inhibitors at day 2. Data are presented in percentages, as compared to absorbance of the control case (no inhibitor). C) Fold growth at day 2 and day 3 as quantified by cell counts using Coulter counter. MEK inhibitor and PI3K inhibitor were added to serum-free medium alone or simultaneously (each at final concentration of 5μM). Error bars represent propagated standard deviations from three biological replicates. D0 plating density = 15,000 cells/cm^2. D) Phase-contrast images of A431 cells in different cultivating conditions at day 3.

The hidden intricacy of the medium conditioning assay

The previously observed growth promoting effect of CM implies the accumulation of diffusive growth-promoting factors but contradicts with the spatially limited nature of many autocrine loops (Lauffenburger, Oehrtman et al. 1998). If cells can efficiently capture the secreted autocrine ligands, it might be impossible to detect such ligands in the supernatant without first inhibiting their interactions with the corresponding receptors (Dempsey and Coffey 1994). To explore these conflicting properties of autocrine systems, we decided to further examine the mechanism that underlies the activity of CM in A431

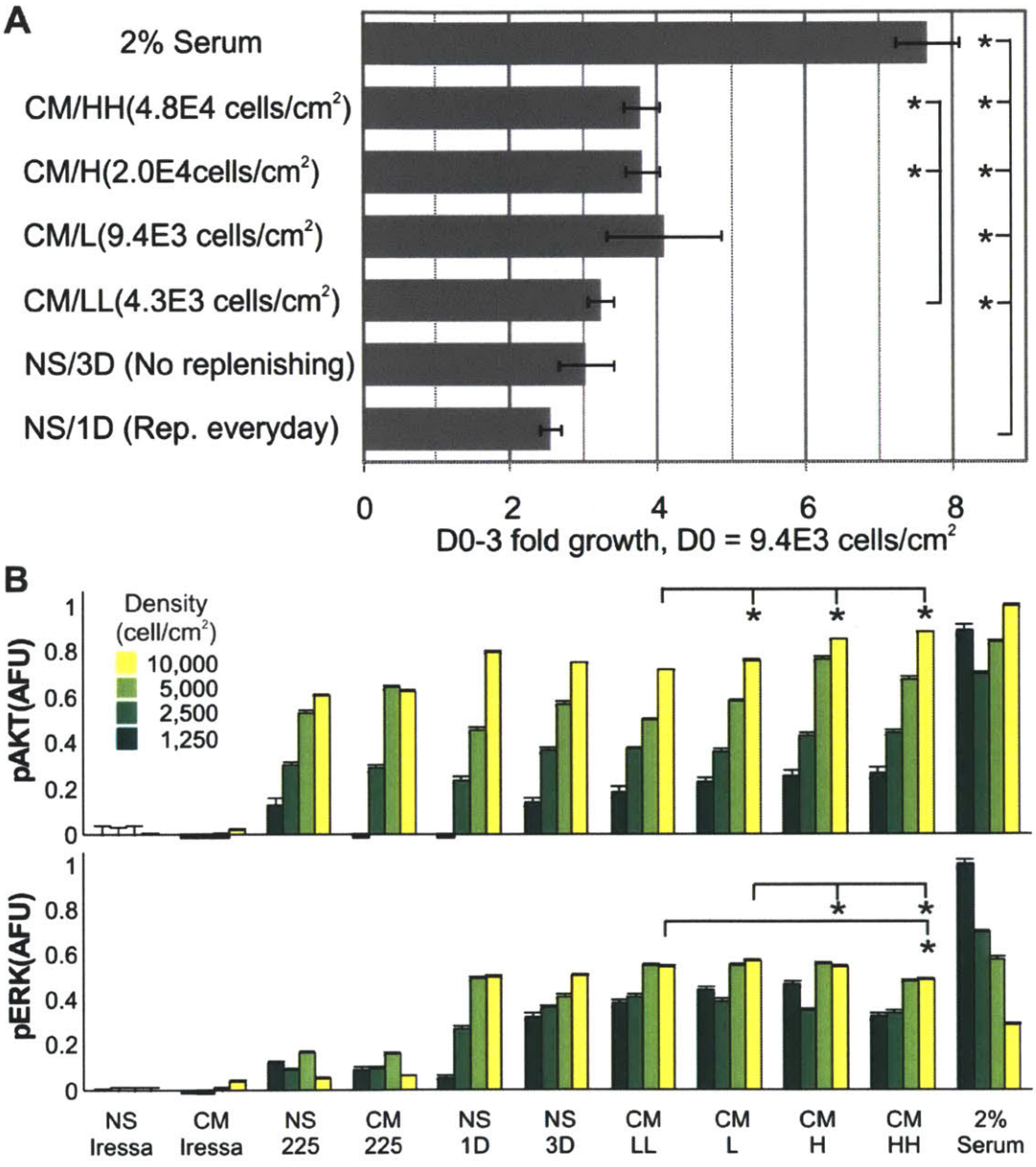

Figure 2-3 Growth-promoting and signal-activating effects of A431-conditioned media
A) Growth increase of A431 cells after three-day cultivation in different media, including CM from different plating densities, serum-free medium with everyday (NS/1D) or no (NS/3D) replenishment. B) AKT and ERK phosphorylation of A431 cells at varying plating densities in different cultivating medium at 72 after serum starvation. (* Statistically significant with $P < 0.05$)

cells. Having identified the underlying mitogenic signaling cascades of A431 growth, we also explored the activation of ERK and AKT by different cultivating media.

First, we attempt to determine the different growth promoting effects of CM that was prepared from A431 cells at different seeding densities. If ligands can diffuse freely into the surrounding fluid, we expect to obtain an increasing accumulation of ligands in CM and a corresponding growth elevation in the testing cell population. We prepared CM by cultivating A431 cells in serum-free media for 24 hours at varying densities, ranging from 4,000 to 40,000 cells/cm^2. To ensure minimal accumulation of waste byproducts, we mixed the prepared CM equally with fresh serum-free medium to acquire 50%CM for all plating densities. Apart from CM, we also cultivated cells in basic medium containing 2% serum as a positive control and serum-free medium, either with and without everyday medium replenishing condition, as negative controls (Figure 2-3A). In fresh serum-free medium, we observed a slight increase in cell growth without everyday medium changing, confirming our previous observation that increased incubation time can increase ligand accumulation (Figure 2-1B). In comparison to cell growth in serum-free medium with everyday replenishment, cells in CM from all plating densities can proliferate at higher rates. When we instead compare growth change among the different CM, growth in CM that were prepared at plating density of 9,400-48,000 cell/cm^2 were observed to actually be comparable while CM that was prepared from 4,300 cells/cm^2 is the only CM condition that exhibit significantly smaller growth change. To explain the observed saturating growth change in CM, we hypothesize that ligand accumulation in CM may reach a steady state. Alternatively, the range of ligand concentration in the different CM may simply fall within the insensitive range of the ligand concentration-growth relationship.

To further investigate the unpredicted growth changes due to different CM conditions, we investigated how the phosphorylation of ERK and AKT might also vary among these different medium conditions. In addition to the regular growth media, we also determined phosphorylation signals when cells were cultivated with EGFR-targeting inhibitors. We used both mAb225 and a small-molecule inhibitor Iressa (or Gefitinib), which has been shown to potently inhibit activity of the tyrosine kinase domains on EGFR (Di Cosimo, Ferretti et al. 2004). To also explore the possibly existing density-dependent effects, we also tested these different medium conditions with cells at varying plating densities (1.25-10 thousand cells/cm^2). Figure 2-3B illustrates ERK and AKT phosphorylation after three-day cultivation in different media. To fully inhibit EGFR autocrine activity, we use Iressa at 10 μM or mAb225 at 1 μM. Signals from all medium types were normalized by the highest signal of 2% serum and the smallest signals from serum-free medium with Iressa at each plating density. Notably, we observe distinct difference between Iressa and mAb225. While Iressa can efficiently inhibit both ERK and AKT phosphorylation, mAb225 can only inhibit ERK phosphorylation. The inability of mAb225 to prevent AKT phosphorylation suggests that the PI3K/AKT pathway may be activated by other mechanisms. Another distinct characteristic of the AKT phosphorylation is its increasing trends with the elevated cell plating densities, which is an effect that is not observed in ERK phosphorylation. When comparing changes of phosphorylation signals among different CM conditions, we surprisingly observe an increasing AKT phosphorylation in CM from elevated cell plating densities. ERK phosphorylation from this same set of medium was found to decrease non-linearly with plating density (pERK in CM/HH is significantly smaller than CM/LL). These observations suggest that CM might contain diffusive factors that are able to activate AKT better than ERK pathways, though our data is still preliminary.

Varying accumulation of EGFR Ligands in conditioned media at different plating densities

To determine the reason for altering effects of CM that was prepared from different plating densities, we determined the concentrations of two EGFR ligands, TGF-α and Amphiregulin, in CM at different time points (Figure 2-4). Using ELISA to measure the absolute concentration of ligands, we found that TGF-α was barely detectable in CM without first adding mAb225 to inhibit its binding with EGFR (i.e., we could only detect TGF-α above ~8,000 cells/cm^2). If we instead co-cultivate the cells with 400-nM mAb225, TGF-α concentration in CM increases by almost 30-fold ($10^{1.5}$) and also elevates at higher plating densities. Surprisingly, we found that Amphiregulin also exists in CM and its concentration

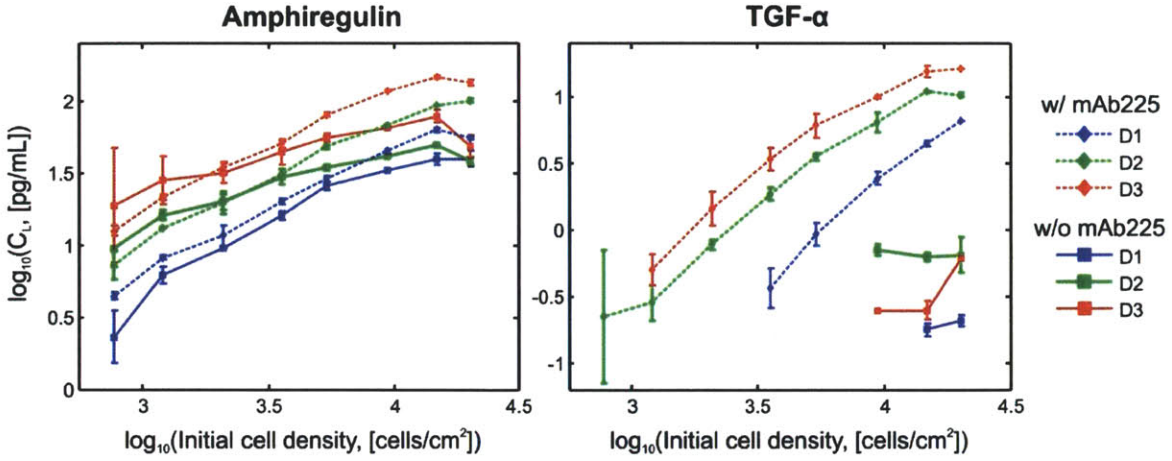

Figure 2-4 Accumulation of secreted EGFR ligands at varying initial plating densities
Concentration of TGF-α and Amphiregulin was determined from conditioned media that were prepared from different plating densities and different conditioning duration. Ligands were measured using standard ELISA for serum-free medium alone (solid lines with square dots) or when co-cultivated with 400-nM mAb225 (dotted lines with diamond dots). Error bars represent propagated standard deviations from two biological replicates.

actually increases with cell densities even without mAb225 addition. The absolute concentration of the Amphiregulin is over 100-fold higher than that of TGF-α (40 VS 0.2 pg/ml at 20,000 cells/cm^2 on day 1). Unlike TGF-α, we did not observe a dramatic change of Amphiregulin concentration with mAb225 addition, implying that Amphiregulin may be captured less efficiently by cells and therefore can propagate more broadly in the supernatant than TGF-α. The dramatic change of TGF-α concentration between the cultivation with and without mAb225 suggests that A431 cells can efficiently capture TGF-α, allowing only very few TGF-α molecules to diffuse into the surrounding fluid. It is important to note the increasing accumulation of both ligands with increasing incubation time, validating that both ligands are in fact secreted by the cells. Because the maximum molar concentration of TGF-α during the regular medium conditioning procedure (without mAb225) is only 0.2 pM (assuming TGF-α molecular weight of 6,000 Daltons (Derynck 1988) and the K_d of TGFα/EGFR binding of 2-3 nM (Ebner and Derynck 1991)), we believe that the observed growth promoting activity of CM is caused by the building-up of Amphiregulin or other ligands that accumulates at higher quantity in CM than TGF-α, the assumed autocrine ligand of A431 cells. We therefore conclude from this experiment that the medium conditioning assay may not be able to exhibit effects of all secreted ligands, especially those ligands that bind more strongly to receptors on cell surface. The medium conditioning assay should not be used to confirm presence or impacts of a specific autocrine loop. Our detection of at least two EGFR ligands in CM also emphasizes the presence of multiple autocrine loops in A431 cells. The ability of TGF-α to bind more strongly to cells may imply its dominating role over other ligands in regulating growth during serum-free cultivation. While we did not investigate this question extensively, it is possible to evaluate significance of a specific ligand using anti-ligand antibodies (Lauffenburger, Oehrtman et al. 1998).

Roles of the ErbB3 receptor in A431 cells

We have previously illustrated the presence of EGFR autocrine loops, with at least two different ligands, and demonstrated the significant roles of the Ras/Raf/MAPK and the PI3K/AKT pathways in regulating A431 cell growth. It was still unclear how the AKT pathway can be activated while we fully inhibited the EGFR autocrine loop. If there is in fact another autocrine loop in A431 cells, the previous results suggest that this autocrine loop must also function together with EGFR to activate AKT

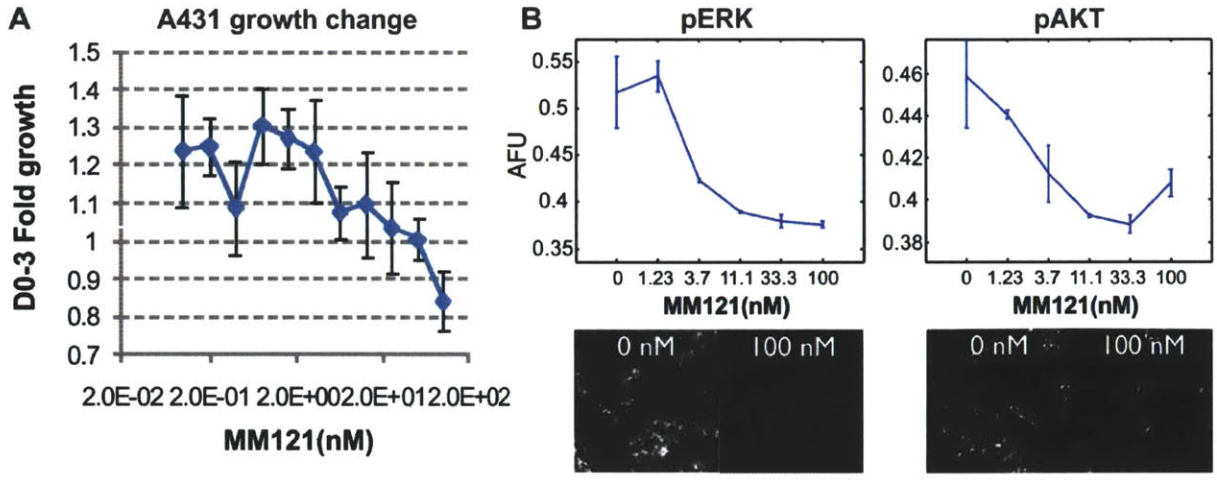

Figure 2-5 Role of the ErbB3 receptor in A431 cells
A) Changes of A431 cell growth after three-day cultivation with varying doses of MM121. B) Phosphorylation signals of ERK and AKT with varying doses of MM121 at 72 hours after serum-starvation. Pictures show aw images for each proteins at the extreme doses of MM121. Error bars represent standard deviations from two biological replicates.

phosphorylation because we can efficiently inhibit AKT phosphorylation using the EGFR inhibitor Iressa. Previous studies showed that A431 cells also express other ErbB-family receptors, including ErbB2 and ErbB3, in addition to the EGFR (Ono, Hirata et al. 2004). ErbB2 cannot bind to any known ligands. ErbB3 can bind to Heregulin (or Neuregulin Type I) but relies on heterodimization with other ErbB-family receptors to activate downstream signaling cascades (Citri, Skaria et al. 2003). A recent study showed that ErbB3 plays a critical role in activating AKT in various cancer tissues and its function can be inhibited using a specific monoclonal antibody MM121 (Schoeberl, Pace et al. 2009). To test whether A431 cells also acquire the ErbB3 autocrine loop, we determined change in A431 cell growth when the cells were co-cultivated with varying dose of MM121 (Figure 2-5A). After three-day cultivation, we found a significant decrease in cell growth with increasing MM121 dose ($p<0.01$ with paired t-test, in comparison with growth without MM121). When we looked at the phosphorylation of major signaling targets, we found that phosphorylation of ERK and AKT all decreases with increasing MM121 concentrations (Figure 2-5B). The previous results strongly substantiate the role of ErbB3 in activating A431 cell growth, even though its growth promoting role may be less significant than EGFR which is expressed at higher amount (2E6 molecules/cell for EGFR versus 1.7E4 molecules/cell for ErbB3 from personal communication with Merrimack). While ErbB3 may be activated by the secretion of EGFR ligands via EGFR/ErbB3 dimerization, the fact that we could not fully inhibit AKT phosphorylation with mAb225 suggests that the EGFR/ErbB3 heterodimers must arise due to non-EGFR ligands, possibly by secretion of Heregulin. Exogenous addition of Heregulin can in fact activate AKT in A431 cells (Chen, Schoeberl et al. 2009). To ensure the presence of the Heregulin/ErbB3 autocrine loop in A431 cells, we have yet to show that Heregulin accumulation in supernatant in fact increases with increasing doses of MM121.

Autocrine ligands initiate unique temporal changes of ERK phosphorylation

Regardless of the prevalence of autocrine loops in cancer cells, the understanding of how autocrine loops initiate mitogenic signaling cascades has been derived mainly from studies with exogenously supplied ligands. To investigate the potential differences between intrinsic versus extrinsic ligand-mediated signaling activation, we compared the temporal change of ERK phosphorylation in A431 cells between the two different activation types. We first obtained changes of ERK phosphorylation due to EGF

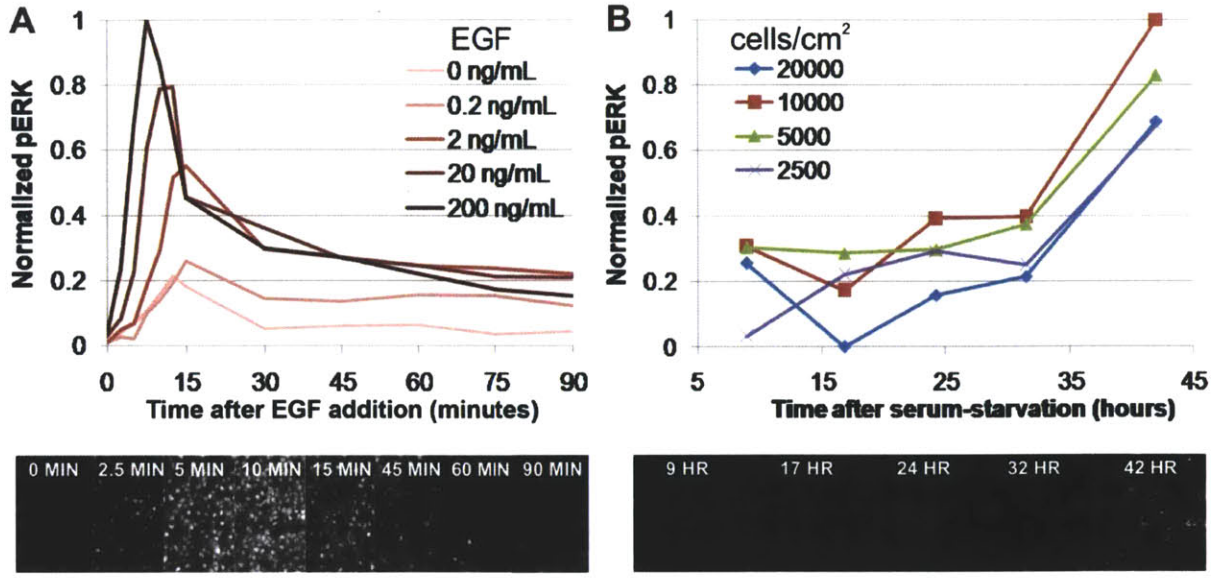

Figure 2-6 Unique temporal changes of ERK phosphorylation from autocrine signaling
A) Dose responses of ERK phosphorylation in A431 cells after addition of EGF at varying doses. B) Changes of intrinsically activated ERK phosphorylation in A431 cells at varying time points after serum starvation for different cell plating densites.

addition at varying doses, ranging from 0-200 ng/mL (Figure 2-6A). With exogenous supply of the EGFR ligand, we observed a temporally increasing ERK phospholylation within 5-15 minutes and a gradual signal decrease between 15-90 minutes. It is also important to note the difference in magnitude and time at which we observe the maximal response for each dose of EGF addition. With increasing EGF concentration, we observed higher magnitude of the signal peak that also occurs at a sooner time point after stimulation. Our results agree well with the previously determined temporal responses of exogenously supplied ligands (Chen, Schoeberl et al. 2009). Unlike the addition of EGF, activation of ERK phosphorylation due to self-secreted ligand via autocrine loops was observed to gradually increase with time (Figure 2-6B). We performed this analysis at varying cell plating densities, hoping to obtain varying levels of autocrine activation with the increasing cell plating densities. Changes of intrinsically-activated ERK phosphorylation for the different plating densities turn out to be more complicated, exhibiting no obvious trend. Regardless of the observed gradual increase of intrinsically activated ERK phosphorylation, their intensities at all plating densities still remain below the peak intensity initiated with EGF addition (compare raw images from intrinsic activation to images at 5-10 minutes due to EGF addition).

Changes of mitogenic signaling activation with altering plating densities

The previous observation of the complex changes of auto-activated ERK and AKT phosphorylation with varying cell plating densities prompted us to carefully examine this characteristic in A431 cells. Unlike the previous analysis, we quantified the single-cell phosphorylation signals for a wider range of plating densities, ranging from 100 to 100,000 cells/cm^2. We compared the generated signals with the mAb225-supplemented cell cultivation to determine the role of EGFR autocrine loops in activating ERK and AKT phosphorylation. We also used either ZSTK474 or PD325901, the PI3K and MEK inhibitors, to generate the true background intensities for AKT and ERK phosphorylation. Figure 2-7 illustrates the measured phosphorylation signals with varying cell plating densities. Without being normalized by background intensities (Figure 2-7A), AKT phosphorylation increases with cell plating

densities and saturates above the plating density of 10,000 cells/cm^2. ERK phosphorylation on the other hand only increases slightly up to plating density of 10,000 cells/cm^2 and decreases above this critical density. To determine the quantitative contribution of EGFR autocrine loops in activating both pathways, we normalized both signals by background intensities at each cell density. A more dramatic increase in ERK phosphorylation is observed with increasing cell density, while AKT phosphorylation elevates with cell plating densities without the previously observed saturation (Figure 2-7B). MAb225 can inhibit ERK phosphorylation effectively, disrupting almost all observed density-dependent changes of ERK phosphorylation. Nonetheless, mAb225 still cannot eliminate the increasing trend of AKT phosphorylation with plating densities. These results suggest that the EGFR autocrine loop contributes more significantly to ERK phosphorylation and also underlies its alteration with cell plating densities. The decreasing ERK phosphorylation at high plating densities must instead be caused by other mechanisms, for example, the density-dependent contact inhibition (Kim, Kushiro et al. 2009). In the case of AKT phosphorylation, because cell cultivation with saturated mAb225 still exhibits a similar density-dependent increase of AKT phosphorylation, we conclude that AKT phosphorylation must be activated mainly by other pathways, possibly by the ErbB3 autocrine loop.

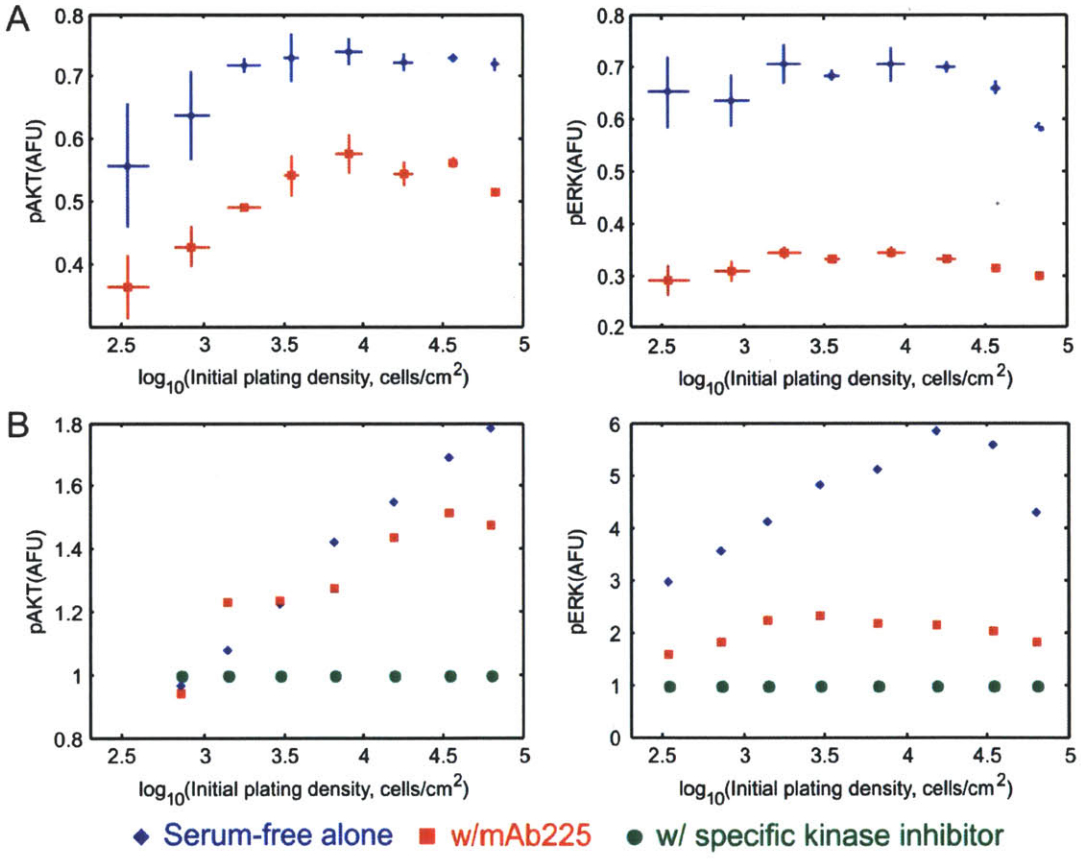

Figure 2-7 Changes of ERK and AKT phosphorylation with varying cell plating densities
A) single-cell averaged AKT and ERK phosphorylation in A431 cells for varying cell plating at 72 hours after serum starvation. The presented signals were calculated from log10(raw intensity)+2.5. Error bars represents standard deviations from three biological replicates. B) AKT and ERK phosphorylation signals at the same conditions but different cell batch, normalized by the background intensities that were generated by incubating the cells with PI3K or MEK inhibitors for 45 minutes before cell fixation.

2.3 Discussion

We have explored in this chapter some of the unique characteristics of autocrine signaling, mainly those that pertain to the autonomous cancer growth. Some of these characteristics such as the phenotypic changes by alteration of cell plating density or growth promotion in conditioned medium are the commonly recognized but frequently misinterpreted characteristics of autocrine loops. The sustained signal activation and the presence of multiple autocrine loops within the same cell type are less appreciated characteristics of autocrine signaling but can provide functional benefits for the acquiring cells. Using A431 cells as our model, we show that the density-dependent phenotypic change and the medium conditioning assay only serve as preliminary screening tools but cannot verify the presence of specific autocrine loops. The use of receptor blocking antibodies is currently the only method for the specific verification of autocrine-loop presence. Using mAb225, we show that inhibition of the EGFR autocrine loops results in elevated accumulation of TGF-α as well as decreasing ERK phosphorylation and cell growth. By measuring the concentration of EGFR ligands in the A431-conditioned media, we illustrate that some autocrine ligands might not actually be present at significant amount in CM due to their efficient capturing by cells. The detection of Amphiregulin at higher quantity in A431-conditioned media illustrates how a single cell type may acquire multiple autocrine loops that operate at different spatial ranges. We also illustrate that A431 may acquire the ErbB3 autocrine loop by showing the critical role of ErbB3 in promoting A431 growth and activating both AKT and ERK phosphorylation. When comparing the activation of ERK phosphorylation from self-secreted ligands versus exogenously supplied ligands, we found that the intrinsic activation causes a gradual increase of ERK phosphorylation in comparison to the fast-rise/slow-delay response due to addition of exogenous factors. We illustrate dissimilar changes of the auto-activated ERK and AKT phosphorylation with varying cell plating densities. The inability of mAb225 to incompletely disrupt AKT phosphorylation further substantiates the possible existence of other autocrine loops. The diminished ERK phosphorylation at high plating densities also suggests the possible involvement of other signaling cues in regulating the mitogenic signaling cascades in A431 cells.

Our analysis of the intracellular signaling cascades in regulating A431 growth emphasizes the complexity in preventing phenotypes that is promoted by autocrine loops. Using small molecules and receptor-blocking antibodies, we showed that at least two ErbB-family receptors exist in A431 cells. While the detected EGFR ligands, TGF-α and Amphiregulin, can only bind to EGFR, it is possible that the A431 cells may also secrete other ligands like Heregulin that can bind directly to ErbB3. Apart from the ErbB-family receptors, other autocrine loops have also been reported in A431 cells including the autocrine loops of IGF-I receptor and IGFII (Guix, Faber et al. 2008) and that of CXCR2 and IL-8/Gro-α (Metzner, Hofmann et al. 1999). We have shown that growth of A431 cells can be fully inhibited using therapeutics that only target the tyrosine kinase activity of EGFR such as Iressa, but it is possible that the functions of other receptor families may only become significant during direct inhibition of the EGFR autocrine loop. In fact, it was shown that Iressa-resistant A431 cells can sustain their growth via mitogenic activation through the IGFI receptors (Guix, Faber et al. 2008). Without addition of cancer therapeutics, this pathway is normally inhibited by the IGF-binding proteins (IGFBPs). Upon long-term treatment of either Iressa or Cetuximab, the investigators showed that expression of IGFBPs is down-regulated, allowing the IGFII/IGF-IR autocrine loop to activate A431 growth via the PI3K/AKT pathway. A similar paradigm is observed in lung cancer cells where mitogenic signals through the EGFR pathway switch to signaling via MET and ErbB3 receptors while the patients are being treated with EGFR-targeting drugs (Engelman, Zejnullahu et al. 2007). Our observation that A431 cells can activate growth via multiple receptor families emphasizes the need for novel therapeutics that can inhibit multiple receptors all at once. Such treatment may be achieved either by a single drug that can simultaneously inhibit multiple receptors at once or simply by using multiple therapeutics.

The observed gradual increase of ERK phosphorylation due to autocrine loops in A431 cells highlights the more physiologically relevant receptor activation due to autocrine signaling in comparison to the temporal signal peaking from exogenous ligands. Such gradual signal activation has been instrumental to the embryonic development in many organisms. In the *Drosophila* egg, The Spitz/EGFR

autocrine loop plays a critical role in sustaining the EGFR activation of the follicle cells (Wasserman and Freeman 1998). This positive feedback loop is initiated by the temporary paracrine secretion of Gurken by the oocyte before the separation of the oocyte and the follicle cells by the vitelline membrane formation. Without this autocrine loop, follicle cells will not be able to maintain EGFR activation, which is necessary to initiate other downstream processes. Another important effect of sustained signal activation is the activation of cell growth. To get through the G1 phase of the cell cycle, it has been illustrated that the mitogen-mediated ERK activation must occur throughout the entire G1 phase. (Weber, Raben et al. 1997; Roovers and Assoian 2000; Meloche and Pouyssegur 2007). Inhibition of MEK even at the end of G1 phase can abolish entry to S phase (Yamamoto, Ebisuya et al. 2006). To ensure prolonged ERK activation, normal cells often require activation of the integrin signaling pathway (Roovers, Davey et al. 1999). In cancer cells, mitogenic activation via autocrine loops alone may be sufficient to create the slow but sustained ERK activity necessary for getting cells through S phase. This characteristic may provide survival benefits to cancer cells that become more aggressive, lacking ability to associate with ECMs (Bringuier, Umbas et al. 1993; Okegawa, Pong et al. 2004).

2.4 Summary

We have explored in this Chapter unique characteristics of autocrine signaling that underlie its complex experimental investigation as well as properties that may provide survival benefits to the acquiring biological system. We showed that modulation of ligand/receptor binding with specific inhibitors still serves as the only accurate method in examining impacts of autocrine loops. To investigate function of autocrine loops in newly discovered biological systems, we will need a novel experimental method that can alter the activity of autocrine signaling without the use of specific inhibitors. The observation that A431 cells secrete at least two EGF-like ligands (TGF-α and Amphiregulin) and also acquire significant activity of the ErbB3 receptor illustrates how an individual naturally-occurring autocrine system may actually acquire multiple autocrine loops. It is therefore important that we take into account the possible presence of all autocrine loops when determining the choice of therapeutics to inhibit cancer growth. The observed non-monotonic changes of mitogenic signals with cell plating densities illustrate possible interplay of autocrine signaling with other environmental cues. To modulate autocrine activity by simply altering the intercellular spacing, we must ensure that the developed method can maintain constant influences of these non-diffusive cues. The analyses performed in this chapter provide fundamental understanding of autocrine systems that is necessary for our development of the cell-patterning platform to measure the combined autocrine activity in cancer cells.

2.5 Material and methods

Cell culture

The A431 epidermoid carcinoma cells were cultivated in DMEM/F-12 medium with Glutamax (Gibco#10565) supplemented with 10% bovine calf serum (BCS), (Hyclone#SH20072.03), 100 U/mL penicillin and 100 μg/mL streptomycin (Invitrogen#15140122) at 37°C in 7.5% CO_2. For passaging, cells were trypsinized with 0.25% trypsin/EDTA (Gibco#25200) and subcultured at 20% confluency. For analysis of intercellular interactions, A431 cells were seeded and cultivated overnight in serum-containing medium to ensure uniform cell attachment at all plating densities. After 24-hour serum starvation (DMEM/F12 with Glutamax supplemented with 100 U/mL penicillin and 100 μg/mL streptomycin), we then washed the cells with PBS and cultivated the cells for another 72 hours in serum-free medium. mAb225 was self purified from the supernatant of 225 hybridoma (Appendix A). MM121, EGF and Iressa were gifts from Sorger Lab. For bulk analysis of cell growth, cell numbers per well were determined using Coulter counter (Beckman).

Measurement of net and total ligand secretion

To determine the secreted amount of EGFR ligands, we first collected the supernatant liquid after 3-day cell cultivation. For long-term storage, the supernatant is centrifuged at 12,000g for 15 minutes and

frozen at -80°C. We measured the amount of human TGF-α and Amphiregulin in the collected supernatant using the DuoSet ELISA development systems (R&D Systems), following the Manufacturer's protocol.

Quantification of phosphorylation signals

We quantified the phosphorylation signals of ERK, AKT and EGFR using fluorescent imaging technique. At the end of the study, cells were fixed by incubating in 2% paraformaldehyde (Electron Microscopy Sciences) diluted in PBS with 0.05% tween-20 (PBST) for 10 minutes. After washing twice with PBST, cells were permeabilized with methanol for 10 minutes. After rinsing twice with PBST, we stored cells in PBST with 1×Halt protease and phosphatase inhibitor cocktail (Pierce, 78440) to preserve the signal for longer storage at 4°C. After blocking with the Odyssey block buffer (Li-cor Bioscience#927-40000) for 1 hour at room temperature, we then incubated the cells with diluted primary antibodies (in Odyssey buffer at 1 in 200) overnight at 4°C. To stain for the phosphorylation signals, we used the following antibodies: rabbit anti-phophorylated EGFR (pY1068, Epitomics#1727), rabbit anti-phosphorylated ERK1/2 (Thr202/Tyr204, Cell Signaling Technology#4377) and rabbit anti-phosphorylated AKT (Ser473, Cell Signaling Technology#4060). After incubation with primary antibodies, we washed the cells three times with PBST and incubated the cells with secondary antibodies for 1 hour at room temperature. We used the Alexa Fluor 647 goat anti-rabbit IgG (Invitrogen). To enable image segmentation, the cells were also counter-stained with DAPI (Invitrogen#D3571) and whole cell stain blue (Pierce#8403501). For counter-staining, we first washed the cells once with PBST and another time with PBS before incubating the cells with whole cell and nuclear stains for 30 minutes. After washing cells twice with PBS, we then imaged the cells using the high-contact screening microscope (CellWorx, Applied Precision). To ensure appropriate segmentation, we chose the concentration of nuclear stain to give at least 10 folds higher in the fluorescent intensity than that of the cytosol region. Quantification of fluorescent intensity per cells were performed with CellProfiler (Carpenter, Jones et al. 2006). Signal of each cell is quantified from the mean intensity of the segmented nucleus area for all phosphorylated proteins.

Appendix A: Purification of murine monoclonal antibody 225 from hybridoma supernatant

To enable inhibition of the EGFR autocrine loops, we need to purify murine monoclonal antibody 225 (mAb225) from the 225 hybridoma. The hybridoma must be cultivated in serum-free containing medium to ensure minimal protein background. We collect the secreted antibodies using commercially available reactor. We then purify mAb225 from the concentrated supernatant from the reactor using the affinity column of protein G. We then check purity of the isolated antibody by running the protein in SDS-PAGE gel. To enable visualization of the antibody, we stain the gel using the standard Coomassie stain.

Materials and device

		Quantity	*Catalog #*	*Price*	*From*
1.	125 mL flask for cell culture	24	30180-036	24	VWR
2.	CELLine™CL-1000	3 flasks	353137	611.10	BD
3.	BD Cell™ MAb Serum-Free Medium	1000 ml	220509	56.28	BD
4.	100 mM L-Glutamine				
5.	Pen/strep				
6.	Amicon Ultra-15, MW 30kDa	8	Z717185-8EA	77.22	Sigma
7.	Pierce Protein G Agarose	2 ml	20398	199	Thermo
8.	Disposable Column Trial Pack	7 pieces	29925	59	Thermo
9.	Small culture dishes (60 x 15)	500	353002	98.55	BD
10.	Spin-X centrifuge tube filters	96	8160	169.06	Corning
11.	Neutralization buffer: 1M Tris HCl, pH 8		H590-04		
12.	Elution buffer: 0.1 M Glycine in water, pH 2.8 (Anything, pH 3.5 or below should work)				
13.	Column storage buffer: 0.02% sodium azide in water				
14.	Binding and washing buffer: 1x PBS				
15.	Incubator with shaker				
16.	Spectrophotometer for measuring protein concentration				

Nutrient media

1. 1 L of BD Cell MAb serum-free medium
2. 10 ml of Pen/strep
3. 10 ml of L-Glutamine

Cultivation of 225 hybridoma cells

1. Stock cells should first be adapted to serum-free mAb medium and frozen with 10% DMSO. Cells should be frozen at 1×10^6 - 2×10^6 cells in 1 ml of nutrient media.
2. To thaw the stock frozen cells, warm up the vial in 37°C water bath for 2-3 minutes. Add 1x (pre-warmed) medium into the cryovial and aliquot the cells into a 15-ml conical tube. Spin the cells down at 1000 rpm for 5 minutes.
3. Aspirate off the supernatant and replenish with 5 ml media. Aliquot 5 ml of cell suspension into 5-cm dish and cultivate at 37°C with 5% CO_2 in a small culture dish, with rotation.
4. After 2 days, the cell concentration should reach approximately 1 million cells/mL.
5. Aliquot the cells into a mini flask and replenish with 10-ml media to obtain $0.2-0.3\times 10^6$ cells/ml in a total of 15 ml. At this point, the cell flask should be aerated and should be incubated with rotation.

6. After 2 days, or until the cell number reaches approximately 1×10^6 cells/ml, the cells are ready for splitting (The doubling time of 225 cells is approximately 24 hours). The cells should be subcultured to obtain $0.2-0.3\times10^6$ cells/ml in the next-round culture.
7. For mAb225 production, use 1 confluent flask filled with 30 mL. Each confluent flask should have 1×10^6 cells/mL. Aliquot the cell suspension into a 50-ml conical tube and spin down at 1000 rpm for 5 minutes. Aspirate off supernatant and replenish with 15 ml nutrient media to obtain 3×10^7 cells at a concentration of 2×10^6 cells/mL.

Important Note It might be necessary to reprenish media even everyday to ensure cell survival. Cell counts should be monitored everyday especially when the hybridoma are cultivated in complete serum-free condition. If cell count become stable or diminish, the medium should be replenished more often.

mAb225 production by medium conditioning using CELLine CL-1000

1. Pre-warm the nutrient media to 37°C
2. Pre-wet the cell cultivation chamber membrane by adding 25 ml media into the nutrient chamber (blue cap) before seeding cells.
3. Loosen the blue nutrient compartment cap to prevent air locking in the cell compartment.
4. Prepare 3×10^7 cells in 15 ml to be filled in the cell compartment.
5. Carefully load cell suspension into the cell compartment using serological pipet. Press the pipet tightly into the black gasket to access cell cultivation chamber. There should be no air left in the cell compartment. Bubbles can be removed by tilting the reactor and aspirating off with the pipet pressed to the gasket.
6. Fill the nutrient compartment with approximately 1 liter of nutrient media (the media can be poured in directly). Make sure to leave about 1 inch of air above the nutrient in the flask.
7. Tighten both the blue and white caps before placing the reactor into the incubator. DO NOT shake the reactor during the next two weeks of mAb secretion. Incubate the reactor at 37°C with 5% CO_2.

Preparation of protein G-resin column

1. Equilibrate protein G agarose and all buffers to room temperature.
2. Carefully pack the column with 2 ml of resin slurry.
3. Equilibrate the column by adding 5 ml of the Binding Buffer and allowing the solution to drain through the column.

   Note: To avoid air bubbles being drawn into the resin, remove the top cap before the bottom cap when opening column.
4. Regenerate column by washing with 12 ml of Elution Buffer. Columns may be regenerated at least 10 times without significant loss of binding capacity.
5. For column storage, wash column with column-storage buffer. When approximately 3 ml of solution remains, replace the bottom cap followed by the top cap on the column. Store columns upright at 4°C.

Purification of mAb225 from the conditioned media

1. After 14 days, aliquot the concentrated media from the white-capped cell compartment into a 50-ml conical tube. Discard the media in the nutrient compartment and the reactor.
2. Cells in the conditioned media should be isolated by centrifugation at 2000g for 30 minutes.
3. Filter the supernatant through a filter-top centrifuge tube (Corning, #430320). Add 10% 10X PBS to the solution to buffer exchange to PBS.

4. Apply the diluted sample to the column and allow it to flow completely into the resin. Do not allow the resin bed to run dry. Save the flow-through liquid for further purification.
5. Wash the Protein G column with 50 ml of the Binding Buffer to remove non-specific binding. Collect run-though liquid and measure their absorbance at 280 nm to confirm that all other proteins are removed. The last fractions should have absorbances similar to Binding Buffer alone (A<0.02).
6. Elute antibodies with 5 ml of Elution Buffer and collect ~0.9 ml fractions. The eluted run-through liquid should be dripped into microcentrifuge tubes, each filled with 0.1 ml neutralization buffer. Mix the tubes by inversion after collection is complete. Monitor the elution by measuring the absorbance at 280 nm.
7. Save and concentrate all of the fractions. The eluted solution should then be concentrated further using Amicon Ultra-15 centrifugal filter unit. Pipet 15 mL protein solution into a filter unit and spin for 12 minutes at 3200g. Repeat this procedure until all of the eluted protein has been concentrated to a volume of 1.5 mL.
8. Add 13.5 mL PBS to the column and concentrate down to 1.5 mL (12 minutes at 3200g). Repeat this PBS buffer exchange once more to dilute the elution buffer 100X.
9. At this point, the concentrated mAb225 can be sterilized by filtering through a 0.22 um Spin-X filter column (spin at maximum speed or ~14000rpm for 1 minute) and stored at -20°C for future use. The recommended storage concentration is 0.5-2 μg/μL.

Coomassie Staining

1. Incubate the gel in 0.5% Coomassie, 50% methanol and 10% acetic acid (to prepare this solution, agitate overnight and filter afterwards)
2. Expose the gel to Coomassie solution for 10 minutes with shaking
3. Rinse with destainer (50% methanol and 10% acetic acid)
4. Cover gel with destainer and boil using microwave
5. Shake until stain comes off from the background
6. Wash and incubate in DI water until the gel swells back to original size

Chapter 3

Technologies for configuring the spatial arrangement of cells

In this chapter, we present our development of engineering techniques to enable the organization of cell culture with precisely defined spatial arrangement. Unlike the standard cell cultivation where cells are randomly positioned on the substrate, cell patterning enables us to pre-configure their intercellular spacing or construct cell clusters with any desired shape. We present in this chapter two cell-patterning techniques: 1) the optimized stencil cell patterning technique and 2) the Stencil-Delineated Electroactive Patterning (s-DEP). Unlike other cell patterning methods, both techniques are designed to be easily integrated with standard biological assays. Per our main objective to develop a generic method for measuring combined autocrine activity in promoting cancer growth, we believe that the introduction of spatial regularity to the standard cell culture will help reveal the direct impact of autocrine signaling while helping to normalize influences of non-diffusive cues. The presented work on s-DEP is a collaborative work with Brian Taff (fabrication of electroactive substrate), Salil Desai (SEM imaging) and Michael Vahey (s-DEP modeling).

3.1 Introduction

Precise spatial organization of tissues underlies lineage specification in multicellular organisms. Via diffusive signaling, distances between sender and receiver cells govern the concentration of the signaling molecules that are exposed to the receiver cells, a parameter that will dictate the ultimate cel response (Francis and Palsson 1997). Via contact-mediated signaling, the relative orientation of a cell to its neighbors defines the cell polarity, a property that underlies asymmetric cell division in most stem cell niches (Fuchs, Tumbar et al. 2004). Because of the critical roles of complex cell arrangement in biology, many engineering approaches have been developed to organize the complex tissue-like constructs (TLCs), or the heterotypic cell clusters with the spatial organization that mimics microenvironment *in vivo*, with the main goal to reestablish such biological niches *in vitro* (Folch and Toner 2000). Cell patterning technologies are methods that were originally used in silicon-based microfabrication but have been adapted for cell localization *in vitro*. In the past decade, various cell patterning techniques have been developed and can be categorized into two main approaches: 1) modification of the substrate surface to promote or inhibit cell adhesion and 2) direct cell manipulation using physical forces. While all techniques enable, in their own ways, a precise cell arrangement within a limited substrate area (~mm^2), only a few can organize precise cell patterning across a large substrate area (~cm^2). Among those, a subset of such techniques can actually be performed consistently and are scalable for biological studies where multiple test conditions are generally needed, and each must contain enough cell samples (> 1,000 cells) to ensure reliable measurement with bulk assays. Finally, a limited number of these methods can establish complex cell structures that contain heterotypic cell populations, a feature necessary to form realistic TLCs.

Stencil cell patterning (Folch, Jo et al. 2000) and dielectrophoretic forcing (Albrecht, Sah et al. 2004; Rosenthal and Voldman 2005) are two cell-patterning methods that acquire limited cell-patterning capability when used on its own but each of these techniques offers unique cell localization characteristics. Stencil cell patterning utilizes a thin, flexible membrane to prevent cells from touching unwanted area while containing through holes that allow cells to be exposed and attach to the substrate. Because of its efficacy in preventing cells from the unwanted area of the substrate without any modification of substrate surface chemistry, stencil cell patterning is an ideal technique for creating cell arrays of adherent cell types. Regardless of its unique features, stencil cell patterning has not been widely used because of its limitation in creating sophisticated shapes and tendency to damage cells. On the other hand, dielectrophoresis creates cell structures by exerting an electrical force to move cells into the desired shape. While DEP allows the arrangement of cells into complex shapes, its unique feature comes at the price of microfabrication of the corresponding electroactive substrate. It is also very difficult to create cell arrays

across a large substrate area using DEP alone. Because of these limitations, both methods when used alone either offer limited cell arrangement capacity or are too complicated for biological studies.

In this chapter, we present the modified stencil-based cell-patterning techniques that feature both scalability and capacity to create complex heterotypic TLCs. With the previous procedure to pattern cells with stencils, the technique cannot be applied with different cell types due to its tendency to damage cells. Difficulty in creating conformal contact between stencil and substrate also prevents precisely defined cell constructs. We first describe the improved stencil patterning method that can consistently establish cell arrays across a large substrate area on standard tissue culture vessels. A simple technique to enable parallel cultivation of stencil-defined cell constructs is also introduced. Having discussed an approach to establish scalable cell arrays, we then present our development of a novel cell patterning technique, the stencil-delineated electroactive patterning (s-DEP). S-DEP allows creation of cell clusters with customizable shapes, positions, and pre-configurable internal cell organization by combining the standard dielectrophoretic forcing with stencil cell patterning. The stencil defines overarching geometries of the cell constructs while negative-dielectrophoretic (n-DEP) forcing guides subgrouping of cells to the desired positions within this pre-defined area. We demonstrate the use of s-DEP by creating arrays of heterotypic cell constructs with internal labeled striation. We use these complex cell constructs to examine cell motion within cell monolayer and find that A431 cells move within the monolayer with a homogenous motion diffusivity independently of their positions. Together, both simple modifications to the original stencil patterning enable the organization of complex heterotypic TLCs that can be scaled up for high-throughput biological studies.

3.2 Results

Optimizing stencil cell patterning for biological studies

Cell patterning will stencils rely on the use of thin, flexible membrane to prevent cells from touching the unwanted area while those that can land on the substrate via through holes end up creating the precisely defined cell structure (Figure 3-1A). Because there is no modification of the substrate surface chemistry, accuracy of the stencil-defined cell patterns relies critically on how well we can seal the stencil on top of the substrate. We describe here three modifications to the original practice of stencil patterning to enable precise cell localization on the regular tissue culture substrate without damaging cells. First, we ensure conformal contact between the stencil and the cultivation substrate by adding a few drops of 70% ethanol on top of the culture substrate before laying down the stencil. Liquid helps remove wrinkles and folding of the stencil membrane, reducing the possibility of cell leakages (Figure 3-1B). We chose to use 70% ethanol to enable removal of liquid after stencil placement on top of the substrate and to create stable seal. To remove ethanol, we simply place the stencil-covered substrate in a vacuum chamber for approximately two hours, a duration that we found to give robust temporary bonding. Too long evaporation time resulted in delamination of the stencil off the substrate. Second, when pouring media or buffer onto the stencil, we observed that a thin film of air can be generated at the bottom of each stencil hole (Figure 3-1C). Because air is composed mainly of nitrogen that does not dissolve readily in water, this gaseous film or what we simply call 'bubbles' can remain up to many hours, preventing cells from touching and adhering to the substrate (Figure 3-1D). We found that smaller stencil holes often generate bubbles that completely cover the whole wells while large holes tend to form bubbles that only cover a partial area of the stencil hole. To prevent bubble formation, we always load any liquid onto the stencil surface in an environment that is filled with 100% carbon dioxide. Like pop soda, carbon dioxide bubbles will be able to quickly dissolve into the covering fluid (Folch, Jo et al. 2000). Finally, removing a stencil from the substrate may damage cells as seen by formation of necrotic blebs (Figure 3-1E). To maintain intact patterned cell patches, we limit the incubation time after loading the cells to prevent cell adhering to the stencil side wall. For A431 cells, 3-5 hours was found to be adequate in promoting cell attachment. Interestingly, we observed that A431 cells can attach more strongly to used stencils than to the freshly made device, even though we have tried multiple cleaning and rinsing methods. A quick pre-experimental

analysis to determine the appropriate incubation time before peeling the stencil off will ensure minimal damage for the different cell types.

Using these techniques, we can consistently create arrays of patterned cell patches for various adherent cell types on the standard 6-well tissue culture plates. To pattern A431 epidermoid carcinoma cells, we can load cell suspension directly onto stencil-covered substrate (Figure 3-2A). For patterning of human embryonic stem cells (hESCs), we need to first coat the substrate with Matrigel. By incubating the device with cold Matrigel overnight, we successfully pattern hESCs with precise cell arrangement. Cells were left for 12 hours before we peel off the stencil. Because of the high selectivity of hESCs to matrigel, we observe only minimal cell migration out of the original patterned areas even after 3 days (Figure 3-2B). A similar procedure can be performed to pattern mouse embryonic stem cells (mESCs), by pre-coating the substrate with gelatin (Figure 3-2C). For all cell types, we successfully create almost perfect cell arrays that span across the whole well area of the regular six-well plate (Figure 3-3A). Missing cell sites may occur from the defects in the stencil membrane or some patches may get removed during the stencil peel-off.

In addition to ensuring precise cell organization, we also developed a new packaging approach to enable high-throughput studies with stencil-defined cell arrays (Figure 3-3B). We first pattern cell arrays of different designs simultaneously on a single microscope slide. After patterning the cells on the slide, a well-separator module can be placed on top of the microscope slide to create isolated cultivating chambers for the different cell-patterning designs. The ProPlate microarray system (Grace BioLabs) provides modular well-separators with standard microtiter plate footprints. These modules are available in different

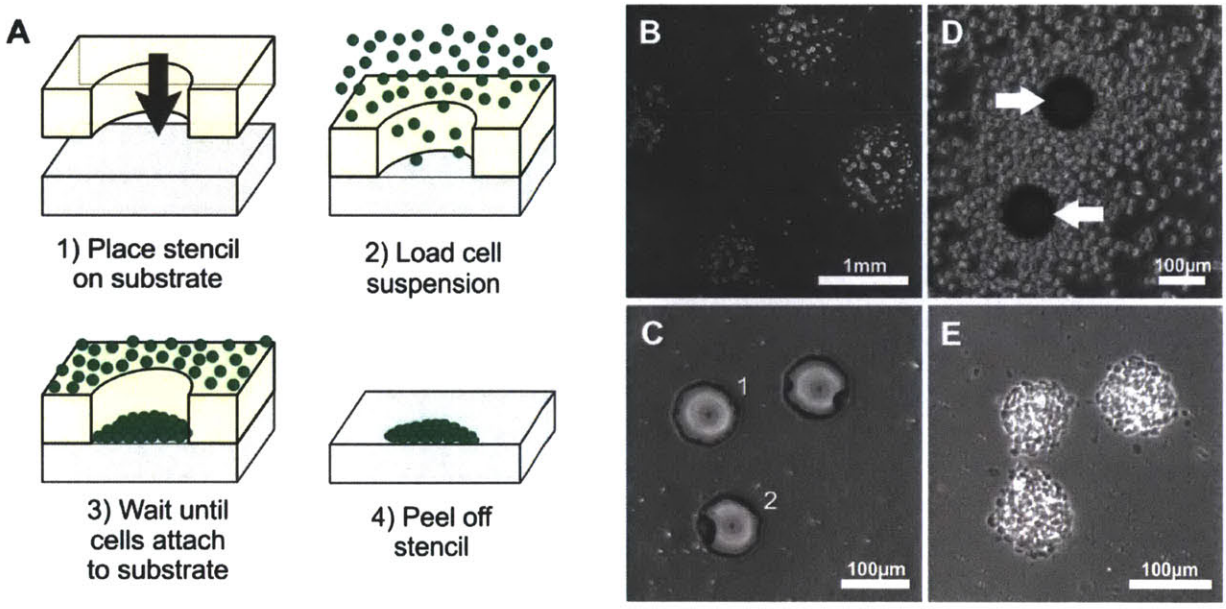

Figure 3-1 Stencil cell patterning and its common complications
A) Standard stencil cell patterning procedure. The stencil is first placed on the substrate to create the temporary microwell with opening to the substrate surface. Cell suspension is then loaded onto the stencil-covered substrate. Some cells will be able to land into the microwell and attach to the substrate. Stencil can then be peeled off, leaving behind the spatially defined cell constructs on the substrate. B) Cell leakage through areas underneath the stencil membrane, giving rise to inaccurate cell structure. C) Bubbles can cover the microwells completely (1) or partially (2). D) Cell crowding around bubbles. E) Cell damage after inappropriate stencil removal.

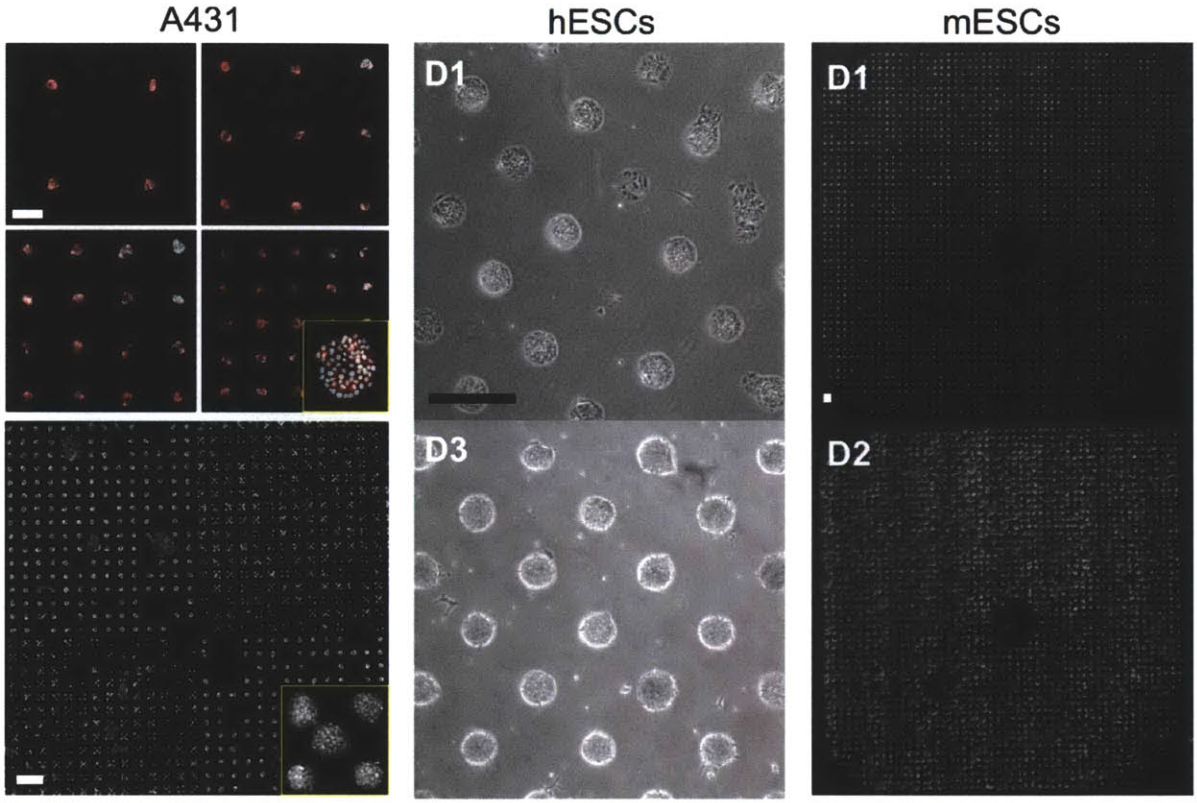

Figure 3-2 Stencil-defined cell arrays of different cell types
A) Patterned A431 cells of varying cell-arrangement designs. B) Arrays of patterned hESCs at one day and three days after stencil peeling off. C) Patterning of mESCs as square arrays across a 2-by-2-cm^2 substrate area. Scale bars, 500 μm.

designs, allowing cultivation of the patterned cells on different substrate areas. To apply the well-separator module onto the microscope slide with pre-patterned cell arrays, we carefully lay down the module on top of the slide that was initially submerged in cultivation medium. The silicone sealer at the bottom of each well-separator module prevents liquid leakage across the wells. After properly aligning the module onto the cell slide, both components are then lifted off the liquid. We then attach spring clips to the slide module, creating separate cultivation chambers for different cell arrays. The assembled slide module can be placed in the available tray set to create a standard microtiter plate that is compatible with high-throughput assaying instruments.

Regardless of its ability to establish precisely defined cell arrays across a large substrate area, stencil cell patterning cannot create cell constructs with complex shapes or multiple cell types. Because its operation relies on the flexibility of the stencil membrane to ensure conformal contact to the substrate, stencil patterning cannot be used with any designs that may cause deformation of the stencil membrane. To illustrate this point, we attempted to pattern parallel stripes of singly aligned cells with stencils (Figure 3-4A&B). Because of the non-rigid nature of the stencil, the adjacent stencil stripes did not remain properly sealed on the substrate but instead became twisted, curled or laid on top of one another. Structures with more balanced center of mass such as circles, squares and perfect triangles were observed to result in more accurate patterns. This constraint limits the use of stencils for creating only cell arrays of simple structures, most often with just one cell type.

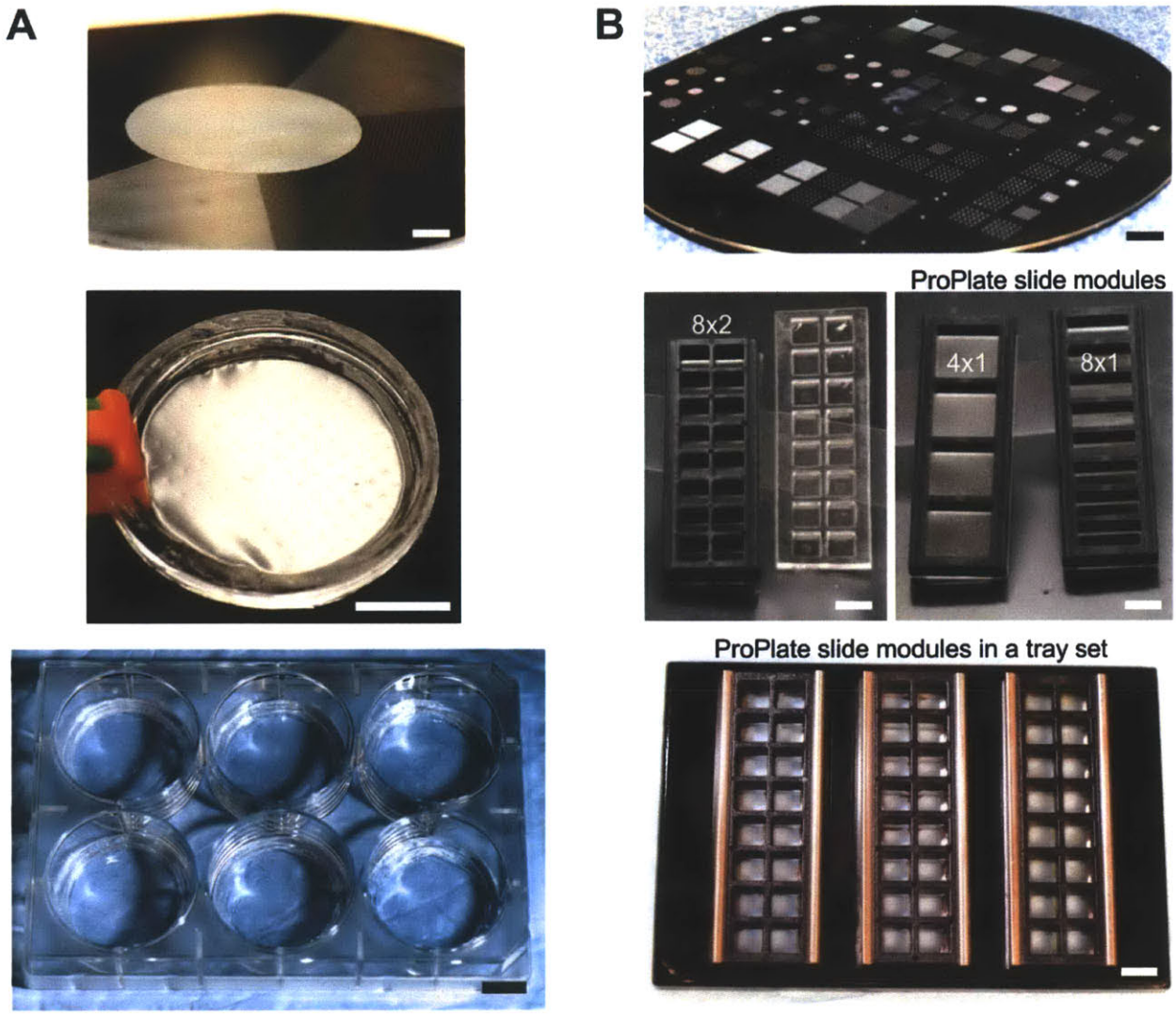

Figure 3-3 Different stencil designs for use with 6-well and 96-well plates
We have developed two formats of cell cultivation substrate for stencil patterning, by pre-designing the microposts on master wafers to support the different stencil shapes. A) Cell arrays can be organized in the standard 6-well plate to establish cell culture with more samples. Here, a round stencil is created to perfectly align within each well of the 6-well plate. B) For high-throughput biological studies, cells can be patterned first on regular microscope slides. The slide with multiple cell array designs can then be cultivated in separate chambers using the ProPlate slide module. The well-separator modules are available in different designs (1x4, 1x8 or 2x8) and can be assembled in a tray set for ease in handling and compatibility with high-throughput instruments. Scale bars, 1 cm.

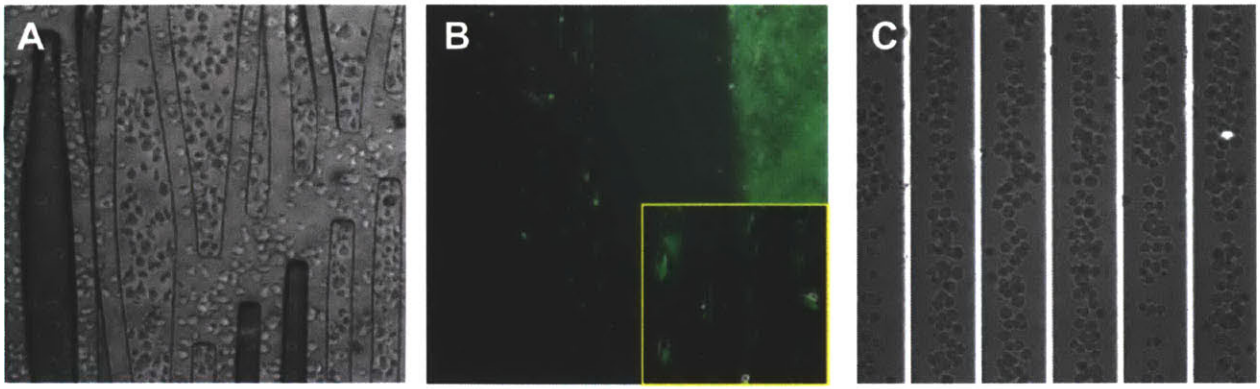

Figure 3-4 Patterning stripes with conventional stencil and DEP forcing
Stencil patterning can only organize simple cell structures. A) Improper alignment of stencils on the substrate. With long stencil stripes, the stencils either bend or lie on top of one another. B) The resulting organization of mouse embryonic fibroblasts from stencil stripes. C) Creation of cell stripes with conventional DEP forcing.

Construction of heterotypic cell patterns with s-DEP

DEP is an electrostatic force that can be generated when we place cells, as polarizable particles, in nonuniform electric fields. Depending on the cell's effective conductivity relative to the surrounding fluid and the frequency of the electric field, cells can be pushed away from (negative dielectrophoresis, n-DEP) or pulled into (positive dielectrophoresis, p-DEP) electrodes, allowing manipulation of cells into the desired patterns. Unlike stencil cell patterning, periodic structures like cell stripes can be more easily fabricated using DEP (Figure 3-4C). To pattern more complex, non-periodic cell shapes, an electroactive substrate with multi-layered electrodes is often necessary. For example, to pattern an array of isolated cell patches, a separate set of electrodes would be needed to levitate cells from touching the background surface (Mittal, Rosenthal et al. 2007). The complex fabrication of electroactive substrate prevents full integration of regular DEP in standard biological studies.

To take advantages of both stencil patterning and DEP, we have developed a novel class of cell patterning called stencil-delineated electroactive patterning (s-DEP) (Figure 3-5). S-DEP utilizes the thin flexible membrane like stencil patterning to prevent cells from touching unwanted area on the substrate. By simply replacing the standard tissue culture substrate with electroactive substrate, S-DEP enables the organization of complex cell structures within each stencil-defined area using n-DEP. We chose to use n-DEP because of its compatibility with standard tissue culture media for mammalian cell cultivation. By placing the stencil on top of the electroactive substrate, we achieved at least two improvements over regular DEP. First, the stencil membrane allows n-DEP to form an array of isolated cell patches of desirable shapes without requiring complex electrode designs. The stencil surface also acts as non-conductive surface that helps reduce the required current to operate s-DEP. In comparison to microcontact printing, s-DEP does not rely on the cell selectivity to specific ECMs, allowing complex cell patterning of any cell types, especially for cells that are genetically engineered but still originate from the same pool. Unlike stencil cell patterning that can pattern only one cell type, s-DEP can create complex cell structures with at least two cell types, and possibly the third one in the background region. In comparison to DEP alone, s-DEP can easily establish arrays of isolated cell patches with complex internal structures.

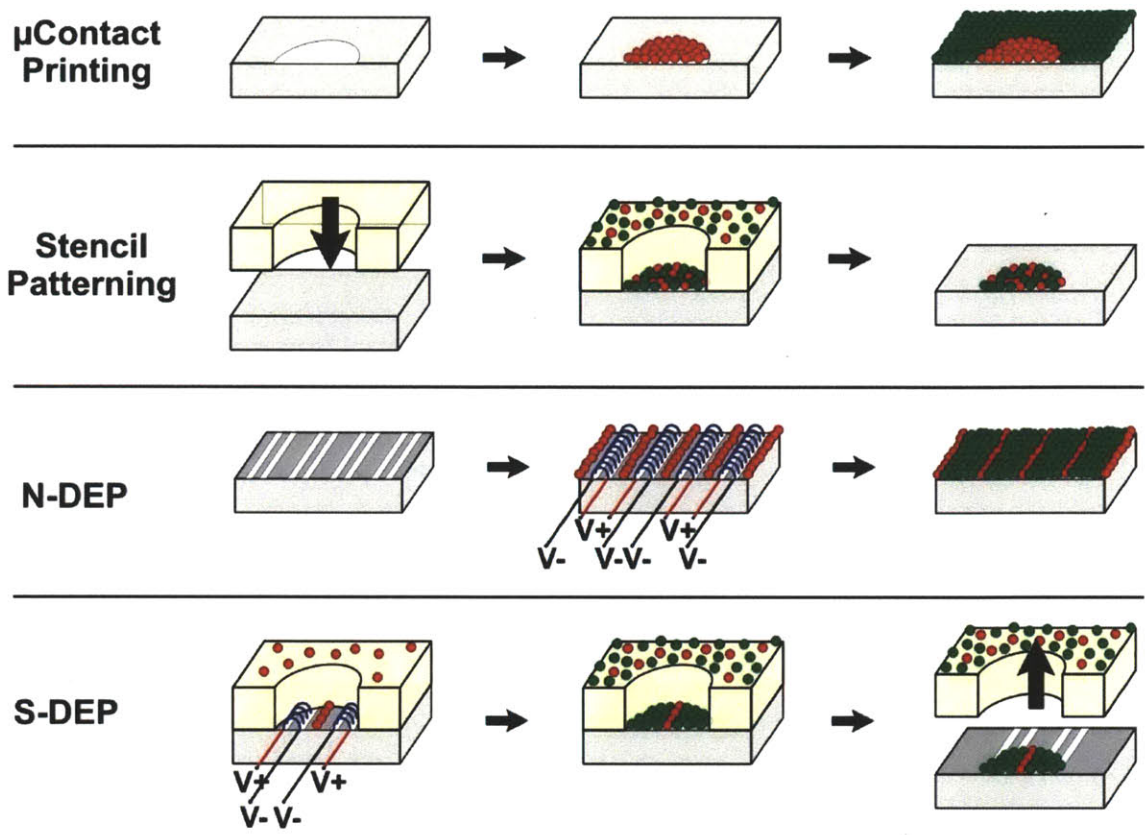

Figure 3-5 Comparison of s-DEP to existing cell-patterning technologies
Microcontact printing can create precisely defined cell structure but relies on cell selectivity to ECMs. This technique therefore cannot be used with cell populations that obtain the same ECM selectivity profile. Stencil patterning allows easy fabrication of cell arrays but can only create simple cell structure of the same cell type. N-DEP can create complex cell structure but cannot generate cell arrays with simple electrode design. S-DEP improves upon the existing technologies, allowing fabrication of cell arrays with complex internal structures while still using technologies that are not overly sophisticated for biology community.

Figure 3-6 illustrates our implementation of s-DEP that we designed to create arrays of cell patches with internal single-cell-width stripes. Our electroactive substrate requires only one layer of interdigitated aluminum electrodes. The s-DEP chip contains 2 sets of 10 main electrodes that span to cover the area of 5×5 cm^2 (Figure 3-6A). The large substrate area implies a significant current necessary to drive the electrodes, even with stencil shielding. Thus, we employ time-multiplexing of the DEP forcing to further reduce the current requirement to run s-DEP. Specifically, we supply the output signal to each consecutive pair of the electrodes using a switching module (Figure 3-6B&C). This electrical unit helps us cycle the input signal through all of these electrode pairs consecutively, reducing the required current that might have been needed to supply the whole substrate all at once. The implemented switching module takes input signal from the standard function generator. The signal cycling speed is controlled by an adjustable knob. With these two input parameters, the switching module can feed out output signals to generate DEP forcing across the whole s-DEP chip. A portable unit has also been implemented to enable easy cell patterning with s-DEP for standard biological studies (Figure 3-6D).

To pattern cells with s-DEP, we first place the stencil on top of the electroactive substrate, again adding a few drops of 70% ethanol to promote its conformal contact with the s-DEP chip. After vacuuming the stencil-covered substrate, we then load the stencil with PBS in the carbon dioxide-filled chamber to prevent bubble formation. At this point, the device is ready to pattern the first cell population (Figure 3-7A). To ensure proper cell alignment, we turn the function generator ON while loading the cell suspension into the device. We successfully create n-DEP forcing to move cells using an input sinusoidal waveform at 750±100 kHz, 8 $V_{peak\text{-}peak}$. Our switching module cycles the output signals through 8 pairs of electrodes at 0.2-2 Hz. As the cells fall down to the bottom of the well due to gravity, the generated n-DEP force aligns cells into stripes within each opening hole of the stencil. After letting cells settle with the DEP forcing turned ON for approximately 1 hour, we then turn the function generator OFF. Depending on

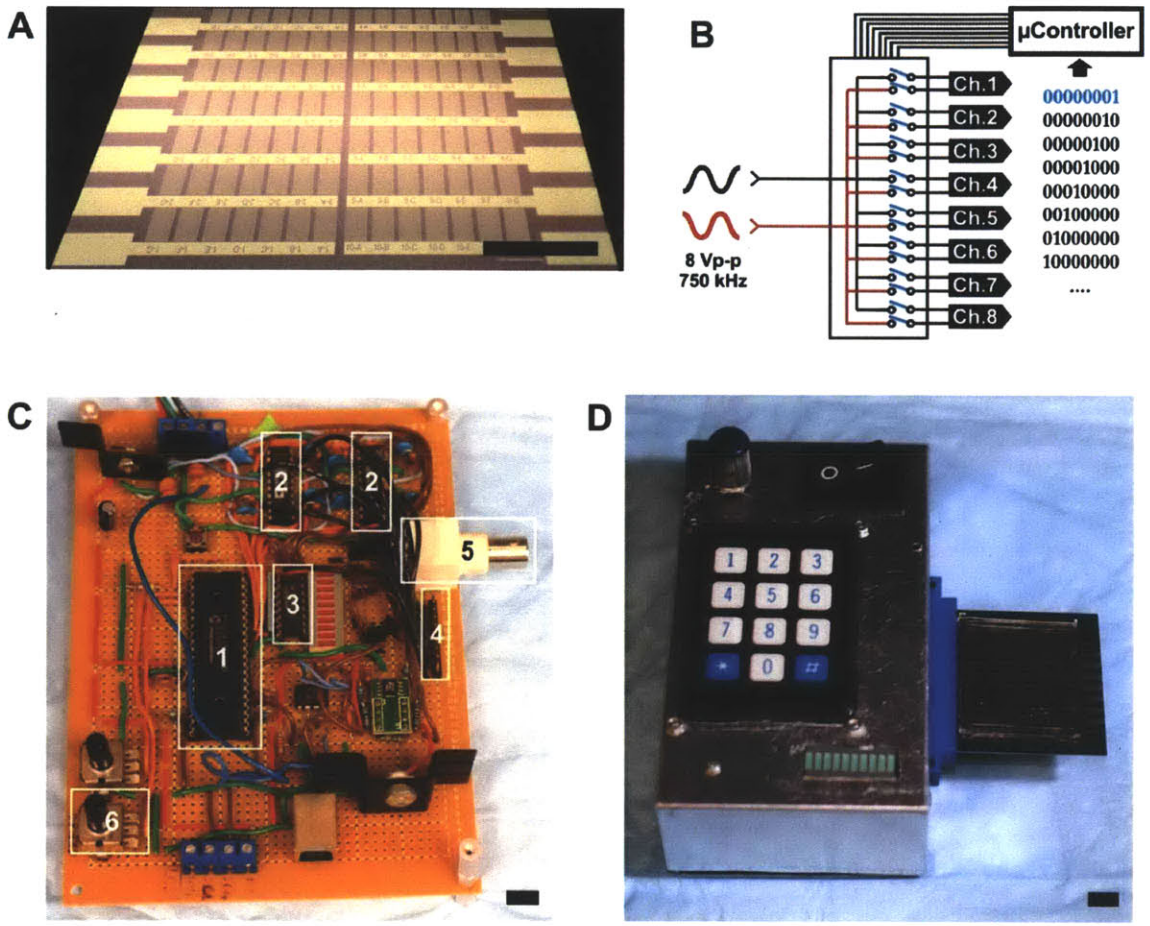

Figure 3-6 Implementation of s-DEP cell-patterning device
A) S-DEP chip are composed of 9 pairs of interdigitated electrodes and each pair only spans to cover a partial section of the whole electroactive substrate. B) Operational design of the input-signal switching module. This unit helps cycle the input signal through all electrode pairs across the substrate area. C) The first prototype of the switching module. The major electrical components include: 1) a microcontroller (PIC16F877A) to regulate the order and the cycling speed of output signals, 2) CMOS analog switches (ADG1434), 3) A\analog-to-digital converter (UNL2803A), 4) output signal pins, 5) input-signal connector and 6) an adjustment knob to control the output-signal cycling rate. D) Packaged s-DEP controller when fully assembled with stencil and s-DEP chip. Scale bars, 1 cm.

the strength of cell attachment during this initial stage, we may decide to wait a little longer to ensure proper attachment of the first cell population. We then load the second cell type into the device. After waiting until both cell types attach to the substrate, we then remove stencil from the substrate, leaving behind arrays of cell patches with internally labeled stripes across the whole substrate area (Figure 3-7B). While the generated cell constructs acquire cell stripes that slightly disperse from the original single-cell-wide stripe design, our experiment shows that s-DEP should be able to easily create cell constructs with less stringent design rule. The result also substantiates the ability of s-DEP to form cell arrays with complex internal organization using technologies that are not too overly sophisticated or inaccessible for biology community.

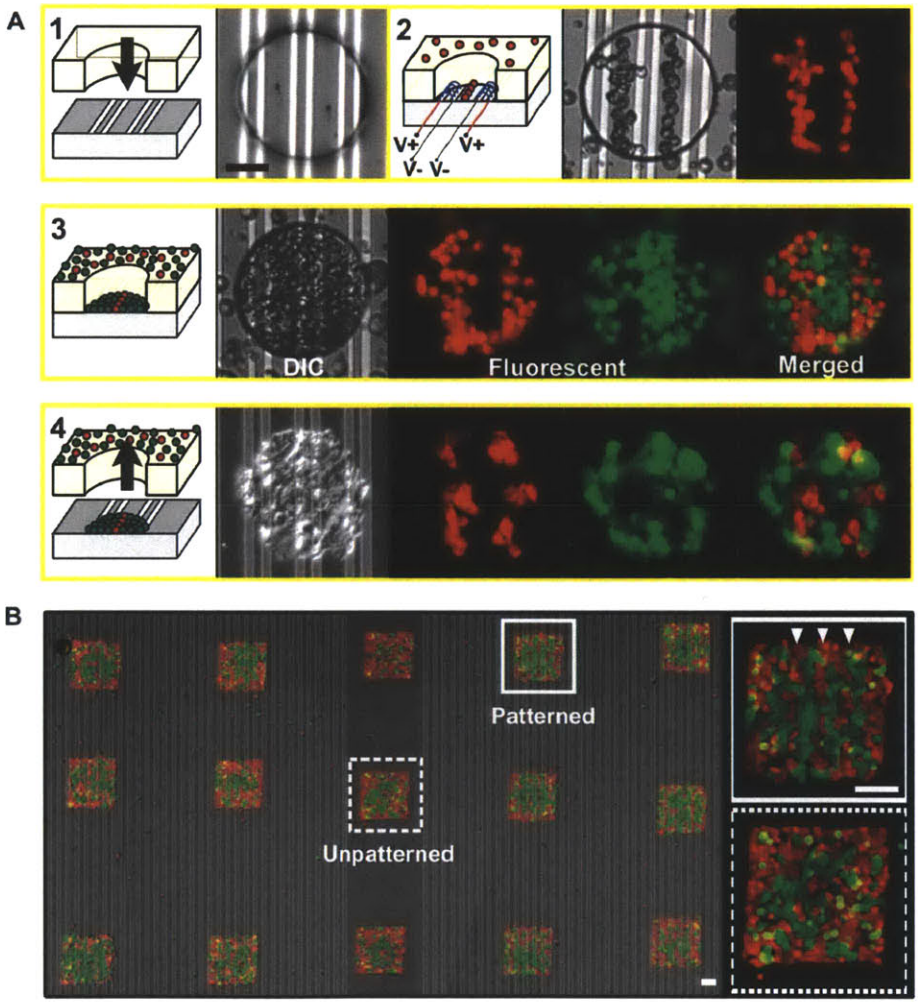

Figure 3-7 S-DEP Patterning

A) S-DEP Patterning Procedure, illustrated with A431 cells. 1) A PDMS stencil membrane is first placed over an electroactive substrate, similar to our standard stencil patterning. 2) After removing bubbles from the stencil-defined microwells, the first cell population is then seeded into the device with the electrodes turned ON to establish cell alignment. 3) After attachment of the first cell type, we can turn the electrodes OFF and load the second cell type. 4) When both cell populations attach well to the substrate, the stencil can be peeled off, leaving behind cell constructs with internally patterned stripes. Scale bar, 50 μm. B) S-DEP enables parallelized complex cell construct formation on a shared substrate. The insets show closer views of example cell constructs with and without stripes (white arrows). Scale bar, 100 μm.

Cell adhesion and motility on S-DEP chip

Because our electroactive substrate is covered partially with aluminum, we were interested in determining how well the cells would be able to attach or move on the substrate, especially at the interface of aluminum electrode and the silicon dioxide background. AFM imaging illustrated that the coated aluminum electrode creates the vertical indentation of approximately 175 nanometers (Figure 3-8). It is thus probable that cells that attach to our s-DEP chip will exhibit some biased motion, as cells are known to be able to respond to nanometer topography (Lim and Donahue 2007). To experimentally characterize these properties and potentially identify methods to promote uniform cell attachment, we first investigated attachment of A431 cells on our S-DEP chip with gelatin coating and/or oxygen-plasma treatment. Gelatin, or denatured collagen, acquires amino acid motifs that can promote cell adhesion with integrin binding. Oxygen-plasma treatment has shown to promote hydrophilicity of many materials (Bodas and Khan-Malek 2006). Based on these hypotheses, we determined changes in cell area of the A431 cells after being cultivated on the substrate with different substrate treatment. We found that adsorption of gelatin can significantly improve cell attachment, as shown by the two-fold increase in cell area (Figure 3-9A&B). Other substrate treatment, even with both gelatin coating and oxygen-plasma treatment, were found to exhibit no distinct change in cell attachment. In addition to cell attachment, we also investigated changes of cell motility on our electroactive substrate. Using two populations of 3T3 cells that were genetically engineered to constitutively express red and green fluorescent proteins respectively, we are able to track cell motion of the minority cell population. Specifically, we mixed red and green cell populations at the 1-to-20 ratio and recorded changes of cell motion on the electroactive substrate with and without gelatin coating for 12 hours (Figure 3-9C&D). Without gelatin coating, we found that fibroblast cells prefer to move along the electrode axis. With gelatin coating, the cells can move more uniformly across the substrate. While cell adhesion and motility are properties that are often cell-specific, both experiments show that we should be able to maintain natural cell attachment and motion while cultivating cells on the non-physiological substrate like our S-DEP chip by pre-coating the substrate with appropriate ECMs.

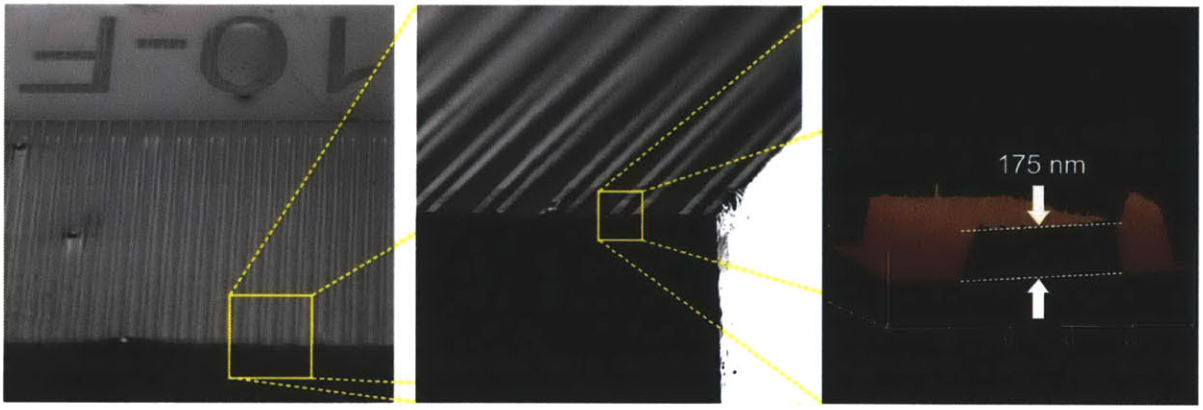

Figure 3-8 Topography of the s-DEP chip
Microscopic view of s-DEP chip surface as imaged by SEM and AFM. Deposition of the electrode layer creates vertical indentation of the electrode in reference with the background substrate surface.

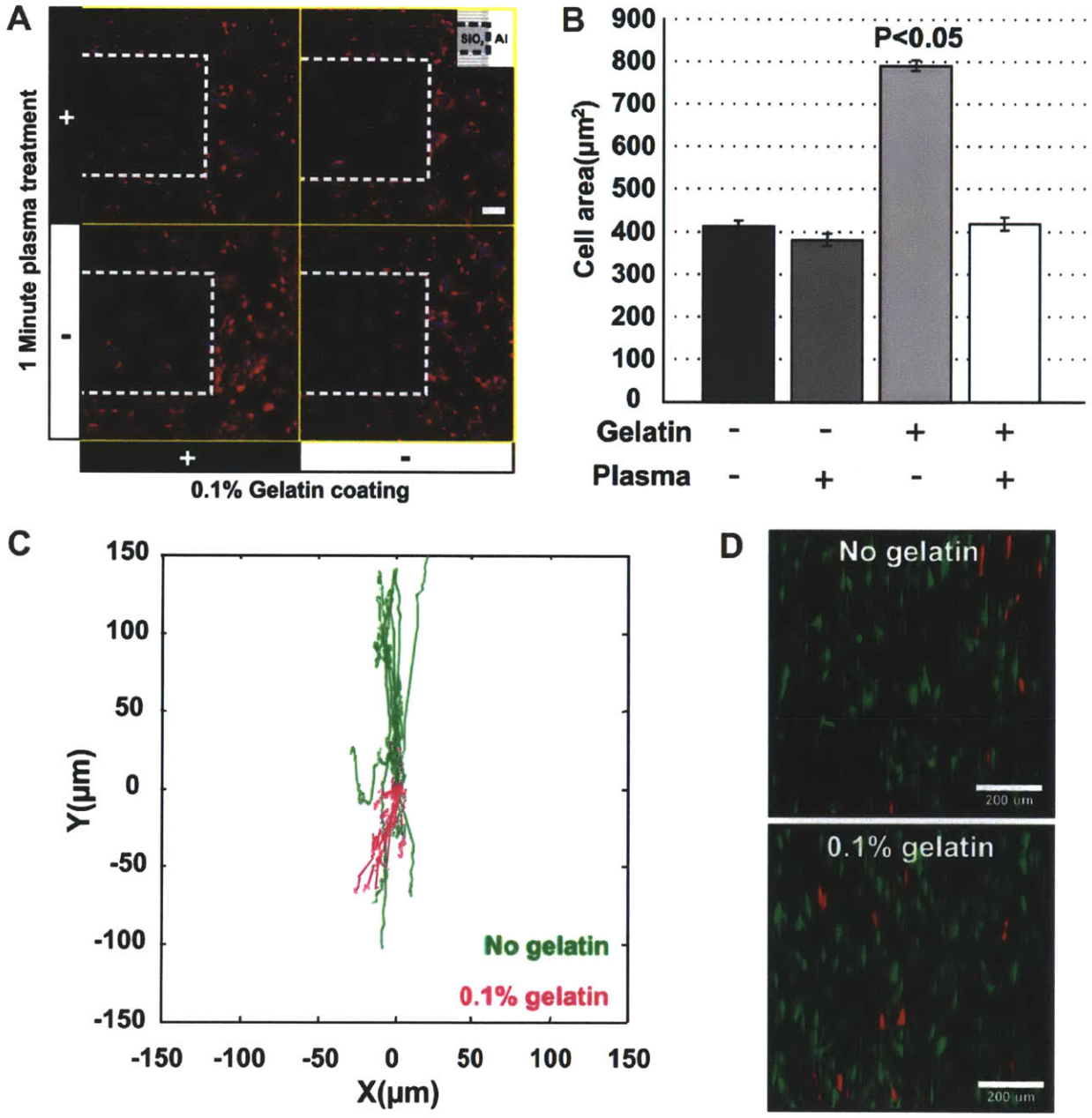

Figure 3-9 Attachment and motion of A431 cells on the s-DEP chip

A) Attachment of A431 cells on the s-DEP chip that is treated with oxygen plasma and/or coated with 0.1% gelatin. Scale bar, 100 μm. B) The calculated area per cell for the different substrate-coating conditions. C-D) Motion of fibroblast cells on the s-DEP chip with and without gelatin coating. We assess cell motility by tracking motion of red-labeled cells, the minority cell population, during our 12-hour time-lapse study. Red and green cells were mixed at 1-to-20 ratio to ensure that all red cells will be spatially isolated from one another.

Investigation of cell motion within cell monolayer using S-DEP

Monitoring cell movement and proliferation within TLCs is key to uncovering the impact of tissue organization in governing cell-decision processes. One important question is to understand whether cell motility plays a role on the commonly observed biased cell proliferation within a clustered cell patch. Contact-dependent growth inhibition is one such phenomenon that can be clearly seen by the preferred cell growth at the edge of physically touching cell cluster (St Croix, Sheehan et al. 1998; Perrais, Chen et al. 2007; Kim, Kushiro et al. 2009). One alternative explanation is that cells which are primed to divide may prefer to move to the edge of cell cluster. Because of such biased motion, we might observe more cell division at the edge instead of at the center of each cell cluster. To test this hypothesis, we used the s-DEP-defined cell stripes to determine whether there is any preferred direction of A431 motion within the patterned cell constructs. Figure 3-10 illustrates the observed change of cell stripes after two days. Cells were labeled using standard live stains (DiI and DiO). The image demonstrates cell motion at different location across each cell patch. Because of the splitting of the stains after cell division, we were unable to track motion of all cells. Nonetheless, we can still observe mixing of both red and green subpopulations and dispersion of the initial striations at all locations across each cell patch. While our result is preliminary and requires cells with permanent reporter protein to enable cell tracking, the result suggests that the commonly observed biased cell growth at the edge of cell cluster should not be caused by directed cell motion. Instead, growth inhibition of cells at the center should occur mainly from growth inhibition due to the alteration of signaling cues at different location of cell patch, for example the effects of contact-mediated growth inhibition (Kim, Kushiro et al. 2009).

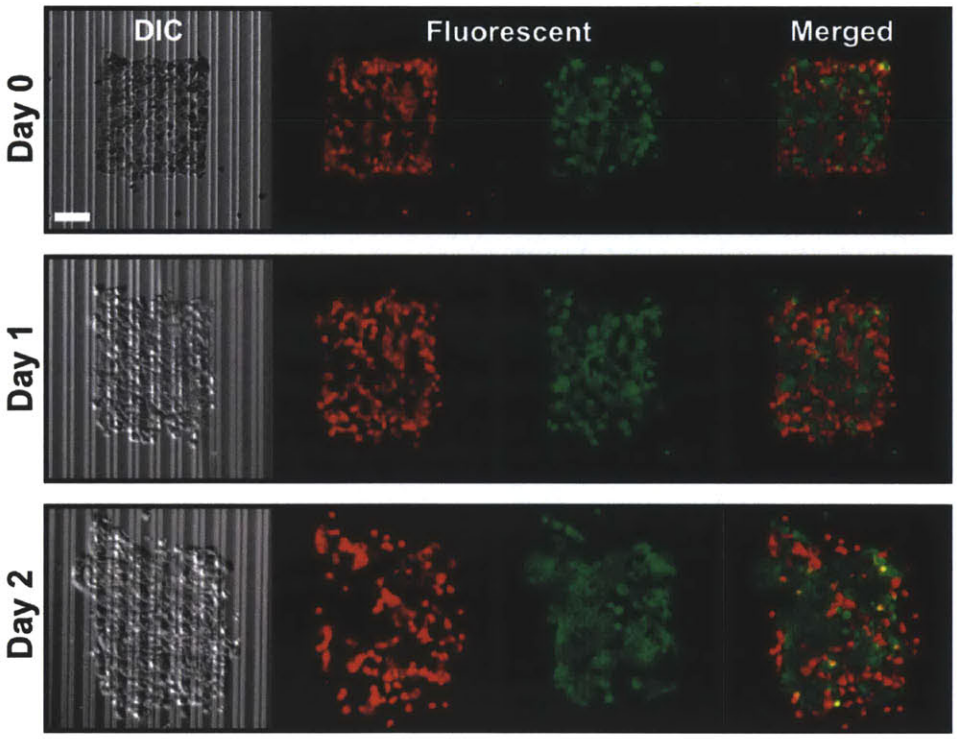

Figure 3-10 Time-lapsed study of striated cell patches
We used s-DEP to create square cell constructs with stripes to study internal motion of A431 cells within cell monolayer. Cells were monitored upto 2 days. The red-colored cell stripes create a conformal map that can be used to interpolate the motion of adjacent cell population. Scale bar, 100 μm

3.3 Discussion

We presented here techniques to create arrays of cell constructs on a large substrate area, also with the option of having complex internal structure. The proposed packaging technique of stencil-defined cell arrays allows the standard stencil cell patterning method to be applied with standard biological assays where multiple test conditions are often needed. Our establishment of s-DEP, taking advantage of both stencil cell patterning and n-DEP, enables the fabrication of complex TLCs on a large substrate area. While we only showed the creation of striated cell constructs, the proposed method can be adapted to create other complex cell structures by changing the electrode design and the shape of the stencil hole. We finally illustrated the use of the striated cell constructs to study cell motion of A431 cells within cell monolayer. The organized cell stripes enable us to interpolate motion of unlabeled cells across the whole cell construct. The observed dispersion of labeled cell stripes at all locations inside each cell patch implies homogenous random motion of cells across the whole cell patch.

While s-DEP has enabled fabrication of cell arrays with complex internal structures, it is important to realize that s-DEP also inherits a few drawbacks from both stencil patterning and regular n-DEP. The precision of cell constructs still relies critically on the establishment of leak-free temporary microwells. The topography of the electrodes on top of the substrate surface adds another source to initiate liquid leakage through the stencil hole. Like DEP, we found that accurate cell organization may only be achieved while we turn the electrodes ON. Without DEP forcing, piling of cells will eventually disperse into the unwanted area. Proper cell density within each stencil hole is therefore a critical factor in achieving precisely-defined s-DEP patterns. We also found that, like other cell-patterning methods, the accuracy of S-DEP depends on the adhesive nature of each cell type. For example, we found that it is very difficult to create cell stripes of embryonic stem cells because of their preference in forming cell clumps while we can easily create such stripes with A431 cells. The possible negative impact of DEP on cell health is another important issue that we cannot neglect when using s-DEP (Desai and Voldman 2011). To ensure minimal damages to the cells, we must maintain the supplied current and voltage across the electrodes to the minimum. Using the output-signaling cycling technique, it is possible to divide the substrate area into smaller sections that are supplied by separated electrode wiring to further reduce the electrical requirements. The use of more conductive metal for electrode fabrication can also help reduce the system load. We may also pre-coat the substrate with appropriate ECM to promote quicker cell attachment to the substrate and to reduce duration of cell exposure to electric fields. Finally, s-DEP requires the use of electroactive substrate that is mostly fabricated with opaque substrate like silicon, limiting our ability to visualize cells with inverted microscope. We attempted to fix this problem by creating the electrodes using indium-tin-oxide (ITO) which is a transparent, conductive chemical. Using the commercially available ITO-coated microscope slides and dry etching, we found that this ITO-based substrate obtains too low conductivity and therefore requires too high voltage to generate adequately powerful DEP forcing that can potentially damage cell health. With the development of advanced materials, it is possible to find a similar chemical to create transparent s-DEP substrate with similar conductivity to standard metal electrodes.

Beyond the study of cell growth and motility, s-DEP provides a platform for investigating cue-response relationship for different cellular phenotypes. To validate the role of contact-mediated cues and its impact in propagating signals across the cell monolayer, we can use s-DEP to spatially define a buffer cell region while we downregulate expression of the interested cell adhesion molecules. To determine the spatial propagation of paracrine signaling, we can also use s-DEP to localize cells that secret diffusive factors into the center of cell constructs and then surround it with the receiver cells. With the appropriate size of cell construct, we might be able to detect phenotypic changes of the receiver cells that correspond well with the spatial distribution of the secreted ligands. While we only illustrated the fabrication of two-dimensional cell structure with s-DEP, it might also be possible to adapt this technology to construct three-dimensional cell aggregates. Technologically, we need to coat the substrate with non-adhesive molecules to prevent cells from adhering to the substrate and develop a method to maintain the DEP-directed positions of the first cell population while loading the second cell type. Such precisely defined heterotypic

three-dimensional cell constructs will enable the study of body planning in vitro and allow the investigation of cell-positioning impact on the differentiation of embryonic stem cells in the embryoid body.

3.4 Summary

We successfully establish techniques to cultivate cells with precisely defined cell positioning. Using stencil cell patterning, we show that cell arrays of simple structures can be fabricated on the standard tissue culture substrates. We illustrate the use of stencil patterning with A431 epidermoid carcinoma cells, and with both human and mouse embryonic stem cells. With the modification of incubation time before peeling off stencils, this technique should be applicable for most adherent cell types. In addition to the simple stencil patterning, we also create a novel cell-patterning technique or s-DEP that can introduce complex internal cell organization within each stencil-defined patch. While our implementation of S-DEP requires the use of non-standard tissue culture substrate, the fabrication of single-layer electroactive substrate is not too complicated. Potentially, end users may be able to purchase such electroactive substrates with simple electrode designs as commercial products, just like standard microscope slides. Both cell-patterning techniques enable us to create a wide range of cell structures. We can use these technologies to establish cell culture with flexible cell arrangement for studying impacts of autocrine signaling on cancer growth.

3.5 Materials and methods

Stencil fabrication

Stencil membrane is molded from a master wafer that is composed on micron-sized posts that match the patterning design (Figure 3-11). The master wafer was fabricated using standard photolithography. Specifically, we first dehydrated the wafer at 200°C for 30 minutes to promote strong attachment of photoresist. SU-8 2050 photoresist (Microchem) was then poured onto the wafer. The required volume of SU-8 is 1-2 mL per each inch of the wafer diameter. We then spin the wafer at 500 rpm/s for 10-15 seconds and then ramp and hole at 1650 rpm for 30 s to yield the resist thickness of 100 μm. We prebake the wafer at 65°C for 4 minutes, immediately switch to 95°C and bake for another 20 minutes. After prebaking process, we exposed the wafer to a UV doze of 10 mW/cm^2/sec for 24 seconds (total exposure energy of 240 mJ/cm^2). The finished master wafer is shown in A. We then perform a post exposure bake (PEB) by first warming the wafer at 65°C for 3 minutes, heating at 95°C for 9 minutes and finally ramping down to 65°C. After PEB, we then develop the wafer by submerging in 1-methoxy-2-propanol acetate for 10-15 minutes. The wafer was rinsed with isopropanol and immediately air-dried using compressed air. To prevent adhesion of master wafer to the silicone later on, we silanized the wafer with vaporized (tridecafluoro-1,2,2-tetrahydrooctyl)-1-trichlorosilane in a vacuum desiccator for at least 3 hours.

After silanization, stencils can be fabricated by applying uniform pressure across the silicone-covered master wafer. We use Polydimethylsiloxane (PDMS) as our molding silicone. The base monomers and the curing agent are mixed at 10:1 ratio by weight. After degassing the mixture, we carefully pour the silicone to the center of the wafer, tilted and rotated the wafer to spread PDMS across the whole area. A transparency film is then placed on top of PDMS, starting from the wafer edge, to prevent sticking of the cured PDMS to the metal plate. We then clamped the wafer between a stack of metal plates, rubber sheath and glass slides on a hot plate as shown in B. After heating at 65°C for 2 hours, the PDMS silicone is cured. Since the PDMS membrane is very thin and deformable, we also attach an annular ring made of PDMS on top of the silicone membrane. To attach the annular ring, we simply paint uncured PDMS to the bottom of the annular ring, place it on the membrane and reheat the device at 65°C for 1 hour. We then cut around the annular ring and carefully removing stencil off the master wafer.

Stencil Patterning procedures

To use stencils for cell patterning, we first clean the leftover curing agent in stencils. We rinse the stencils in series of solvents: acetone, isopropanol, and 80% ethanol and finally in water for 12 hours

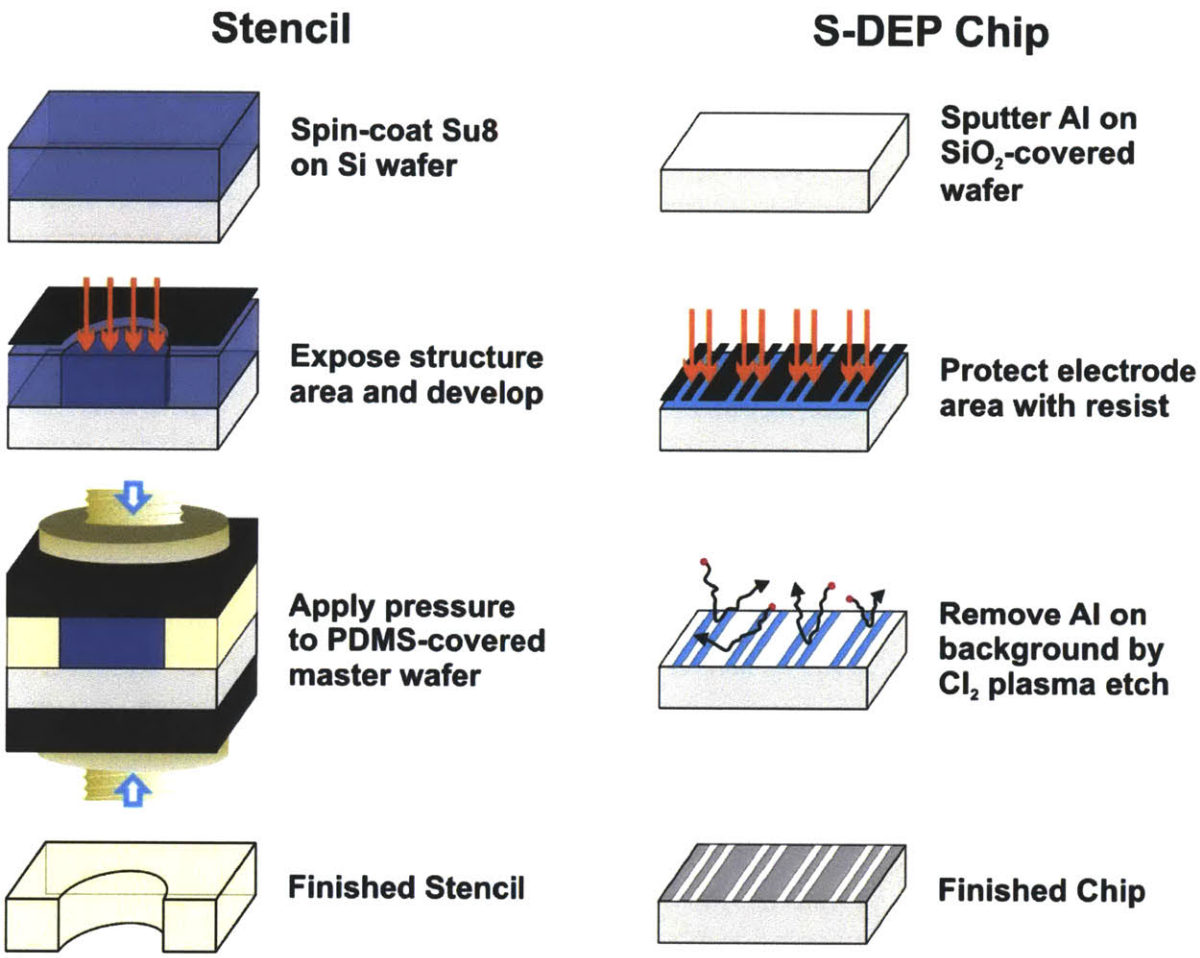

Figure 3-11 Fabrication of stencil and S-DEP chip
Stencil is casted from a master wafer that was microfabricated using standard photoliphographic technique. We use SU8 photoresist to create the microposts on the silicon substrate. We use Polydimethylsiloxane (PDMS) to create the stencil membrane. To fabricate the s-DEP chip, we coat a thin layer of aluminum on top of silicon dioxide-covered silicon substrate. Positive photoresist is used to establish electrode design and prevent aluminum etching by chlorine plasma. After etching, we obtain aluminum electrodes with the pre-defined geometry.

during each step. We then air-dried the stencil and autoclaved it for sterility. To use the stencil for cell patterning, the stencil is first placed onto the substrate that was added with a few drops of ethanol to ensure conformal contact. We then put the attached components in a vacuum desiccator to vaporize ethanol for approximately 2 hours. To ensure sterility, we expose the device under UV for 15 minutes. To load liquid onto the stencil in CO_2-filled chamber to prevent formation of bubbles within each stencil hole. To load cells into the device, we first removed most solution in the device but leave enough liquid to prevent reformation of bubbles. We then load cell suspension into the device. Within the first 5-10 minutes, we left the device untouched, allowing cells to sink to substrate surface. After waiting long enough to ensure adequate cell attachment to the substrate (between 3-5 hours for A431 cells), we rinsed the device with PBS a few times before removing the stencil. Cultivating medium is added to the area surrounding the stencil to reduce cell damage during stencil removal. A final rinse is done using cell cultivation medium.

Electroactive substrate fabrication

We fabricate our electroactive substrate by depositing aluminum onto SiO_2-covered silicon substrate and etch aluminum off to match our electrode design (Figure 3-11). Specifically, we first clean the silicon wafer and thermally grow 1.5μm-thick oxide layer on top of its surface. After cleaning the processed wafer with piranha, aluminum is then deposited on top of the wafer by sputtering to achieve 0.5 μm-think aluminum blanket surface. A 1 μm-thick positive resist is coated on top of the wafer by spin-coating. We then develop the photoresist while having the mask of our electrode design laid on top of the wafer. After removing the uncured photoresist, we then specifically remove the aluminum film that is not covered by photoresist using chlorine plasma etching. A thick layer of positive resist is then coated on top of the wafer as protective layer. The wafer is then diced using die saw. Right below the experiment, the protective layer of positive resist is easily removed by quickly rinsing in acetone.

Designing S-DEP electrodes

To design s-DEP electrode geometry, we use our in-house mathematical model to help determine efficacy of our initial intuitively-selected electrode shape. By further refining the electrode geometry that can give the most correct cell alignment in our simulation, we can achieve the electrode design that can successfully pattern cells with s-DEP (Figure 3-12). To create the simulation of cell movement, we first model the formulated electric field in three dimensions using finite-element modeling (COMSOL). Based on the generated electric field, we then calculate dielectrophoretic forcing and gravity on each cell based on the initial cell positions that were randomly placed inside the modeling space. The positions and forces on each cell are then updated at every time step until a defined time point is reached.

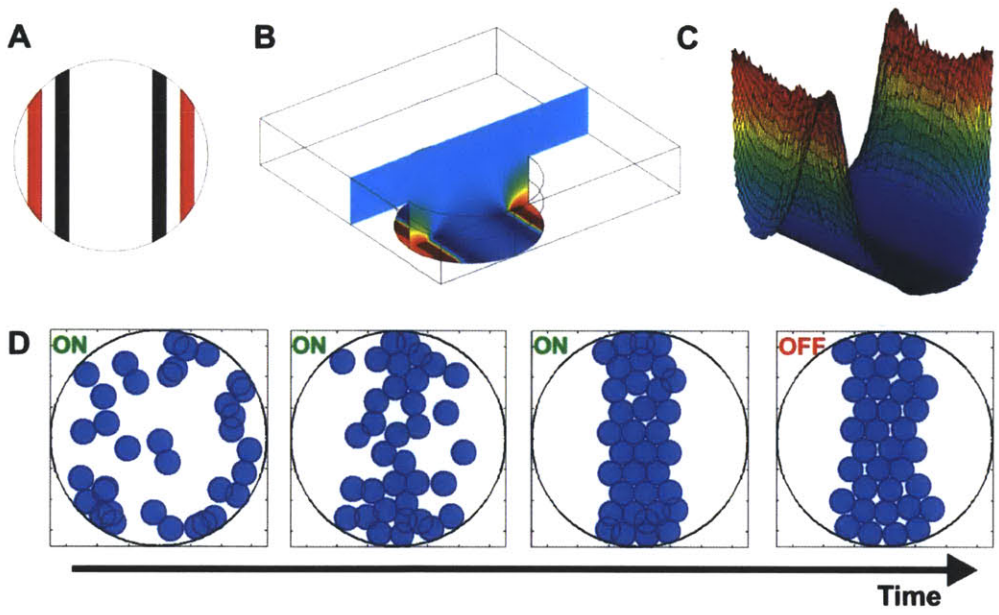

Figure 3-12 Simulation of cell positioning for different electrode designs
A) Electrode design for creating a slap of cell structure within the circular cell constructs. B) Simulated potential field in the s-DEP well. C) Energy field ($|\text{electric field}|^2$) associated with the input electrode design. D) Our particle simulation predicts cell motion with respect to the modeled electric field. DEP force was calculated as a function of relation cell position within the s-DEP well.

Chapter 4

Mathematical modeling of autocrine ligand binding with varying cell arrangement

We have discussed previously unique characteristics of cells that acquire autocrine loops and explored cell-patterning techniques that can help introduce spatial regularity to the standard cell culture *in vitro*. We will explore in this chapter how changes of cell arrangement can affect ligand/receptor binding in autocrine systems. In addition to getting captured by the originally secreting cells, autocrine ligands that propagate further in the supernatant can also be captured by adjacent neighbors. Throughout this chapter, we define *autocrine* trajectories as the diffusion paths of ligands that land on the originally secreting cells. Ligands that can diffuse broader and ultimately get captured by the non-secreting cells are defined here as having *paracrine* trajectories. It is important to note how both definitions are defined here in inference with location of the individual cell in the cell culture, in comparison to the less stringent definition that are termed based on the types of secreting and receiving cells. A stochastic model is developed here to help predicts changes of ligand capture with altering cell arrangement. To explore the impacts of cell arrangement, we use the developed model to distinguish changes in ligand binding, both at the *global* and *local* length scales. Continuum models are also developed to gain quantitative insights on the effect of cell arrangement. The continuum models discussed in this chapter was a collaborative work with Michael Vahey.

4.1 Introduction

Autocrine signaling is a complex biological process that we have gained past insights from the availability of mathematical modeling. Unlike other modes of chemical signaling that we can evaluate their roles on phenotypic regulation from the standard dose-response study, cells with autocrine loops acquire an intrinsic ligand supply that can misinform the relationship between phenotypic changes due to exogenous ligand supply. To verify the presence of a specific autocrine loop, detection of the underlying autocrine ligand in the supernatant is also challenging and, in many cases, requires full inhibition of ligand/receptor binding (Dempsey and Coffey 1994). With mathematical simulations, previous investigators were able to identify transport parameters that govern the intrinsic properties of autocrine loops, namely the relative production of ligands and receptors (DeWitt, Dong et al. 2001), the ligand/receptor affinity (DeWitt, Iida et al. 2002), and ligand diffusivity (Shvartsman, Wiley et al. 2001). High ligand/receptor production ratios, low ligand/receptor binding or high ligand diffusivity was shown to underlie the broader spatial propagation of autocrine ligands in space.

A unique characteristic of most natural autocrine systems is the variation of cellular phenotypes with the alteration of cell plating densities during *in vitro* cultivation. This property originates from the ability of autocrine systems to respond to their self-secreted ligands. Regardless of its prevalence, such density-dependent phenotypic change has not been accurately described by existing mathematical models of autocrine signaling. The random positioning of cells in the conventional cell culture creates heterogeneous boundary conditions of cell surface that prevents our ability to obtain the analytical solutions of ligand accumulation in the supernatant. Without any simplification of the cell-surface boundary conditions, such system must be solved with numerical methods that not only requires bulky computational resources but also cannot explicitly illustrate relative importance of different transport/kinetic parameters. To obtain the analytical solutions of ligand transport in autocrine systems, most existing models often assume the cell-surface boundary condition with a single spatially-isolated cell (Lauffenburger and Cozens 1989; Forsten and Lauffenburger 1994; Oehrtman, Wiley et al. 1998; Shvartsman, Wiley et al. 2001). To describe the effects of varying cell plating densities, these models simply modulate the liquid volume per cell, a parameter that still does not take into account the possible diffusive exchange of ligand molecules between adjacently positioned cells. In order to examine the

complete and accurate impacts of cell arrangement on ligand/receptor interactions, we require a mathematical model that can analyze changes of ligand binding for a variety of cell-positioning configurations.

Recently developed stochastic models of autocrine systems have enabled the examination of ligand binding in autocrine systems for various families of input cell arrangement (Batsilas, Berezhkovskii et al. 2003; Berezhkovskii, Batsilas et al. 2004; Berezhkovskii, Makhnovskii et al. 2004). Unlike most existing continuum models of autocrine systems that describe the averaged ligand distribution using the diffusion equation, these stochastic models monitor random walks of all secreted ligands. By empirically describing the numerical simulation of ligand paths, the experimenters establish simple relationship between ligand capturing for different input cell surface geometry. Depending on the survival time of each ligand in the surrounding fluid, some ligands may get captured by the originally secreting cell (ligands with *autocrine trajectories*) while others that propagate more broadly may instead land on neighboring cells (ligands with *paracrine trajectories*). Due to the spatially-varying nature of paracrine trajectories (Batsilas, Berezhkovskii et al. 2003) and the variation of intrinsic parameters among different autocrine loops, we hypothesize that cell arrangement can critically influence ligand capturing in autocrine systems at diverse length scales. The global cell density across the whole substrate would define the baseline ligand concentration while local cell density may exhibit a more critical role in spatially localized autocrine systems. With the availability of the stochastic model to study changes of ligand binding with various classes of cell-positioning geometry, it would be useful to determine the relationship between local and global cell densities and how they interact with intrinsic properties of autocrine loops. When will the global cell density dominate the effect of local cell density? Is there a specific cell arrangement that can amplify impacts of the local cell density in regulating cellular phenotypes that can potentially cause cell-to-cell variability in the initially uniform cell population?

We present in this chapter an analysis of how cell arrangement plays a role on ligand capture in autocrine system, both at the local and global length scales, and also exhibit its interactions with major intrinsic properties of autocrine loops. Following the approach by Monine *et al.* (Monine, Berezhkovskii et al. 2005) to determine ligand accumulation and complex formation, we take advantage of the symmetry of square-latticed arrays of circular patches to explore the impacts of cell arrangement at different length scales. Effects of global cell density are investigated by altering the array spacing for a fixed patch radius. Impacts of local cell density on the other hand are compared by changing the patch radii for a fixed global cell density. Our analysis identified two extreme modes of the intercellular communication in autocrine systems: the *communicative* and the *isolated* modes. The unique characteristics of each spatial regime were validated by simplified continuum models. Having characterized the interplay between local and global cell densities, we then examined the synergy between cell arrangement and the intrinsic properties of autocrine loops in governing the significance of autocrine signaling in regulating cellular phenotypes. Our study provides a preliminary simulation platform for determining the appropriate cell arrangement for the experimental characterization of autocrine loops with cell patterning methods.

4.2 Theory

Our analysis aims at developing a mathematical model that can distinguish local versus global impacts of cell arrangement on ligand binding in autocrine systems. After exploring different cell arrangement structures, we identified multiple unique characteristics when positioning cells as square-latticed arrays of circular patches. Because of its simple symmetry, the cell-covered area fraction (σ) is found to be proportional to the square ratio of the patch radius (r_{patch}) and the centroid-to-centroid patch spacing ($R_{c\text{-}c}$):

$$\sigma = \frac{\pi r_{patch}^2}{R_{c-c}^{\ 2}}. \qquad [4\text{-}1]$$

To investigate the local impact of cell arrangement, we can determine changes of ligand capture for different patch radii of the same σ. As long as we maintain the same cultivation area, we can ensure the

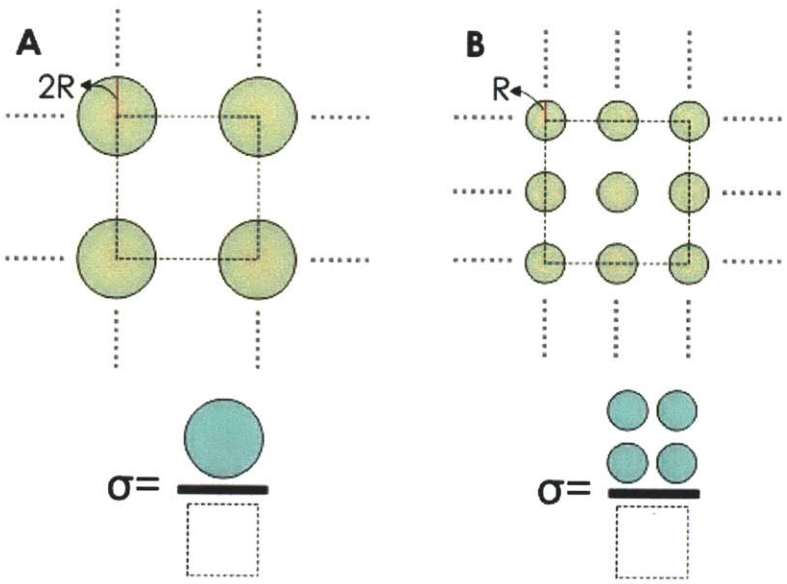

Figure 4-1 Examining impacts of cell arrangement with cell arrays
To isolate the global and local impacts of cell arrangement in autocrine systems, we investigate the changes of ligand capturing for the systems of square-latticed arrays of circular patches with varying patch radii and array spacing. Because of the symmetry of this design, we can modulate the patch radius while maintaining the same initial area fraction covered by cells (σ). (A) Cell patches in this design have the radius of $2R$ and σ of $1\times4\pi R^2$/square area. (B) By maintaining the same $r_{patch}/R_{c\text{-}c}$ ratio, the array with patch radius of $1R$ can be designed to acquire the same σ. If we cultivate cells with both designs on the same cultivation area, the concentration of accumulated ligands in the covering medium should be equal without any ligand consumption by cells. Because cells with autocrine loops can in fact bind and uptake some ligands, any observed differences of accumulated ligand concentration between these two designs must there arise due to the unequal local impacts of cell arrangement. These families of cell arrangement can also be obtained for other patch radii while maintain the same σ.

same total cell count on the substrate, or same global density. If cells cannot bind or consume any secreted ligands, all designs of the same σ should acquire the same global ligand concentration. Any differences of the ultimate cell response must therefore arise as a result of the dissimilar local concentration. We can also investigate the global impact of cell arrangement by simply comparing ligand capture with different σ but the same patch radius (Figure 4-1).

Stochastic model of square-latticed arrays of cells that acquire a single autocrine loop

Regardless of the symmetry of the square-latticed array of circular cell patches, such cell arrangement still gives rise to mixed boundary conditions for our ligand transport analysis. We use the boundary homogenization technique developed by Shvartsman and colleagues to simplify the heterogeneous boundary conditions of densely-plated cell surface (Batsilas, Berezhkovskii et al. 2003; Berezhkovskii, Batsilas et al. 2004; Berezhkovskii, Makhnovskii et al. 2004; Berezhkovskii, Monine et al. 2006). The cell surface is modeled as a uniform boundary condition with effective ligand trapping rates that consolidate all transport properties of the original boundary conditions, including geometry of cell positioning, the affinity between ligands and receptors and the receptor area density. Based on the analyses performed in these previous studies, we can describe the probability density function of ligands on the cell surface due to their interactions with the receptors from:

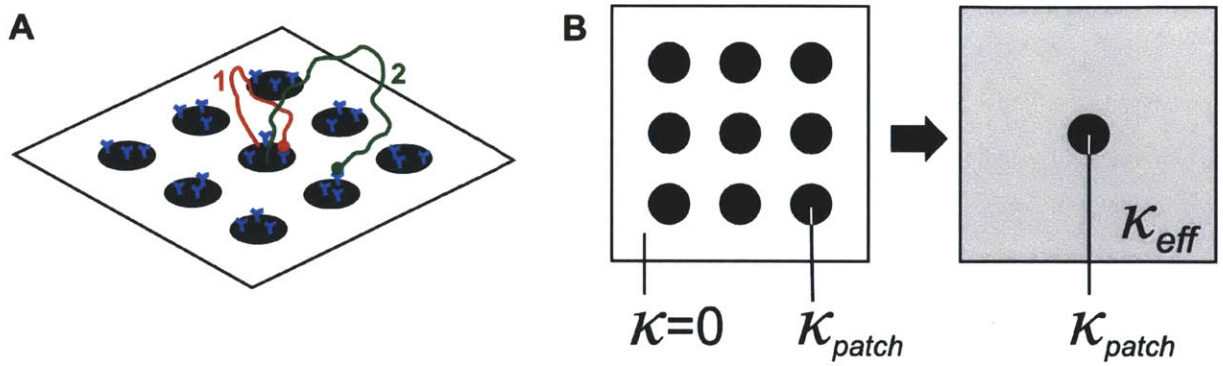

Figure 4-2 Boundary homogenization of cell-surface
A) Ligand molecules that are secreted from the patterned cell array can either bind to the original secreting patch (autocrine trajectory, #1) or land on the neighboring patch (paracrine trajectory, #2). B) To simplify the heterogeneous boundary conditions of cell surface (reflective wall on substrate surface and absorptive areas on cell patches), capturing of ligands with paracrine trajectories are described by the effective trapping rate κ_{eff} while binding of ligands with autocrine trajectory is governed by the same trapping rate, κ_{patch}.

$$D\frac{\partial p(x,y,z,t)}{\partial z}\bigg|_{z=0} = \kappa p(x,y,z=0,t). \qquad [4\text{-}2]$$

The trapping rate κ (has the same unit as velocity, m/s) will vary, depending on the types of ligand trajectories (Figure 4-2). Capturing of ligands with autocrine trajectories has shown to be independent of the array geometry, and can be described by the patch trapping rate κ_{patch}.

$$\kappa_{patch} = \frac{k_{on} n_{patch} R_{total}}{\pi r_{patch}^2 N_A} = \frac{k_{on} R_{total}}{\pi r_{cell}^2 N_A} = k_{on} r_{total} \qquad [4\text{-}3]$$

Ligands with paracrine trajectories are dependent on cell arrangement and were found to be governing by the effective trapping rate κ_{eff} which was defined as

$$\frac{1}{\kappa_{eff}} = \frac{\pi r_{patch}}{4DF(\sigma)} + \frac{1}{\sigma\kappa_{patch}}, \qquad [4\text{-}4]$$

where

$$F(\sigma) = \frac{\sigma(1 + A\sqrt{\sigma} - B\sigma^2)}{(1-\sigma)^2}. \qquad [4\text{-}5]$$

A and B are constants that vary with different lattice geometry of the patch array, namely A=1.62, 1.75, 1.37 and B=1.36, 2.02, 2.59 for triangular, square and hexagonal lattices of circular patches (Berezhkovskii, Monine et al. 2006). In the case of randomly-distributed patches, A=0.34 and B=-0.58. D is the ligand diffusivity; N_A is the Avogadro's number; R_{total} is the total number of receptors per cell; r_{total} is the total number of receptors in the unit of molar per area; n_{patch} is the number of cells per patch; r_{patch} is the patch radius; r_{cell} is the cell radius; and k_{on} is the association rate constant of ligand/receptor binding.

With these trapping rates, we can determine the ligand survival probability (the probability that a released ligand from the cell surface has not been recaptured by cells) following the previously developed approach (Monine, Berezhkovskii et al. 2005). In brief, the total survival probability of ligands in the supernatant can be approximated from the summation of survival probability of both the autocrine (S_{au}) and paracrine trajectories (S_{para}) (Figure 4-3).

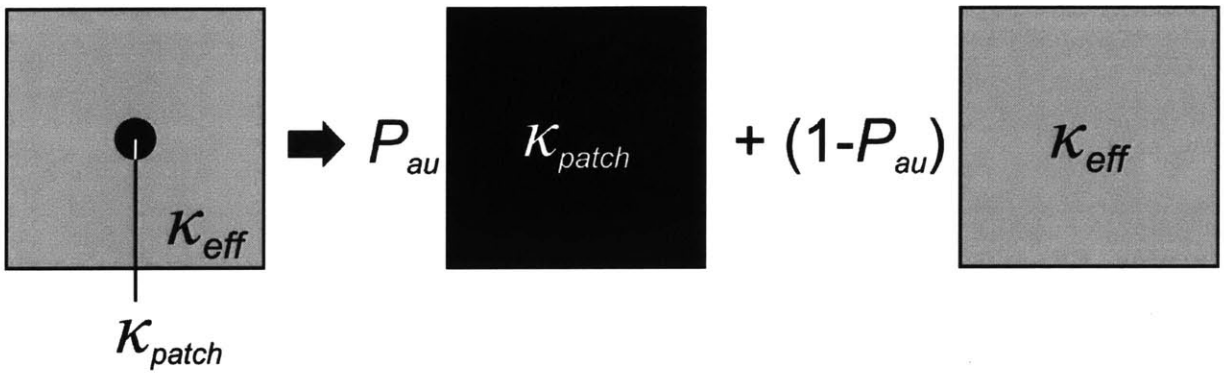

Figure 4-3 Calculation of ligand survival probability

Having simplify the cell-surface boundary conditions using the boundary homogenization technique, we can approximate the total ligand survival probability in the supernatant from the summation of survival probability of ligands with both autocrine and paracrine trajectories.

$$S(t) \approx P_{au} S_{au}(t) + (1 - P_{au}) S_{para}(t) \qquad [4\text{-}6]$$

From the analysis by Batsilas *et al.*(Batsilas, Berezhkovskii et al. 2003), the fraction of ligands with autocrine trajectories can be determined from:

$$P_{au} = \frac{\kappa_{\text{patch}} r_{\text{patch}} / D}{\kappa_{\text{patch}} r_{\text{patch}} / D + 4/\pi}, \qquad [4\text{-}7]$$

To solve for the survival probability for each type of ligand trajectories, one must first determine the probability density function of the ligand particles across the fluid height (z-axis). Because diffusion of ligands along the lateral (x-y) and vertical (z) axes occur independently, the ligand propagators (or the Green's function) along both directions can be solved separately. Because we only care to determine the bulk ligand concentration in the supernatant and the averaged complex formation on cell surface, we will only solve for the vertical propagator $G(z,t)$. We define $G(z,t|z_0)$ as the particle probability density in finding ligand at the distance z from the cell-surface boundary at time t after each ligand has started its path at a distance z_0 from the cell surface. The solution of vertical propagator has been extensively described in Monine *et al.* (Monine, Berezhkovskii et al. 2005). In brief, the vertical propagator when considered as a function of the starting plane z_0 must satisfy the following one-dimensional diffusion equations:

Governing equation:

$$\frac{\partial G}{\partial t} = D \frac{\partial^2 G}{\partial z_0^{\,2}} \qquad [4\text{-}8]$$

with the following initial condition and boundary conditions:

$$G(z, t = 0 \mid z_0) = \delta(z - z_0) \qquad [4\text{-}9]$$

Boundary conditions:

$$D\left.\frac{\partial G(z,t\mid z_0)}{\partial z_0}\right|_{z_0=0} = \kappa G(z,t\mid 0)$$
$$\left.\frac{\partial G(z,t\mid z_0)}{\partial z_0}\right|_{z_0=h} = 0 \qquad [4\text{-}10]$$

Based on this definition, the survival probability of ligand that starts from the plane z_0, $S(t|z_0)$ is then calculated by integrating the vertical propagator across the fluid thickness (0 to h):

$$S(t\mid z_0) = \int_0^h G(z,t\mid z_0)dz\,. \qquad [4\text{-}11]$$

By solving this particle survival probability in the Laplace domain and later set z_0=0, the following solutions in the Laplace domain can be obtained for the survival probability of both autocrine and paracrine trajectories.

$$\hat{S}_{au}(s) = \frac{\sqrt{D}[\exp(2h\sqrt{s/D})-1]}{\sqrt{D}[\exp(2h\sqrt{s/D})-1]s + k_{patch}[\exp(2h\sqrt{s/D})+1]\sqrt{s}} \qquad [4\text{-}12]$$

$$\hat{S}_{para}(s) = \frac{\sqrt{D}[\exp(2h\sqrt{s/D})-1]}{\sqrt{D}[\exp(2h\sqrt{s/D})-1]s + k_{eff}[\exp(2h\sqrt{s/D})+1]\sqrt{s}}\,. \qquad [4\text{-}13]$$

Following the approach developed by Monine *et al.* (Monine, Berezhkovskii et al. 2005), we then determine the concentration of accumulated ligands in the surrounding fluid, $L(t)$, from the ratio of total number of ligand molecules in the supernatant to the medium volume. The total number of ligand molecules in the covering fluid can be determined from convolution of the total ligand release rate from cell surface $I(t)$ and the total ligand survival probability $S(t)$.

$$L(t) = \frac{\sigma}{A_{cell}h} I(t) * S(t) = \frac{\sigma}{A_{cell}h}\int_0^t I(\tau)S(t-\tau)d\tau. \qquad [4\text{-}14]$$

The total ligand release rate $I(t)$ is the summation of two processes: 1) novel ligand secretion $Q(t)$ and 2) dissociation of ligand-receptor complexes.

$$I(t) = Q(t) + k_{off}C(t)\,. \qquad [4\text{-}15]$$

We determine the rate of change of complex formation based on the mass balance of the ligand capturing rate, $-I(t)*S(t)$, and the loss of complex molecules due to ligand/receptor unbinding (k_{off}) and the internalization of bound receptors (k_e).

$$\frac{dC(t)}{dt} = -\int_0^t I(\tau)\frac{dS(t-\tau)}{d\tau}d\tau - (k_{off}+k_e)C(t)\,. \qquad [4\text{-}16]$$

Putting everything together with the initial condition $S(t=0)=1$, we can then solve for the concentration of ligands in the extracellular medium and the concentration of generated complexes simultaneously from the following equations in the Laplace domain and numerically determine the time-varying solutions using the inverse Laplace transformation.

$$\hat{L}(s) = \frac{\sigma}{hA_{cell}}\frac{Q_{cell}}{s}\frac{\hat{S}(s)\left[s+k_e+k_{off}\right]}{\left[s+k_e+k_{off}+k_{off}\left(s\hat{S}(s)-1\right)\right]} \qquad [4\text{-}17]$$

$$\hat{C}(s) = -\frac{Q_{cell}}{s}\frac{\left(s\hat{S}(s)-1\right)}{\left[s + k_e + k_{off} + k_{off}\left(s\hat{S}(s)-1\right)\right]} \qquad [4\text{-}18]$$

Note also that the ligand secretion rate $Q(t)$ is assumed here to be a step function, $Q(t)=Q_{cell}u(t)$. The ligand secretion function in the Laplace domain $\hat{Q}(s)$ is therefore equal to Q_{cell}/s.

Continuum models of ligand binding

To understand the mechanism that underlies the steady-state behavior at both spatial extremes, we attempt to model changes of ligand capturing analytically using continuum models. To obtain these models, we solve the diffusion equation for steady-state propagation of secreted ligand, $\nabla^2 L = 0$, subject to the boundary condition:

$$-D\left[\mathbf{n}\cdot\nabla L\right]\Big|_S = q - k_e r_{total}\frac{L_S}{\left(K_M + L_S\right)} \qquad [4\text{-}19]$$

for boundary elements S corresponding to cell surfaces, and $-D\left[\mathbf{n}\cdot\nabla L\right]\Big|_S = 0$ otherwise. Here, the Michaelis-Menten constant, K_M is defined as $K_M \equiv (k_{off} + k_e)/k_{on}$. L_S is ligand concentration on cell surface; q is the ligand secretion flux (equal to $Q_{cell}/(N_A A_{cell})$ in the unit of moles·area^{-1}·second^{-1}); r_{total} is the area density of total receptor on the cell (equal to $R_{total}/(N_A A_{cell})$ in the unit of moles·area^{-1}·cell^{-1}) and N_A is the Avogadro's number. In the communicative regime, cell patches can be approximated as a confluent monolayer of cells, with secretion and receptor density scaled by the cell-covered area fraction σ. For this case, the steady-state ligand concentration is uniform everywhere and equal to L_S. Applying the boundary condition in equation [4-19] gives:

$$L_S = \frac{K_M}{\frac{k_e r_{total}}{q} - 1} \quad \text{for } \sigma \to \pi/4. \qquad [4\text{-}20]$$

Note that if $q \geq k_e r_{total}$, the rate of ligand secretion overwhelms the maximum rate of complex internalization and no steady-state concentration exists regardless of the value of σ. This value of L_S results in the equivalent amount of bound receptors (c) given by q/k_e.

At the opposite extreme of cell density where $\sigma \to 0$, it is also possible to obtain analytical results. To do this, we use confocal ellipsoidal coordinates (Hilbert 1999) in which $a = b = r_{patch}$ and $c = 0$, corresponding to a flat, circular patch of cells with radius r_{patch}. To simplify the problem, the ligand concentration is constrained to depend only on the ellipsoidal coordinate where we define the confocal ellipsoid constant ξ as $\xi = 1/2\left[(r^2 - r_{patch}^2) + \sqrt{(r^2 - r_{patch}^2)^2 + 4r_{patch}^2 r^2}\right]$. We then obtain the ligand concentration in this new coordinate equal to:

$$L(\xi) = L_S\left[1 - \frac{2}{\pi}\tan^{-1}\left\{\frac{\xi^{1/2}}{r_{patch}}\right\}\right] \qquad [4\text{-}21]$$

Note that the boundary condition of equation [4-19] cannot be satisfied exactly by this expression since the flux normal to the cell patch (proportional to $\partial L/dz$) is not constant over the patch's surface ($\xi = 0$). Nonetheless, we found the averaged flux over the surface of the cell patch $\left\langle dL/dz|_{z=0}\right\rangle = -4L_S/\pi r_{patch}$. Using this approximation in equation [4-19] gives the surface concentration L_S for a flat, circular patch in isolation:

$$L_S = \frac{\pi r_{patch}}{8D}\left[-\left[\frac{4D}{\pi r_{patch}}\right]K_M + q - r_{total}k_e + \left\{\left(\left[\frac{4D}{\pi r_{patch}}\right]K_M\right)^2 + 2(r_{total}k_e + q)\left[\frac{4D}{\pi r_{patch}}\right]K_M + (r_{total}k_e - q)^2\right\}^{\frac{1}{2}}\right]$$

$$L_S = \frac{\pi r_{patch}}{8D}\left[\left(\frac{4D}{\pi r_{patch}}\right)K_M + (r_{total}k_e - q)\right]\left[-1 + \left\{1 + \frac{\left(\frac{16D}{\pi r_{patch}}\right)qK_M}{\left[\left(\frac{4D}{\pi r_{patch}}\right)K_M + (r_{total}k_e - q)\right]^2}\right\}^{\frac{1}{2}}\right] \quad [4\text{-}22]$$

Equation [4-22] is valid for any parameter values, assuming $(r_{total}k_e/q) > 1$ (so that a steady-state exists). If we further assume that the surface concentration remains low relative to the dissociation constant K_M (this would be the case, for example, if endocytosis dominates secretion ($r_{total}k_e/q >> 1$) or diffusion of ligand away from the patch dominates binding and secretion ($DK_M/qr_{patch} >> 1$)), the ligand concentration at the cell surface in the isolated regime is accurately approximated by:

$$L_S \approx \left[\frac{qK_M}{\frac{4DK_M}{\pi r_{patch}} + r_{total}k_e}\right] \quad [4\text{-}23]$$

This result can be obtained either by linearizing the square root term within equation [4-22], or by solving equation [4-19] directly for $K_M >> L_S$. From equation [4-23], the concentration of bound receptors can be determined and further simplified as a function of dimensionless parameters as follows:

$$c \approx \left[\frac{r_{total}}{\frac{4DK_M}{q\pi r_{patch}} + \frac{r_{total}k_e}{q}}\right] \quad [4\text{-}24]$$

$$c = \frac{q}{k_e}\left(\frac{\frac{r_{total}k_{on}r_{patch}}{D}}{\frac{4}{\pi}\frac{k_e + k_{off}}{k_e} + \frac{r_{total}k_{on}r_{patch}}{D}}\right) \quad [4\text{-}25]$$

$$c = \frac{q}{k_e}\left(\frac{\frac{k_e}{k_e + k_{off}}\frac{r_{total}k_{on}r_{patch}}{D}}{\frac{4}{\pi} + \frac{k_e}{k_e + k_{off}}\frac{r_{total}k_{on}r_{patch}}{D}}\right) \quad [4\text{-}26]$$

$$c = \frac{q}{k_e}\left(\frac{\upsilon Da}{\frac{4}{\pi} + \upsilon Da}\right) = \frac{q}{k_e}P_{au} \quad [4\text{-}27]$$

Here, we have introduced here two groups of dimensionless parameters. First, υ defines the probability of receptor internalization and is defined here as $\upsilon \equiv k_e/(k_{off} + k_e)$. Da is the commonly recognized Damköhler numer and defined here as $Da \equiv (r_{total}k_{on}r_{patch})/D$. We found that the ratio of these two dimensionless parameters $\upsilon Da/(4/\pi + \upsilon Da)$ is equal to the recapturing probability of ligand with autocrine trajectories (P_{au}) when taking into account its consumption due to complex internalization by

cells (Batsilas, Berezhkovskii et al. 2003). Note also that when $r_{patch} >> (4/\pi)/(\upsilon r_{total} k_{on}/D)$ (*i.e.* for sufficiently large cell patches) the solution for the isolated cell patch converges to that for the communicative regime (q/k_e). Accordingly, for cell patches significantly larger than this critical size, cell signaling (as parameterized by the fraction of bound receptors) between neighboring patches becomes insignificant, as essentially all communication occurs within a single patch.

4.3 Results

Ligand accumulation and capturing with varying cell arrangement

Having developed a stochastic model that can be applied to flexible cell arrangements, we put the model to the test by comparing its prediction of ligand accumulation to our experimental measurement using the TGFα/EGFR autocrine loop in A431 cells as our study model. It has been illustrated that the spatial propagation of ligands can be inferred from the analysis of ligand capture (DeWitt, Dong et al. 2001). Autocrine loops with smaller fraction of captured ligands (F_{LC}) acquire longer survival time in the supernatant and thus obtain broader spatial propagation. Following this principle, we asked how ligand capturing would change with the alteration of cell arrangement, both at the local and global length scales. The F_{LC} was determined from two different ligand fluxes, 1) the total ligand secretion rate, $Q(t)$, and 2) the net ligand secretion rate, $L(t_{end})/(t_{end}-t_0)$. The difference between these two fluxes represents the rate of ligand consumption by cells. F_{LC} can then be obtained by normalizing the ligand consumption rate by the total ligand secretion rate (Figure 4-4A). Because the amount of ligands in the covering fluid can be experimentally measured using ELISA (Chapter 2), we compare the simulated cell density-ligand accumulation relationship to our experimental measurement. Supplementation of mAb225 at the saturating dose (450 nM) enables the measurement of total ligand secretion rate. Figure 4-4C&D illustrates net and total ligand secretion rates from both mathematical simulation and our experimental measurements at 72 hours after serum starvation. We determined bulk concentration of TGF-α in the collected supernatant from different cell plating densities. The averaged ligand secretion rate per cell was then determined by normalizing the per-well ligand concentration with the total cell counts per well. To simulate ligand accumulation, we used the transport and kinetics parameters that were experimentally identified from previous studies (Table 1). The total secretion rate of TGF-α is set to 33.6 molecules/cell/hour to match the averaged value from our measurements at all plating densities (Figure 4-4D, red square dots). Overall, the stochastic model can accurately predicts the qualitative trend of ligand binding changes with the alteration of global cell densities. We found that the total ligand concentration per well linearly increases with the elevating cell plating density, validating our modeling assumption to use a constant total ligand secretion rate (red square dots in Figure 4-4C&D). Without receptor-blocking antibodies, we observe a general decrease in net ligand secretion per cell with increasing plating densities (blue square dots in Figure 4-4D). This result implies the improving ability of cells to capture the secreted ligand when cells are positioned more adjacently to one another. This postulation can be quantitatively validated from the corresponding increase of ligand-capture fractions (F_{LC}) with increasing cell plating densities (Figure 4-4B). The observed change of ligand capture with increasing plating densities may underlie the commonly observed density-dependent growth change during *in vitro* cultivation of mammalian cells (Lauffenburger and Cozens 1989).

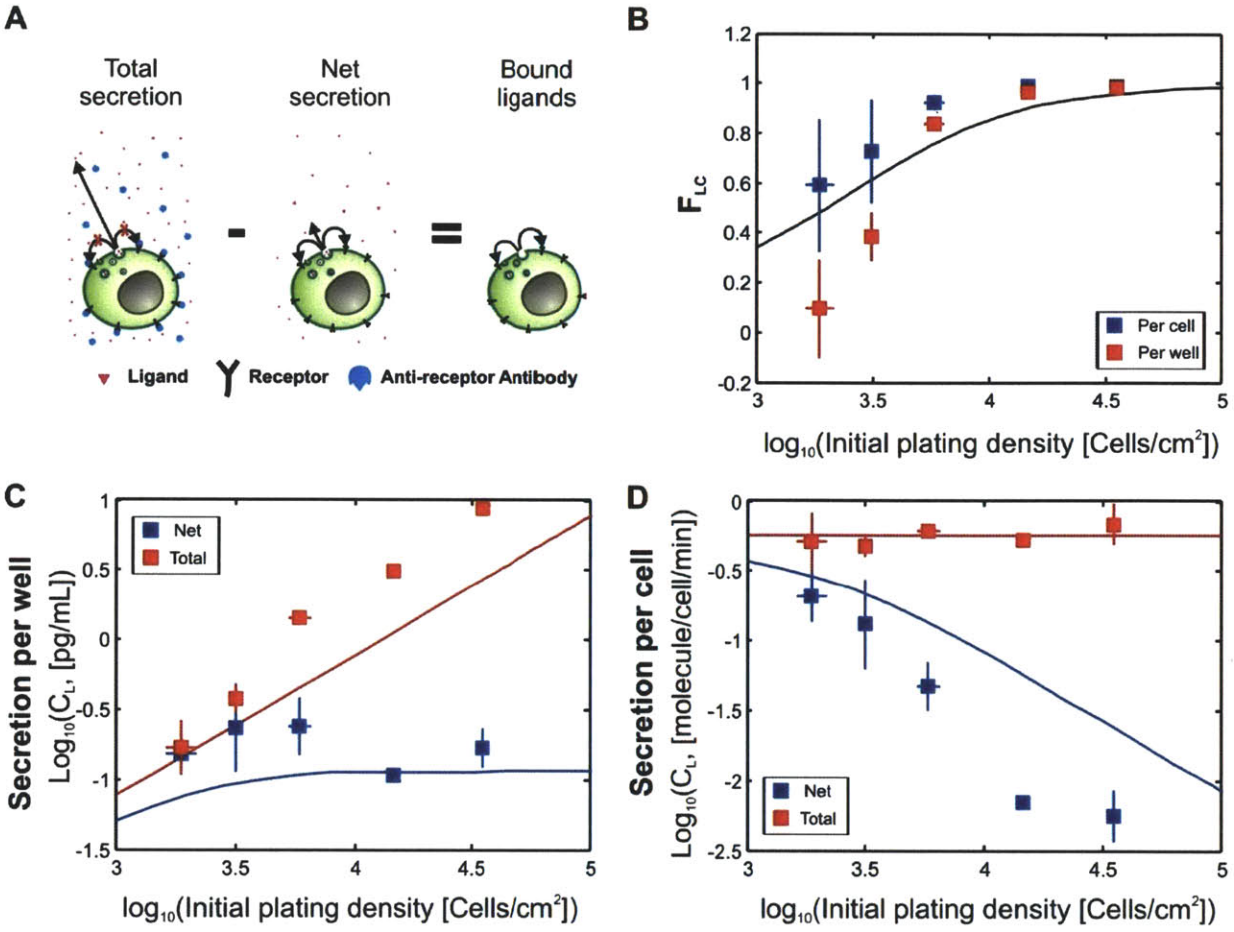

Figure 4-4 Changes of ligand capturing with varying cell plating densities

A) The amount of bound ligands can be inferred from the difference between total and net ligand secretion. Experimentally, total ligand secretion can be obtained by co-cultivation the cells with the EGFR-neutralizing monoclonal antibody 225. B) Fractions of captured ligands (F_{LC}) with varying cell plating densities (F_{LC}=1-$[L]_{net}/[L]_{total}$). F_{LC} from the experimental measurement (colored dots) is plotted along with the modeling prediction (black line). C) The per-well concentration of TGF-α. (D) The per-cell concentration of TGF-α. The experimental measurements (colored square dots) are plotted together with prediction from the stochastic model (colored lines). Error bars represent propagated standard deviations from two biological replicates. Parameters used: D=2.5×10^{-6} cm^2/s, k_{on}=7.83×10^8 cm^3/(moles-s),k_{off}=0.27 minute^{-1}, k_e=0.08 minute^{-1}, R_{total} = 3×10^6 molecules/cell, Q=0.5638 molecules/(minute-cell), r_{cell}=7 μm, liquid volume = 100 μL, substrate area = 0.3165 cm^2.

Temporal changes of ligand/receptor complex formation with altering cell arrangement

Having determined the modeling parameters that can optimally predict ligand accumulation and capturing in A431 cells (experimentally measured transport parameters are often reported as a tentative range, Table 1), we use the developed model to examine the temporal change of ligand/receptor binding with varying cell plating densities. By plotting the number of generated complex molecules with varying cell plating densities for the different time points, we can demonstrate the transition of complex formation between the two extreme global cell densities (Figure 4-5A). The number of complex molecules between the densities of 100 to 100,000 cells/cm^2 increases with time and reach the same maximal complex number. With increased incubation time, the transition to maximal complex number also occurs at smaller cell plating densities (leftward curve shift). With an attempt to explore the impact of local cell density, we also performed a similar analysis for the square-latticed arrays with the patch radii of 50 and 100 microns (Figure 4-5B). Independently of the patch radius, we observed that complex molecules reach steady states at two distinct array spacing, at densely-packed spacing ($R_{c\text{-}c} = 2\times r_{patch}$) and at broadly-positioned spacing ($R_{c\text{-}c} = 1024\times r_{patch}$). For example, the number of generated complex molecules with the patch radius of 50 microns exhibits complex formation that varies between ~3 molecules/cell at $R_{c\text{-}c} = 1024\times r_{patch}$ to ~7 molecules/cell at $R_{c\text{-}c} = 2\times r_{patch}$. Thus, the dense cell array defines the maximal complex formation while the spatially-isolated array marks the baseline complex formation. Interestingly, the arrays with both 50 and 100-micron patch radii both acquire the same number of complex for very dense array. For the arrays with spatially isolated patches, the 100-micron arrays exhibit higher complex number than that of the 50-micron arrays. Because all simulations were performed using the same substrate area and thus the

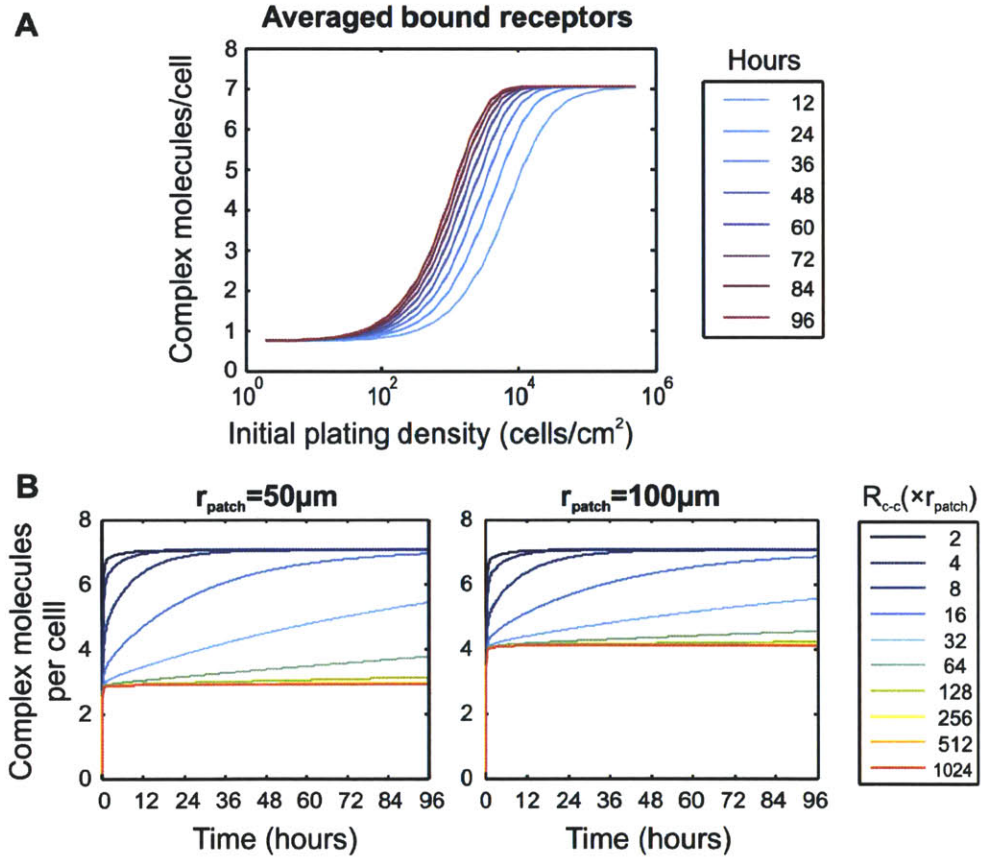

Figure 4-5 Temporal change of complex formation for different cell-positioning geometry
A) The number of bound receptor per cells with varying cell plating densities is simulated at varying time points. B) Change of complex formation from the square-latticed cell arrays of circular cell patches with the patch radii of 50 and 100 μm. The array spacing was altered from $2\times r_{patch}$ to $1024\times r_{patch}$ (legend).

same global density, the observed difference in complex formation from both designs must occur due to their different local cell density. The previous result illustrates that the impact of cell arrangement on ligand/receptor binding is temporally dynamic and shows that the local impact of cell arrangement can manifest itself in the variation of complex formation.

Relationship between local and global cell densities and its impact on ligand/receptor interaction

To further investigate the previously observed impact of local cell density and its connection with the global cell density, we used the developed stochastic model to examine changes of ligand/receptor binding while we systematically modulated the geometric configuration of square-latticed cell arrays of circular patches. We determined changes in ligand/receptor binding for multiple patch radii while choosing the corresponding array spacing that gives rise to the same cell-covered area fractions (σ), ranging from 10^{-6} to the maximum value of $\pi/4$. With increasing σ (increasing global cell densities), we observe a decrease in the net ligand secretion rate per cell or the corresponding elevation of ligand capturing from all patch radii (Figure 4-6A). At very small and very large σ, complex formation (Figure 4-6B) is found to reach two distinct equilibriums that do not depends on global cell density. With small σ, we observe distinct differences in the equilibrium complex number among the different patch radii. Specifically, arrays with larger patch sizes acquire higher F_{LC} and complex formation than those with smaller patches. Such local impact of cell arrangement on ligand/receptor binding is found to diminish

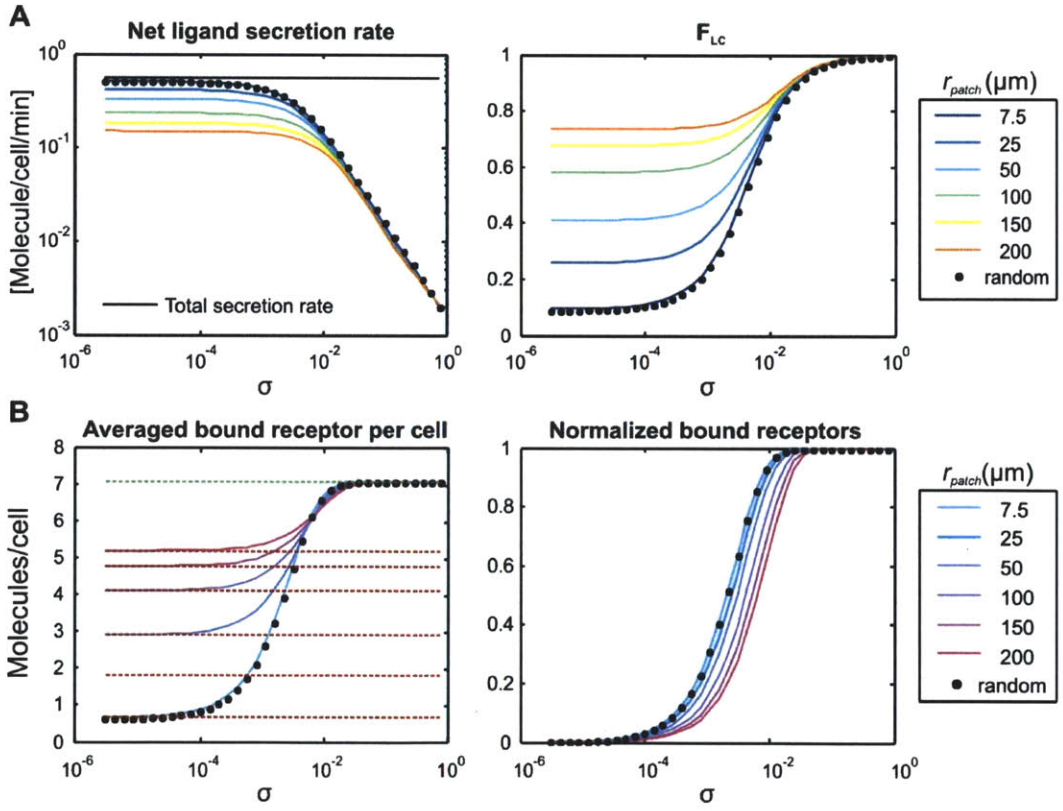

Figure 4-6 Predicted complex formation at 72 hours for varying cell arrangement geometry
To investigate the relationship between local and global cell densities, we systematically modulate both the patch radius (r_{patch}) and the array spacing ($R_{c\text{-}c}$) for a fixed range of σ between 10^{-6} and $\pi/4$. A) Net ligand secretion rate and the fraction of captured ligands are determined for different array geometry. B) Changes of complex formation with varying σ and patch radii are also determined with the stochastic model. The prediction from continuum models at both extreme length scales are also calculated (dotted lines). To determine shifting of the σ-complex formation relationship for varying local cell densities, we normalize all plots by the maximal and minimal number of the generated complex from all array designs.

and soon become insignificant at larger σ. By normalizing the calculated number of bound receptors (Figure 4-6B), we can observe a rightward shift of the σ-complex formation relationship with increasing patch radii. In other words, complex formation becomes increasingly desensitized to the global impact of cell arrangement when the effect of local cell density critically influences changes in ligand binding. This assumption holds true as long as the complex formation still does not reach the maximum equilibrium. Finally, it is important to note the closely matched behaviors of ligand capturing between randomly plated cells (black dots in Figure 4-6) with the square-latticed arrays of single-cell patch (r_{patch} =7.5 microns). This result implies the spatially limited nature of the TGFα/EGFR autocrine loop in A431 cells that gives rise to equivalent ligand capturing between the two cell arrangement designs, either random or square-latticed array.

Because our stochastic model is a numerical analysis, it is unclear which model parameters actually contribute to the observed changes of ligand binding with the modified cell arrangement. To gain some insights for the underlying mechanism, we used the developed continuum models of autocrine ligand transports at the two extreme global densities. Because ligand binding reaches steady states at these two spatial regimes, the complex mixed boundary conditions of the square-latticed cell arrays can be simplified, allowing us to determine the analytical forms of generated complex molecules. For the spatially-isolated cell arrays, we approximate the boundary condition of cell surface as a single circular patch on an infinite reflective wall. For the dense arrays, we can approximate cell surface simply as a homogenous monolayer. Using the same transport parameters of the TGF-α/EGFR autocrine loop in A431 cells, we found that the prediction of complex formation by these two continuum models agrees well with our numerical estimations from the stochastic model at both spatial extremes (green and red dotted lines in Figure 4-6B). We found that the equilibrium complex number at large σ is equal to the ratio of ligand secretion rate and the rate of complex internalization (Q/k_e). At small σ, the steady-state complex formation can be easily determined from the same ratio of ligand secretion and the rate of complex internalization multiplied by the probability of self-captured ligands ($P_{au} \times Q/k_e$).

The identified analytical solutions of the steady-state complex formation at both spatial extreme regimes provide us important insights about the mechanism that underlie impacts of cell arrangement on ligand binding in autocrine systems. First, the ratio of ligand secretion rate and complex internalization rate represents the required balance of two important fluxes at steady states, ligand source and ligand sink. At both spatial regimes, such steady states cannot occur if this balance cannot be practically generated in the autocrine system. Mathematically, such steady-states can only be achieved when the number of generated complex molecules is smaller than the total receptors. Second, because a spatially isolated cell patch cannot interact diffusively with other patches (at least within the observe time scale), it makes sense intuitively that the steady-state of complex formation in this spatial regime is mathematically found to be equal to the maximum complex formation multiplied by the probability of self-captured ligands (P_{au}). Because P_{au} is a function of patch radii (P_{au} increases with elevated patch sizes), the observed change of complex formation with the alteration of patch sizes also makes sense mathematically. Finally, by comparing the difference in complex formation between the two steady states, we can reason that the extra ligand binding must arise due to the diffusive exchanges among the neighboring cell patches or more commonly known as the paracrine trajectories (P_{para}=1-P_{au}). To highlight the difference in cell-to-cell diffusive interaction between the two spatial steady states, we define the effect of cell arrangement on ligand binding at very large σ as the '*communicative*' mode and at small σ as the '*isolated*' mode. Between these two extreme length scales, we will also define the temporally dynamic changes of ligand capturing due to spatially-varying paracrine interactions as the '*critical*' spatial range. It would be interesting to explore how the identified impacts of cell arrangement also interplay with intrinsic characteristics of autocrine loops such as the relative production rates of ligands and receptors and the ligand/receptor affinity.

Interactive impacts of cell arrangement and ligand/receptor productions on ligand propagation

It was illustrated that the relative production rates of ligands and receptors that underlie a specific autocrine loop critically influence the spatial propagation of autocrine ligands (DeWitt, Dong et al. 2001). Specifically, an autocrine system with relatively higher ligand production than receptor availability was shown to acquire broader ligand propagation in the surrounding fluid, behaving like true paracrine system. Having identified impacts of cell arrangement on ligand capturing, we thus seek to investigate the connection between cell arrangement and the relative ligand/receptor production in regulating ligand binding. First, we examine changes of F_{LC} with varying σ for a fixed patch radius of 50 microns and a variety of ligand/receptor production ratios (Q/R_{total}), using the previously optimized parameters of A431 cells as the baseline trend (Figure 4-7). Because the total receptor number is linearly proportional to the receptor production rate (s $\approx k_e r_{total}$ and q/s= 2.8×10^{-6} in A431 cells), it is mathematically accurate that we determine the ligand/receptor production ratios by simply modulating Q and R_{total}. To change the Q/R_{total} ratio, we equally adjust both Q and R_{total}. For example, to increase the Q/R_{total} ratio by a factor of 100, we assign the new ligand secretion rate to $Q\times10$ and the new total receptor to $R_{total}\times0.1$. Having modulated the Q/R_{total} ratios ranging from 10^{-6} to 10^{6} folds (Figure 4-7A), we found that an increase in Q/R_{total} causes the steady-state F_{LC} in the *isolated* mode to diminish and the overall F_{LC}-σ curve to shift rightwards. Increases of the Q/R_{total} ratios above 1000 folds result in disappearance of the *communicative* mode, suggesting that the two major spatial modes of the intercellular communication may not actually exist simultaneously in some autocrine systems. With the decreasing Q/R_{total} ratios, the differences of F_{LC} between the *isolated* and *communicative* regimes become less significant, implying the gradual disappearance of the density-dependent phenotypic change. We also examine the connections between the local cell density and the ligand/receptor production ratio in regulating ligand binding by determining changes of the F_{LC}-Q/R_{total} curves with varying patch radii (Figure 4-7B). An increase in patch sizes exhibits no effect in the *communicative* regime but causes a rightwards shift of the F_{LC}-Q/R_{total} curve in the *isolated* regime. In summary, an increasing cell density at either the local or global length scale is found to limit the impact of

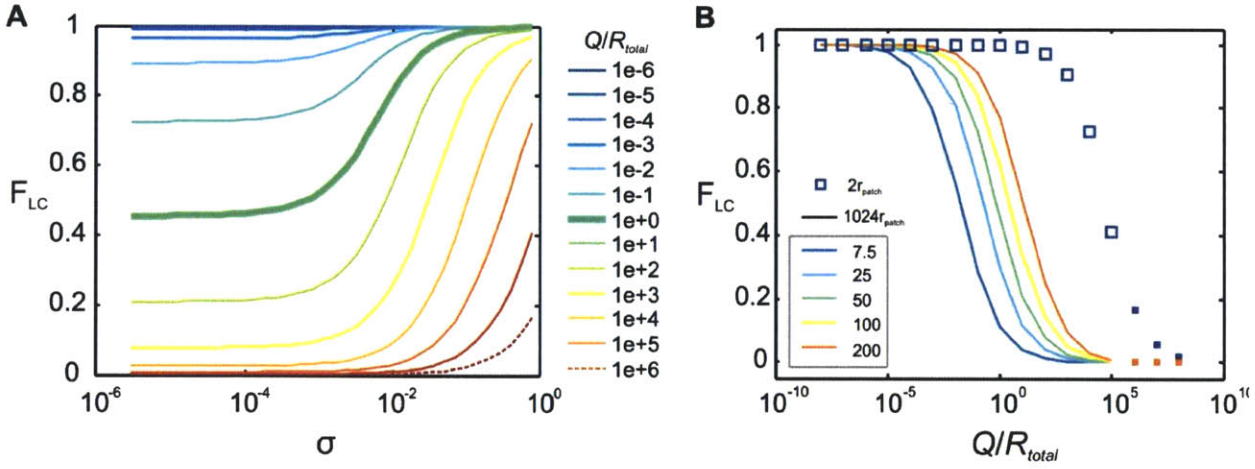

Figure 4-7 Change of autocrine ligand capturing with varying ligand/receptor production ratios
A) To investigate the interplay between cell arrangement and the ligand/receptor production ratios and its impact on ligand capturing, we used the developed model to predict changes of F_{LC} with varying σ for a fixed patch size of 50 microns while we also modulate the Q/R_{total} ratios between 10^{-6}-10^{6}. The Q/R_{total} of 10^{6} (dotted line) is found to give complex number greater than R_{total}, suggesting that steady states cannot occur with this set of parameters. B) To also determine the impacts of local dell densities on the relationship between ligand/receptor production ratios and ligand propagation range, we also perform similar analysis for multiple patch radii (shown in legend in the unit of microns). While no difference is observed in the communicative mode, an increase in patch radii results in a rightward shift of the F_{LC}-Q/R_{total} curve. Orange and blue dots represent parameter sets that cannot establish steady-states of complex formation.

the ligand/receptor production ratio to expand the propagation range of ligands in supernatant. With increasing cell densities, it makes sense that more ligands can be captured by the cell surface, instead of diffusing away into the surrounding fluid.

Roles of cell arrangement on the impact of ligand/receptor affinity on ligand propagation range

Like the ligand/receptor production ratio, the affinity between ligand and receptor also affects the spatial propagation of autocrine ligands. Ligands with poorer affinity to the corresponding receptor were observed to exhibit broader propagation range (DeWitt, Iida et al. 2002). Because an increase in ligand/receptor affinity can be mathematically simulated by either increasing the association rate (k_{on}) or decreasing the dissociation rate (k_{off}), we investigated changes of ligand binding with changes of cell densities in association with the separate modification of k_{on} and k_{off}. Figure 4-8A illustrates the impact of ligand/receptor affinity to the F_{LC}-σ relationship. Similar to the decrease in the Q/R_{total} ratio, an increase in

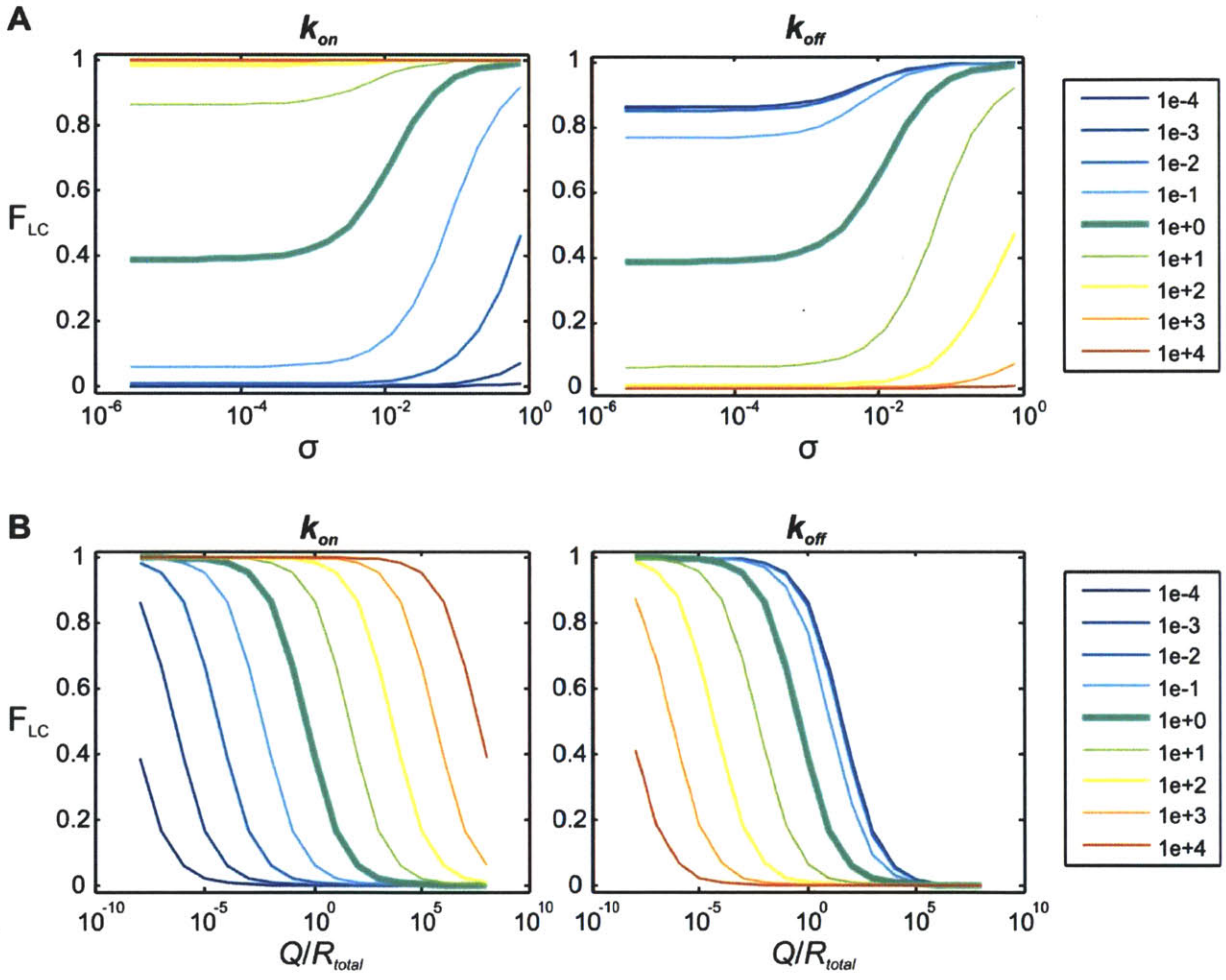

Figure 4-8 Changes of autocrine ligand capturing with varying ligand/receptor affinity
A) Changes of the F_{LC}-σ relationship with varying ligand/receptor affinity, either via changes of association (k_{on}) or dissociation rate constants (k_{off}). Each parameter is modulated from 10^{-4} to 10^{4} folds (shown in legend). An array with the fixed radius of 50 microns and the instrinsic parameters of the TGFα-EGFR autocrine loop in A431 cells are used to generated the baseline trend (bold lines). Increase in k_{on} or the decrease in k_{off} results in increasing steady-state F_{LC} and the leftward shift of the F_{LC}-σ curves although the effect of decreasing k_{off} seems to be saturated with the modification ratio below 10^{-3} folds. B) Impact of ligand/receptor affinity on the F_{LC}-Q/R_{total} relationship. Increase in ligand/receptor affinity desensitizes the impact of ligand/receptor production ratio on the ligand propagation range.

k_{on} elevates the steady-state F_{LC} in the isolated mode and also shifts the F_{LC}-σ curve leftwards. While a decrease in k_{off} seems to exhibit a similar effect, its effect becomes insignificant with the modification factor below ~10^{-3}. While further analysis is needed to describe the different effects of k_{on} and k_{off}, the underlying cause must stem from how the effect of ligand/receptor dissociation (k_{off}) is mathematically associated with the internalization rate (k_e) of bound receptors (see Equation [4-26]). When combining the impact of ligand/receptor affinity to the changes of Q/R_{total} ratios, we found that a decrease in ligand/receptor affinity, either by decreasing k_{on} or increasing k_{off}, generally shifts the F_{LC}-Q/R_{total} curve leftwards, representing the broader ligand propagation in space (Figure 4-8B). The limited impact of decreasing k_{off} was similarly observed. The previous results emphasize how the intrinsic properties of an autocrine loop can critically affect both ligand capturing and the propagation range of uncaptured ligands in the surround fluid. These unique properties of each autocrine loop will define the rate of change of complex formation between the isolated and the communicative modes as well as the range of global cell densities where we observe the most critical change of complex formation.

4.4 Discussion

We have adapted a previously developed stochastic model of autocrine signaling to investigate the impact of cell arrangement geometry on ligand capturing of various types of autocrine loops. By positioning the cell surface as square-latticed arrays of circular patches with varying patch sizes and array spacing, we were able to illustrate both the global and local impacts of cell arrangement. Our model identified two major modes of the intercellular communications in autocrine systems. The *communicative* mode occurs at high global cell densities and can be best characterized by the free exchange of secreted ligands between the adjacent cell clusters. Because of this characteristic, local impact of cell arrangement is insignificant in this spatial regime. In the *isolated* mode, cells can only bind to ligands that are self-secreted from cells within the same cell cluster and occurs at very low global cell densities. Because of its inability to interact with other cell patches, ligand binding is purely governed by the shape and size of the cell cluster. The local impact of cell arrangement therefore dominates in this spatial regime. Between these two communication modes, cells within the *critical* spatial range gradually generate complex molecules that will soon reach the maximum equilibrium value. We showed mathematically that such temporal change of complex formation occurs due to diffusive exchange of ligands via paracrine trajectories. The above results emphasize the unique interplay between local and global cell densities in governing ligand binding in autocrine systems. Such transport characteristics underlie the commonly observed change of cellular phenotypes with the alteration of cell plating densities in autocrine systems.

We also use the developed model to investigate the synergistic impacts between cell arrangement and intrinsic properties of autocrine loops in governing ligand binding. Using parameters of the TGFα/EGFR autocrine loop in A431 cells as our baseline trend, we determined changes of ligand capturing with the modulation of ligand/receptor production ratio as well as the ligand/receptor affinity. We observed that only a limited range of these intrinsic properties of autocrine loops can give rise to the full behavior of intercellular communication in autocrine systems. For example, increasing the ligand/receptor production ratios above 1,000 folds resulted in the disappearance of the *saturation* regime. On the other hand, a too large increase in receptor production can cause the cell to always remain in the saturated regime, resulting in no density-dependent changes of ligand capturing. It is interesting to find that the parameters of the unmodified TGF-α/EGFR autocrine loop in A431 cells already falls within the effective range of intrinsic parameters. Some of the engineered autocrine systems, while being customized to secrete more ligands, may not actually exhibit significant role of autocrine signaling in regulating cellular phenotypes (Joslin, Opresko et al. 2007). Our study thus provides an approach to help assess whether a specific autocrine loop already acquires critical impacts of cell arrangement and whether perturbation of a specific intrinsic parameter will in fact result in the amplification of autocrine phenomena.

It is important to recognize that our analysis and the developed model were designed to specifically characterize cells with only a single autocrine loop. In many cancer cells, the cells can acquire

multiple autocrine loops, and each will exhibit its own unique characteristics of ligand/receptor interactions and diffusive ligand exchanges. Some of the existing autocrine loops may not exert critical impact on receptor activation naturally but its effect may be amplified due to clinical intervention such as the use of therapeutics to inhibit another more dominant autocrine loop (Zhou, Peyton et al. 2006; Guix, Faber et al. 2008). To make the model more clinically relevant, one potential direction would be to expand the model to include multiple autocrine loops. Taking the ErbB-family receptor system as an example, a single receptor family can already acquire different modes of autocrine loops (Chen, Schoeberl et al. 2009). A secreted ligand can bind to multiple receptors all at once. At the same time, the cells may secrete multiple ligands. Depending on its unique binding characteristics, diffusivity in medium and relative production rate in comparison to the corresponding receptor, only a few ligand/receptor pairs may contribute more significantly to regulate a specific phenotype. A good model of an autocrine system should therefore be able to predict the dominant ligand/receptor pairing and its quantitative contribution to activate all associated receptors.

Another important physiological regulation network that should be included in models of autocrine systems is the modification of either receptor availability or ligand secretion rate with the gradually increasing receptor binding. Such intrinsic modulation of ligand/receptor production ratio can occur due to the close-looped nature of autocrine systems. It is possible that the downstream gene targets of the activated receptors could change the expression level of the signaling molecules or related enzymatic processes that in turn temporally modulate the characteristics of autocrine loops. While our model did not include this process, such rejection may be justified by the usually elongated time scale of gene expression changes (order of several hours to days). In addition to the negative feedback control due to expressional changes of the downstream gene targets, other more immediate feedback regulation may also exist (Freeman 2000). Phosphorylation of the signaling molecules by kinases is a well-regulated process and counter-balanced by the function of phosphatases. While the availability of phosphatases is assumed to be in excess during receptor activation due to exogenous ligand supply, it is unclear how phosphatase concentration may alter during autocrine activation. The JAK-STAT autocrine loops can be similarly affected by the suppressors of cytokine signaling (SOCS) which can inhibit STAT phosphorylation. While our model did not include these complicated regulatory networks, our analysis shows that this simple simulation can provides a simple platform to preliminarily estimate the potential impact of cell arrangement for the different autocrine loops. Together with our established cell-patterning methods to experimentally organize cell culture as square-latticed arrays of circular patches, we should be able to determine the importance of these complex regulatory networks and include the regulatory pathways that are essential for creating more accurate simulation.

4.5 Summary

We successfully established a mathematical model that enables our prediction of ligand capture changes with varying cell arrangement. By defining the cell surface as square-latticed arrays of circular patches with varying patch sizes and array spacing, we were able to illustrate changes of ligand binding as a function of both local and global cell density. The model predicts two distinct spatial modes of autocrine signaling with changes of cell arrangement. Ligand binding in the *isolated* mode is predicted to be critically dependent on local density, or practically the patch size and shape or cell arrays, because cells are unable to exchange ligands diffusively across the different cell patches. On the opposite end, the *communicative* mode exhibits uniform ligand capturing, independently of the array and patch designs. These insights help us acquire the appropriate cell-patterning designs to investigate impacts of autocrine signaling in maintaining cancer growth. Specifically, we can alter the array spacing while maintaining the same cultivation area and patch shape across the substrate to exhibit changes of ligand capturing due to altering global density. To study impacts of local density, we can compare the ultimate cell response among design of the same cell-covered area fraction but with altering patch designs, either size or shape.

Table 1

Cellular kinetic Parameters	Values	References
Molecular weight of TGFα	~6 kDa (soluble form) 17kDa (pre-mature form)	(Thornley and Jones 1992)
V_{LT}, TGFα production in A431	3.6 pg/10^6 cells per 20 hours 10 ng/million cells per day ~36 molecules/cell/hour	(Thornley and Jones 1992) (Reiss, Stash et al. 1991) My result
V_R, synthesis rate of EGFR in A431	72,000 sites/cell/hour	(Krupp, Connolly et al. 1982)
R_s(t=0), Steady-state surface EGFR per each A431 cell	2.5-2.8×10^6/cell 1.45-6.36×10^5/cell	(Jones, Heiss et al. 1993) (Reiss, Stash et al. 1991)
K_D, Dissociation constant between TGFα and EGFR	1.1, 1.4 nM 2.08, 10.56 nM 2.2 nM 6.3 nM	(Jones, Heiss et al. 1993) (Reiss, Stash et al. 1991) (Ebner and Derynck 1991) (French, Tadaki et al. 1995)
k_{on}, association rate constant between TGFα and EGFR	4.3×10^7±3.8×10^6 $min^{-1}M^{-1}$	(French, Tadaki et al. 1995)
k_{off}, dissociation rate constant between TGFα and EGFR	0.27±0.02 min^{-1}	(French, Tadaki et al. 1995)
k_{eR}, internalization rate constant of unbound EGFR	0.03 min^{-1}	(Wiley, Herbst et al. 1991)
k_{eC}, internalization rate constant of EGFR bound to EGF	0.022 min^{-1}	(French, Tadaki et al. 1995)
k_{eC}, internalization rate constant of EGFR bound to TGFα	Assumed same as EGF	
Fraction of degraded internalized receptors	0.45	(French, Tadaki et al. 1995)
k_{der}, Degradation rate constant (B82 cells) **In A431 cells**	0.045-0.07 min^{-1} 0.043 h^{-1}	(French, Sudlow et al. 1994) (Krupp, Connolly et al. 1982)
k_{rec}, Recycling rate constant	0.058	(Herbst, Opresko et al. 1994)
EGFR down-regulation rate in A431	$T_{1/2}$ = 2-3 hr	(Krupp, Connolly et al. 1982)
$D_{TGFα}$, Diffusion coefficient of TGFα in medium	~1.2×$10^{-10}$$m^2$/s	(Kojic, Kojic et al. 2006)

Chapter 5

Uniformly-shaped cell-patterning array as a method for determining direct autocrine impacts on cancer growth

Having developed technology to create cell cultivation platform with the precisely defined cell arrangement and investigated both local and global impacts of the relative cell positioning on ligand capture of autocrine systems, we will illustrate in this chapter the advantages of uniformly-shaped cell arrays as a method to screen for the presence of autocrine loops. We will first examine the complex interactions of signaling cues to control growth of randomly-plated cells and examine how these cues are modulated with the alteration of cell plating densities. We will then show how the uniformly-shaped cell arrays will help minimize the influences of non-diffusive signaling cues in controlling cancer growth, allowing the impact of autocrine loops to be revealed. Because we can modulate autocrine loops by simply changing geometry of cell arrays, the experiment performed in this chapter substantiates the developed platform as a general method to investigate autocrine signaling, requiring no prior knowledge of the underlying ligand/receptor pairs or any specific inhibitors.

5.1 Introduction

Since 1980 when the autocrine hypothesis was first proposed (Sporn and Todaro 1980), many autocrine loops have been discovered in various cancer types (Sporn and Roberts 1992). Even though its role in supplying mitogenic signals to cancer cells has been validated (Mendelsohn 1997; Mendelsohn and Baselga 2006), autocrine signaling has still been an ineffective target for clinical cancer treatment. Therapeutics that are designed to target autocrine loops either exhibit treatment benefits only in limited tumor types (Paez, Janne et al. 2004; Cappuzzo, Hirsch et al. 2005) or fail after long-term use (Wang and Greene 2008; Nguyen, Kobayashi et al. 2009). Gefitinib and Cetuximab are the most commonly used EGFR-targeting drugs. Gefitinib, an ATP analog, inhibits tyrosine phosphorylation of EGFR and is approved for clinical use in non-small-cell lung cancers (NSCLCs). Cetuximab, a human:murine chimeric monoclonal antibody, prevents binding of EGFR to its cognate ligands and is now commonly used in metastatic colorectal cancers. While both drugs have exhibited improved treatment efficacy over conventional chemotherapy, evidence shows that patients who initially respond to anti-EGFR therapeutics may develop tumor recurrence (Wheeler, Huang et al. 2008; Nguyen, Kobayashi et al. 2009). Such resistance was initially determined to be caused by a second mutation in the kinase domain of EGFR (Kobayashi, Boggon et al. 2005; Pao, Miller et al. 2005; Balak, Gong et al. 2006) but recent studies in NSCLCs discovered an alternative resistance mechanism without any genetic mutations. These recurring tumors instead promote their growth through alternative autocrine loops. Swapping of autocrine loops in these cells has been shown to occur among the ErbB-family receptors (Zhou, Peyton et al. 2006) or with other receptor types such as c-Met (Engelman, Zejnullahu et al. 2007) and Insulin-like growth factor receptor (Guix, Faber et al. 2008). Such emerging, unpredicted roles of untargeted autocrine loops recapitulate the need for the exploration of novel autocrine loops and their roles in maintaining cancer growth.

Due to the limited experimental methods for examining autocrine signaling, only a handful of autocrine loops have been accurately characterized as the true cause of cancer growth. Existing approaches focus on the validation of specific autocrine loops using therapeutic agents such as receptor-blocking antibodies (Lauffenburger, Oehrtman et al. 1998; DeWitt, Dong et al. 2001; Joslin, Opresko et al. 2007). These methods require prior knowledge of the underlying ligand-receptor pair as well as the availability of specific perturbing molecules. To study the potential role of autocrine loops on tumor recurrence, one requires a method that must be able to investigate both *known* and *unknown* autocrine loops. Alteration of cell seeding densities has long been used as a preliminary method to screen for autocrine phenomena. Because cells with autocrine loops can share secreted ligands with adjacent

neighbors via diffusive paracrine exchange (Oehrtman, Wiley et al. 1998; Batsilas, Berezhkovskii et al. 2003), one should be able to amplify the impacts of autocrine signaling on cancer growth by modulating these paracrine trajectories. Theoretically, ligand sharing can be promoted by simply decreasing the diffusion distance between cell neighbors. Practically, this requirement has been obtained by altering seeding densities in the randomly-plated culture (Oehrtman, Wiley et al. 1998). Unfortunately, previous studies showed that changes of cell plating density can also modulate other environmental cues. For example, in endothelial and smooth muscle cells, the variation of cell seeding density was found to affect both cell morphology and cell-cell contact (Nelson and Chen 2002). Densely plated cells were found to acquire more direct cell-cell contacts but reduced cell spreading. Because of the more dominant impact of cell morphology, these cells are commonly observed to exhibited growth arrest at high seeding density. Using a defined cell localization technique to maintain uniform cell spreading, an increase in cell-cell contacts was found to actually promote growth (Nelson and Chen 2002). In human mammary epithelial cells, proliferation is controlled by a complex interplay between cell-cell contacts and diffusible signaling cues (Kim, Kushiro et al. 2009). Direct cell-cell contacts give rise to growth inhibition, but only when the concentration of the necessary growth factor lies below the required threshold. These studies illustrate the complex interactions of environmental cues to regulate cell growth and emphasize difficulties in examining the contribution of a specific cue without the appropriate normalization of growth effectors.

This chapter examines how autocrine signaling and its interaction with other environmental cues influence cancer growth changes. Combining cell patterning technology, high-throughput single-cell imaging, and mathematical modeling, we present a novel platform for investigating the contribution of autocrine signaling in promoting cancer growth. With the availability of cell patterning technology to precisely localize cells on the substrate, we hypothesized that the arrangement of cells as arrays of uniformly-shaped patches would help equalize growth-affecting impacts of non-diffusive signaling cues. The modulation of paracrine exchanges of self-secreted ligands can then be achieved by altering the array spacing. We chose to work with the A431 cell line, epidermoid carcinoma cells that are known to express the TGFα/EGFR autocrine loop (Van de Vijver, Kumar et al. 1991; Fan, Lu et al. 1994) for two reasons. First, A431 cells overexpress EGFR, a genetic lesion that is commonly observed in various cancer tissues (Mendelsohn and Baselga 2006). Second, EGFR is a member of the ErbB-family signaling cascade, the best characterized mitogenic pathway (Wiley, Shvartsman et al. 2003). To test our hypothesis, we first examined the interactions of growth-affecting cues in randomly-plated culture. Our results showed that the observed density-dependent growth change was not mainly contributed by EGFR autocrine loops while contact-mediated cues through E-cadherin was found to cause growth arrest at high plating densities. Then, using stencil cell patterning to precisely localize cells, we showed that the uniformly-shaped cell culture can reduce heterogeneity of non-diffusive signaling cues while still enabling the variation of global cell density. Arrays of uniformly-shaped cell patches were found to exhibit increasing cell growth with decreasing array spacing. We then developed a mathematical model to explain how changes in cell positioning systematically affect diffusive exchanges of secreted ligands. Our study validates the modulation of autocrine impacts by the simple change of intercellular spacing, but only when the impacts of other signaling cues are normalized, and provides a platform to screen for cancer cells that critically rely on autocrine loops in sustaining their growth.

5.2 Results

Randomly-plated cell culture as inaccurate platform for exhibiting autocrine activity

While the alteration of cell seeding density has been a common approach to screen for the presence of autocrine loops, its ability to validate quantitative characteristics of autocrine signaling is hampered by the fact that phenotypes such as cell growth are influenced by multiple environmental cues, each of which changes with cell density. Because of the non-uniform cell arrangement in randomly-plated cell cultures, we hypothesized that various signaling cues would be varyingly perturbed by the modulated cell seeding densities, making it very difficult to determine changes and contribution of a particular signaling cue in controlling the ultimate cell response. Using A431 cells as our model autocrine system,

we began by investigating the efficacy of seeding-density modification as a method to uncover the influence of autocrine loops on growth regulation. Plating cells at various starting densities and then allowing them to grow for 72 hr, we observed a non-monotonic growth change with varying seeding densities (Figure 5-1A). Specifically, we found an increase in cell growth at plating densities up to ~5,000 cells/cm^2. Above this critical density, fold growth decreases gradually with increasing seeding density.

To examine the possible contribution of autocrine signaling on the observed density-dependent growth change, we chose to specifically investigate the role of the EGFR autocrine loop because of the known presence and critical role of the TGFα-EGFR autocrine loop in A431 cells (Derynck, Goeddel et al. 1987; Van de Vijver, Kumar et al. 1991). It has been shown that the anti-EGFR monoclonal antibody 225 (mAb225) can inhibit growth and reduce intrinsic ERK activation in A431 cells (Masui, Kawamoto et al. 1984; Mendelsohn, Masui et al. 1987). A recent study also showed that the physical interaction between Cetuximab (the human chimeric form of mAb225) and the domain III of EGFR structurally occludes binding of EGFR to its cognate ligands (Li, Schmitz et al. 2005). If the EGFR autocrine loop is the sole contributor of the observed density-dependent growth change, fold growth should be independent of cell density during the cultivation with mAb225. Using a saturating dose of mAb225 (450 nM), we observed a general decrease in cell growth at all plating densities, but the density-growth relationship still exhibited a density-dependent and non-monotonic trend (black circles, Figure 5-1A). To ensure that the observed result was not caused by the limited sensitivity of bulk cell counting, we also determined growth changes

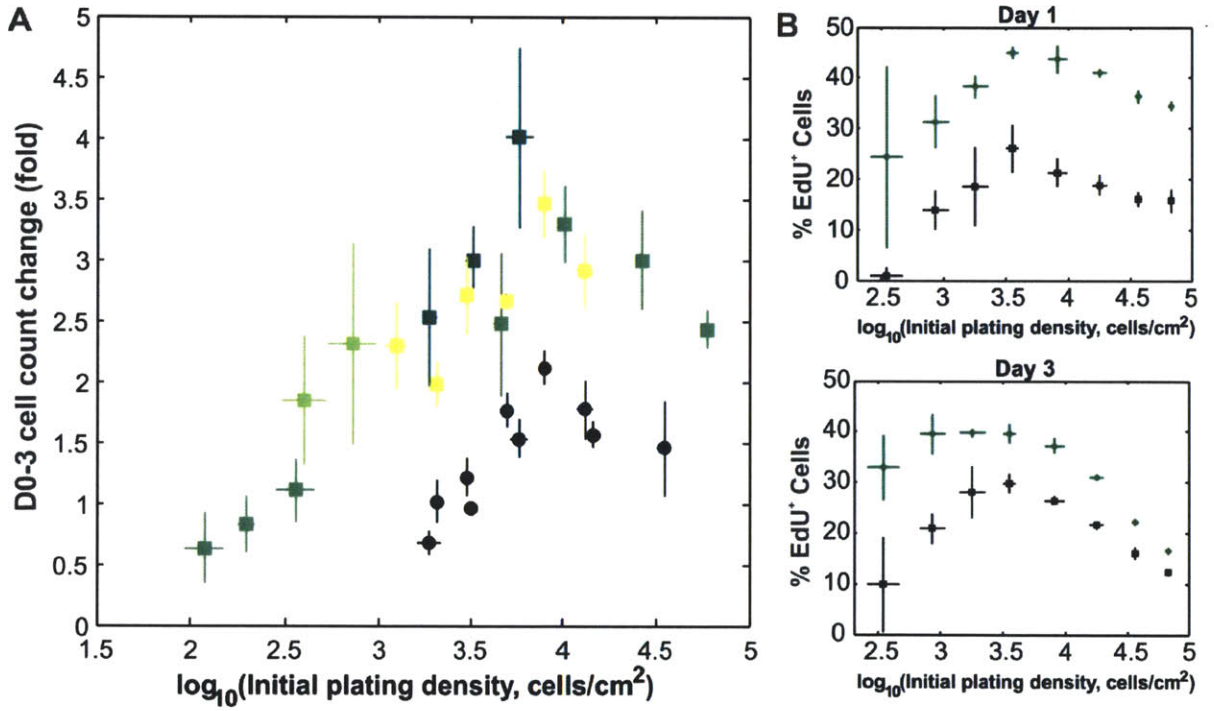

Figure 5-1 Growth change with the alteration of initial plating density of randomly-plated cells
A) Change of cell growth at varying plating densities as quantified by bulk cell counting with Coulter counter. Cells were initially plated in serum-containing media to ensure uniform cell attachment at all plating densities. After 24-hour serum-starvation, cells were cultivated for another 72 hours in serum-free medium alone (colored square) or with addition of 450-nM mAb225 (black circle). The color of the square dots represents experiments on different days with different passage number. Error bars represent standard deviations from at least two biological replicates. B) Growth change with altered plating density as quantified by single-cell analysis of EdU incorporation at 24 and 72 hours after serum-starvation. Cells were cultivated in serum-free medium alone (green diamond) or with 450-nM mAb225 (black square). Error bars represent standard deviations from five biological replicates.

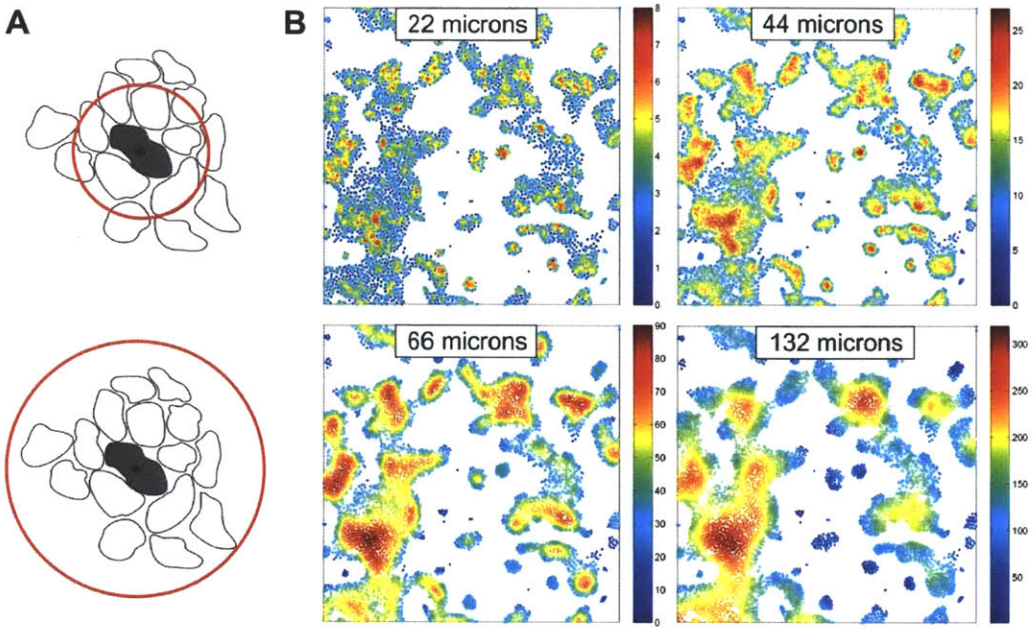

Figure 5-2 Experimental measurement of local cell density
A) Measurement of local cell density with two different neighbor radii. Small neighbor radius can be used to investigate signaling cues with spatially-limited effects. Larger neighbor radius enables the investigation of signaling cues with broader spatial operation. B) Spatial distribution of neighbor counts at four different neighbor radii. Color represents the ranges of neighbor counts.

with altering plating densities using EdU incorporation, which, like BrdU, gets incorporated into newly synthesized chromosomes during S phase. The results still exhibited a non-monotonic variation of EdU^+ fraction with plating density at both 24 hours and 72 hours (Figure 5-1B). Interesting, we observed that the impacts of growth reduction with increasing plating density becomes even more pronounced at 72 hours. Below the critical density of ~5000 cells/cm^2, the EdU^+ fractions change more slowly with the elevated plating density while growth of cells above the density of 30000 cells/cm^2 is found to decrease to almost half of the EdU^+ fraction at 24 hours. Addition of mAb225 was found to decreases the EdU^+ fraction at all plating densities while still maintaining the non-monotonicity. These results illustrate the significant role of the EGFR autocrine loop in promoting A431 cell growth but also show that we cannot presume the presence of autocrine loop based only on the observed growth change with altering initial plating densities. In the case of A431 cells, we instead showed that the density-dependent growth change must be contributed more significantly by other environmental cues.

Because of the spatially-limited nature of autocrine loops and the non-uniform cell arrangement in the randomly-plated culture that can give rise to heterogeneous cell clustering, it is possible that we might still be able to illustrate the presence of autocrine loops by determining changes of cell growth with local cell density. Experimentally, we can approximate local cell densities from the distribution of neighbor counts based on the different pre-defined neighbor radii (Figure 5-2). Using the neighbor radius of 44 microns, we observed both the similar and the differing characteristics from day-1 and day-3 samples (Figure 5-3). First, we observed diminishing cell growth with the increasing number of neighbors at both time points. Nonetheless, day-1 samples at all plating densities seem to exhibit the same density-growth change relationship. On day 3, however, densely-plated cells exhibit less EdU^+ incorporation than sparsely plated cells at all local cell densities. These results show the temporal amplification of the growth decrease with increasing cell densities (both local and global length scales). In comparison to cell culture in serum-free medium alone, addition of mAb225 causes growth decrease at all local and global densities, but still exhibits more pronounced density-dependent growth inhibition at later cultivation time. Overall, our

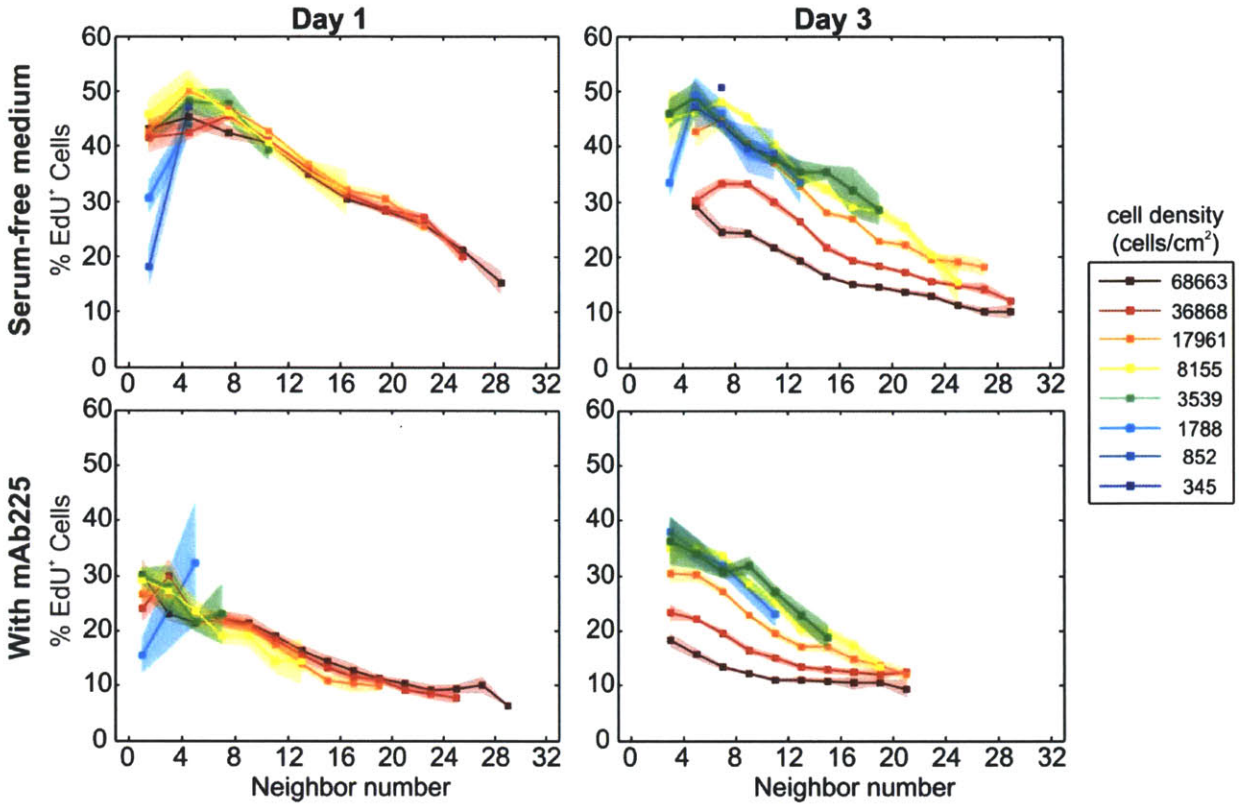

Figure 5-3 Growth change with varying local density
Changes of EdU incorporation with varying neighbor number at different initial plating densities when A431 cells were cultivated in serum-free medium alone or with saturated mAb225. The colored regions represent ranges of the 95% confidence intervals. The legend illustrates the corresponding initial plating densities (cells/cm^2). The number of neighbors was analyzed using the neighbor radius of 44 microns.

analysis of phenotypic changes with altering local cell density still exhibits the density-dependent growth change that does not correspond directly with the predicted effects of the EGFR autocrine loop (should promote A431 growth). The presence of autocrine loops in A431 cells thus cannot be directly inferred from the observed growth change with either local or global cell densities. To validate the presence of EGFR autocrine loops in the randomly plated culture, we still require specific inhibitors such as the receptor-blocking antibodies to directly perturb autocrine loops.

Cell-cell contacts exhibit both negative and positive roles on growth of randomly-plated A431 cells

To validate the role of non-diffusive signaling cues on the observed density-dependent growth change, we decided to investigate the role of contact-mediated signaling. Alteration of cell seeding densities has been illustrated to affect EGFR binding to the exogenously supplied EGF in A431 cells (Lichtner and Schirrmacher 1990). Cell-cell contacts that increase with the elevated plating densities were shown to cause biased EGFR localization to cell junctions and the decrease in the total number of high-affinity EGF receptors. Additionally, direct attachment of spatially isolated cells to E-cadherin-coated microspheres was observed to cause growth arrest in A431 cells (Perrais, Chen et al. 2007). These studies substantiate the significant role of contact-mediated cues in regulating A431 growth. The anti-E-cadherin monoclonal antibody SHE78-7 was shown to effectively prevent E-cadherin function in colon, breast and lung carcinoma cells, giving rise to growth recovery in a dose-dependent manner (St Croix, Sheehan et al. 1998). To investigate the role of E-cadherin-mediated cell adhesion in regulating A431 growth, we examined growth change as a function of both local and global cell density in the presence of varying doses of SHE78-7. After cultivating the cells with the addition of SHE78-7 for 3 days, we found that inhibition of E-cadherin-mediated cell adhesion causes distinctly different growth changes between low

and high plating densities (Figure 5-4A). With increasing doses of SHE78-7, cells at high plating densities exhibit an increase in mean EdU signals while sparsely plated cells demonstrate decreased growth (mean EdU signals are used here to enable statistical mean comparison among different wells). In other words, E-cadherin-mediated cell-cell contacts were found to inhibit cell growth at high plating densities but can also promote growth of spatially isolated cells.

When we examined growth change as a function of local cell density, the EdU^+ fractions become less dependent on the global cell density with increasing concentration of SHE78-7 (Figure 5-4B); changes of EdU^+ fractions with altering local density collapse onto one similar trend with increasing inhibition of

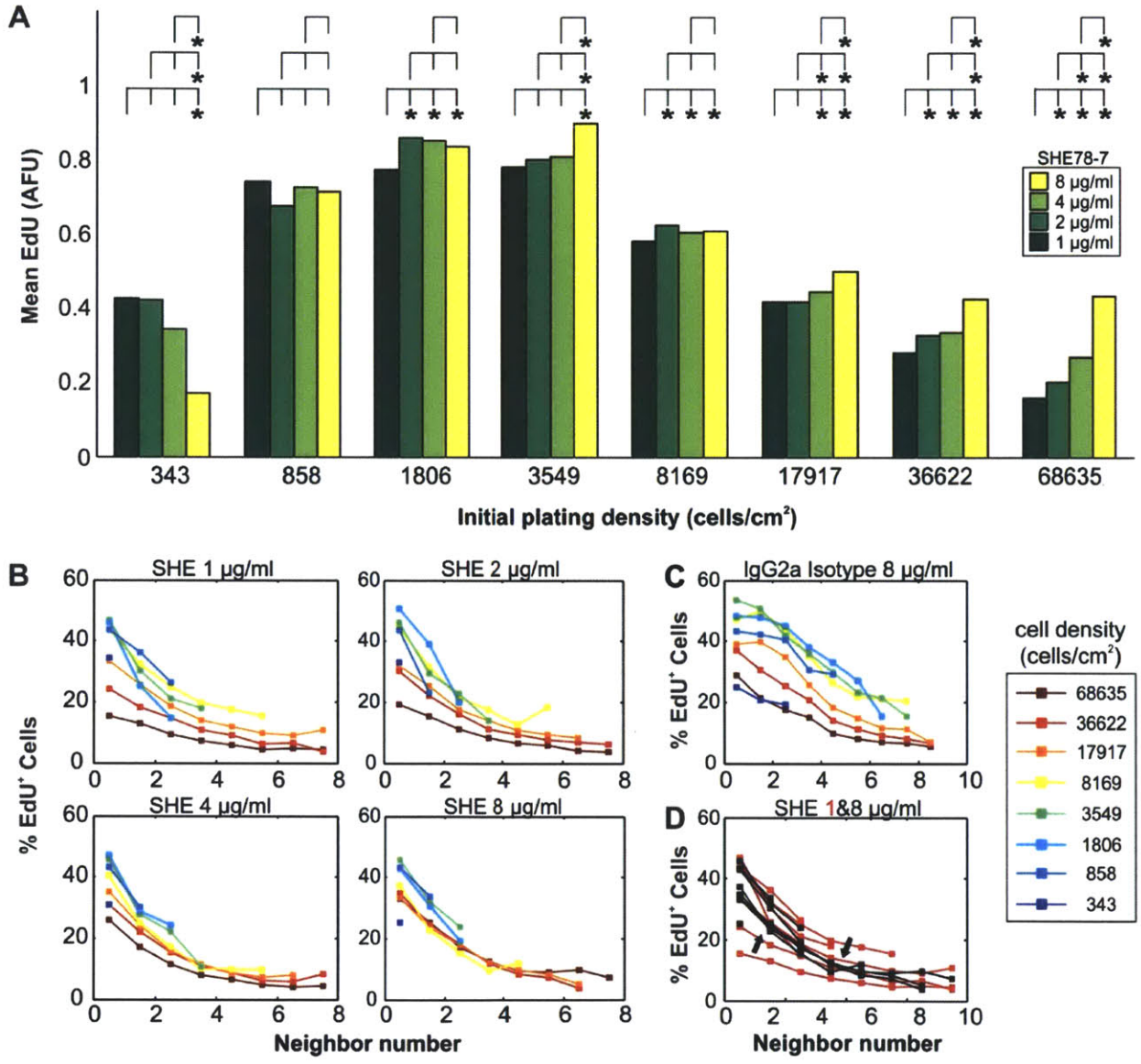

Figure 5-4 Effects of contact-mediated signaling on the density-growth relationship
A) Changes of EdU incorporation with varying global cell densities and doses of SHE78-7 (from 1-8 µg/ml). *, significantly different with $p<0.05$. B) Changes of EdU incorporation with varying local cell densities in the presence of SHE78-7. C) Changes of EdU incorporation with varying local cell densities using IgG2a isotype control. D) Overlaid results with 1 µg/ml (red) & 8 µg/ml (black) of SHE78-7. B-D) Legend annotates the corresponding initial plating densities (cell/cm^2) and the number of neighbors was analyzed using the neighbor radius of 22 microns.

E-cadherin. The curves of local density-EdU$^+$ fraction relationship at high plating densities shift downwards while those of low-density cells shift upwards (Figure 5-4D). Regardless of the diminishing role of global cell density with the inhibition of E-cadherin binding, we can still observe a decrease in EdU$^+$ fractions in cells with more neighbor number at any doses of SHE78-7 and at any global cell density. The persisting growth inhibition of cells with more neighbors can arise from two major reasons. First, it is possible that we did not add enough SHE78-7 to fully inhibit E-cadherin function. Alternatively, such growth inhibition may arise due to other environmental cues that may also function at the similar length scale as E-cadherin-mediated signaling.

We tested the first hypothesis by culturing cells with higher dose of SHE78-7 (25 μg/ml) and also examined both early (1 day) and late (3 days) responses (Figure 5-5). Results were also compared with the addition of EGFR-neutralizing antibody, the mAb225. Similar to our previous experiment (Figure 5-4A), addition of SHE78-7 reduces growth at low plating densities but promotes growth of densely-plated cells, although its growth inhibiting effect only becomes prominent at day 3 (compare %EdU$^+$ at densities aove

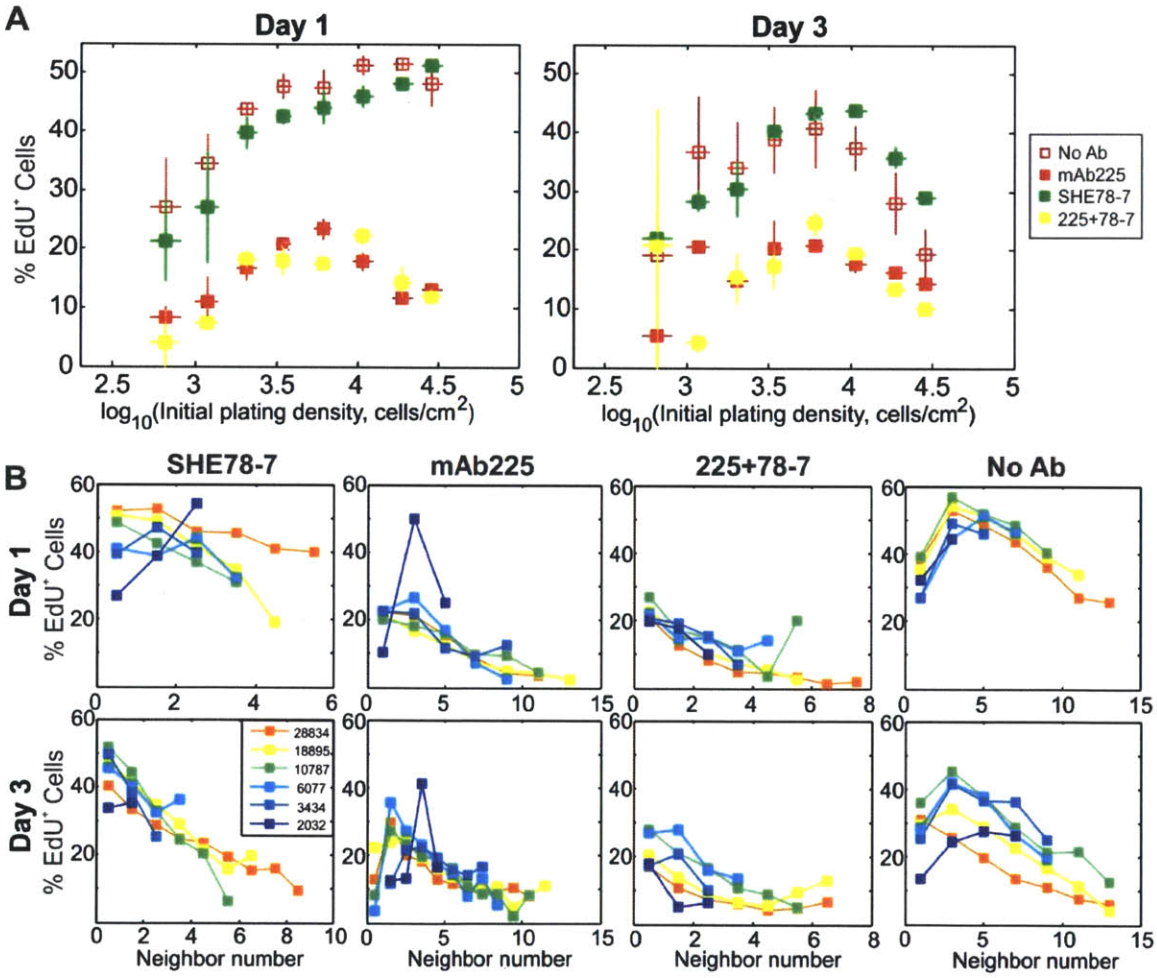

Figure 5-5 Density-dependent growth change with double neutralizing antibodies
A) Changes of EdU incorporation with varying global cell densities for various cultivating conditions including: serum-free medium alone (unfilled red), with 450-nM mAb225 (filled red), with 25-μg/ml SHE78-7 (green), with both mAb225 and SHE78-7 antibodies (yellow). EdU incorporation was determined at both day 1 and day 3 after serum starvation. B) Changes of EdU incorporation with varying local cell densities for various cultivating conditions. Legend annotates the corresponding initial plating densities (cell/cm^2). The number of neighbors was analyzed using the neighbor radius of 22 microns.

10000 cells/cm^2 between green solid squares versus red unfilled squares in Figure 5-5A). Cultivation of cells with both SHE78-7 and mAb225 exhibits a similar growth inhibiting effect as when using saturating mAb225 alone; growth diminishes almost equally at all plating densities (compare yellow and filled red squares with unfilled red squares in Figure 5-5A). We then attempted to distinguish effects of different neutralizing antibodies by analyzing changes of EdU incorporation with varying local cell densities (Figure 5-5B). Addition of 25-μg/ml SHE78-7 seems to help minimize the growth-inhibiting impact of E-cadherin at the local length scale at day 1 but its effect becomes dominated by the more pronounced role of growth inhibition at day 3, only functioning to exhibit a collapsed density-growth relationship (compare results of SHE78-7 between day 1 and day 3 in Figure 5-5B). Effects of mAb225 are comparable to other previous studies (compare results from the addition of mAb225 between Figure 5-3 and Figure 5-5B). Overall, we still observe the diminishing growth with increasing local cell densities from all cultivating conditions (Figure 5-5B). Because our simultaneous inhibition of both EGFR autocrine loop and E-cadherin-mediated cell adhesion still cannot negate the non-monotonic changes of cell growth with cell plating density, we think that environmental cues other than these two pathways must exist and also play a critical impact on the observed growth change with altering plating densities. Nonetheless, our previous studies have proven the growth promoting effect of EGFR autocrine loop at all plating densities and the temporally increasing effects of E-cadherin, especially to inhibit A431 growth at high plating density.

Changes of autocrine ligand capturing with the altered plating densities

Our previous analyses show that we cannot validate the presence and determine the quantitative contribution of EGFR autocrine loops in promoting A431 cell growth from only monitoring changes of cell growth with altering local or global cell densities (Figure 5-1). We can only illustrate contribution of the EGFR autocrine loop in promoting A431 cell growth when comparing cell growth with and without the EGFR-neutralizing antibody (Figure 5-3). Because of the existing roles of other signaling cues, it is difficult for us to interpolate from changes of cell growth whether capturing of the autocrine ligand in fact varies with the elevated plating densities. To determine whether changes of the intercellular spacing can actually modulate paracrine trajectories of the secreted ligands, we directly measure the capturing of EGFR ligands, TGF-α and Amphiregulin, with altering cell plating density. Expression of TGF-α has previously been reported as the primary EGFR ligand in A431 cells (Derynck, Goeddel et al. 1987; Thornley and Jones 1992), although Amphiregulin has been shown to be secreted only by keratinocytes, which are similar epithelial cells (Piepkorn, Lo et al. 1994). We determined the amount of captured EGFR ligand by comparing the amount of ligand in the supernatant after cultivation with and without mAb225 (Figure 5-6). With saturating concentrations of mAb225, none of the secreted ligands can bind to EGFR on the cell surface but instead will be left in the supernatant. We define this measurement as the *total* ligand secretion, C_L^{total}. Without the antibody to block EGFR binding, some ligand will be captured and consumed by both originally secreting cells and adjacent cells, releasing a net discharge of ligand into the supernatant, defined here as *net* ligand secretion, C_L^{net}. We can then calculate the fraction of captured ligands (F_{LC}) by cells from $1 - (C_L^{net} / C_L^{total})$.

We find that A431 cells secrete both TGF-α and Amphiregulin and that the F_{LC} for both ligands are density-dependent (Figure 5-6B). The discrepancy between the per-cell and per-well calculation of F_{LC} could occur due to the variation of ligand secretion rate with time as a result of possible feedback regulators of cell growth. The TGF-α/EGFR autocrine loop exhibits an increase in F_{LC} from 0.1-0.6 at 1900 cells/cm^2 to ~1 at 35,000 cells/cm^2. In contrast, the Amphiregulin/EGFR autocrine loop has a more modest increase in F_{LC}, changing from 0.6-0.8 at 1900 cells/cm^2 to 0.8-0.9 at 35,000 cells/cm^2. Because of the larger increase in F_{LC} of TGF-α with increasing global cell density, it is likely that the TGF-α/EGFR interaction may function as the more dominant autocrine loop in causing growth changes with altered plating density. On the other hand, because the F_{LC} of Amphiregulin only increases slightly with changing global density (F_{LC} change of 0-0.3), the Amphiregulin/EGFR interaction may contribute to the observed general increase in A431 growth during serum-free cultivation all plating densities. It is also interesting that almost all secreted TGF-α was recaptured by the cells at the highest plating density (F_{LC}=0.91-0.92) while Amphiregulin only reached a maximum F_{LC} of 0.8-0.9 (p=0.08 when assuming equal variance).

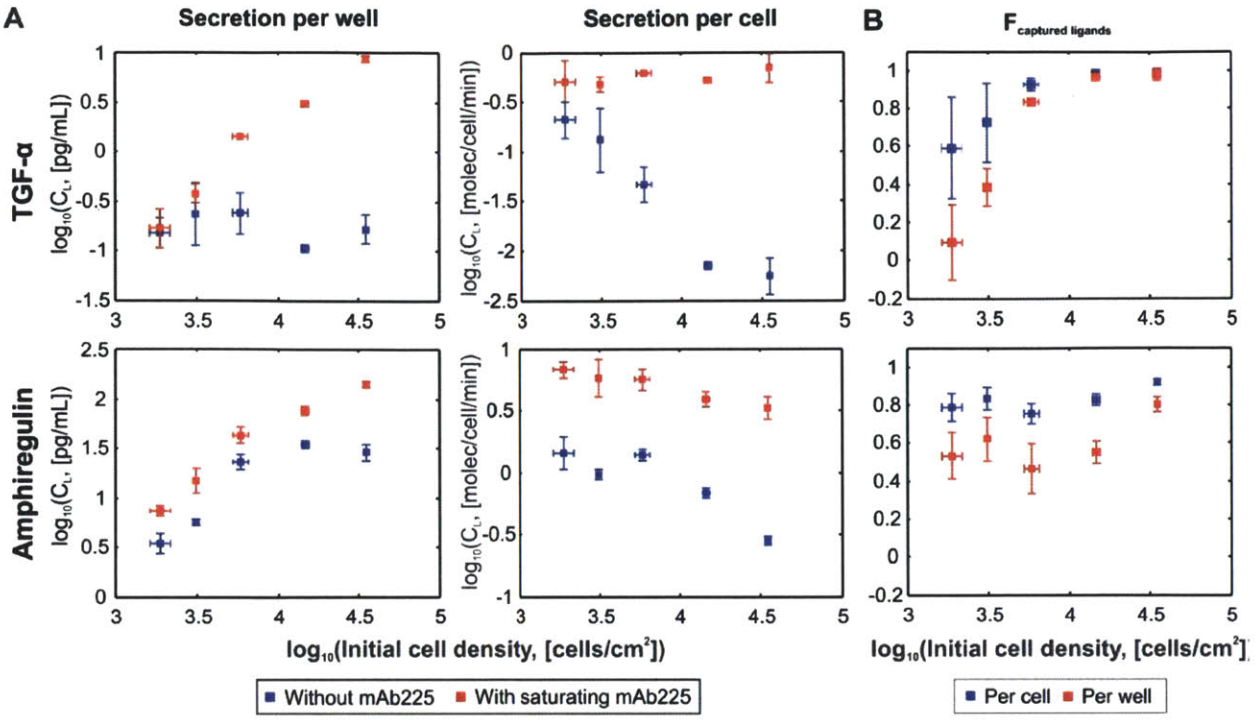

Figure 5-6 Accumulation of secreted EGFR ligands at varying initial plating densities
Cells were cultivated for three days in serum-free media with or without EGFR-blocking antibody 225. The amount of TGF-α and Amphiregulin was quantified using ELISA. A) Concentration of accumulated ligands in the supernatant after three-day cultivation in serum-free medium alone (blue square dots) or with saturated mAb225 (red square dots). Measurements were obtained as concentration per well or normalized by the endpoint cell count of each medium condition and the total cultivation time to obtain ligand secretion rate per cell. B) The calculated fraction of of captured ligands for both TGF-α and Amphiregulin. Both per cell (blue) and per-well (red) F_{LC} were obtained for all tested plating densities, demarcating the tentative range of actual ligand capture. Error bars in all plots represent propagated standard deviations from two biological replicates.

This observation is consistent with the 3× lower affinity of Amphiregulin versus TGF-α to EGFR (Shoyab, Plowman et al. 1989). This previous analysis of EGFR ligand capture illustrates the increasing autocrine ligand capture with modulated intercellular spacing even though we could not observe the corresponding phenotypic changes from the measurements of growth in randomly-plated cell culture.

Arrays of uniformly-shaped cell patches reveal impacts of autocrine signaling on A431 growth

Our previous analysis illustrated the limitation of randomly-plated cell culture to exhibit the direct contribution of autocrine signaling in promoting cell growth. With the availability of cell-patterning technology to precisely localize cells on the culture substrate, we were interested in developing a cell cultivation method that can ensure uniformity of non-diffusive signaling cues while the intercellular spacing is being modulated. We hypothesized this platform would help disclose impacts of intrinsic diffusive signaling cues on growth regulation while we alter the global cell densities. Among the existing methods to perform cell patterning (Folch and Toner 2000), stencil cell patterning emerges as the most suitable practice for our study (Folch, Jo et al. 2000). Microstamping enables the fabrication of cell patterns with more complex shapes, but this technique typically limits cell growth to the originally defined adhesive area, which is undesirable for our studied phenotype like cell growth (Tan, Tien et al. 2002; Nelson, Raghavan et al. 2003). Stencil cell patterning, on the other hand, involves the use of a single elastomeric membrane with predefined through-holes that match the intended cell locations (Figure 5-7A).

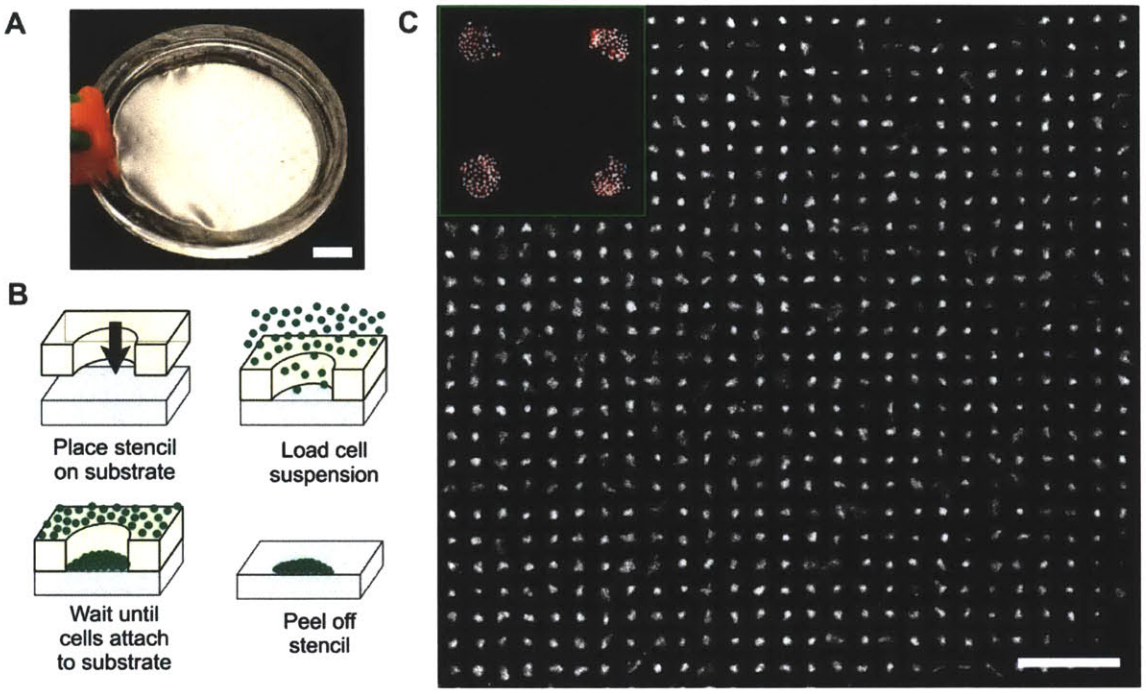

Figure 5-7 Stencil cell patterning
A) A finished stencil made of PDMS. Scale bar, 5 mm. B) To pattern cells with a stencil, we first place the stencil on an ethanol-wetted substrate to ensure its full conformal contact. Cell suspension is then loaded onto stencil in a carbon dioxide-filled chamber to prevent bubble formation within each well. After cells land into each microwell and attach to the substrate, stencil can be peeled off, leaving behind the cells on the substrate. C) Precise positioned cells across a large substrate area using stencil patterning technique. The pattered cells can grow naturally outside their original circularly-shaped area. Scale bar, 2 mm.

To pattern cells with a stencil, we place stencil on top of the regular tissue culture substrate. Cells that can sink into the stencil holes will be able to attach to the bottom substrate. After peeling the stencil off, precisely defined cell constructs are left on the substrate (Figure 5-7B). This method enables us to precisely localize cells in such a way that they can grow beyond their originally patterned sites across a large substrate area (Figure 5-7C).

In order to develop a platform for investigating autocrine signaling using cell-patterning, we had to incorporate several features into the platform to enable the isolation of diffusive signaling cues from other growth-influencing regulators. We localized cells initially as circular patches of a uniform size across the whole substrate area so that we can maintain non-diffusive signaling cues constant across the whole array. Cell patches were positioned as square-latticed arrays to ensure consistent spacing between the adjacent patches and to simplify image acquisition and post-experimental referencing. To modulate the diffusive exchange of secreted ligands, we varied array spacing while maintaining the same cultivation area to achieve the equivalent plating densities of 200-20,000 cells/cm^2, the global density range that we previously observed critical changes in cell growth. These global densities are also equivalent to the patch spacings of ~60 to 5 patch radii and cell-covered area fractions (σ) of 10^{-4} to 0.1 (Figure 5-8). Another feature critical to our approach is that we design each patch to contain multiple cells. Although arrays of isolated cells may appear to help prevent complex growth regulation due to contact-mediated cues, cells will eventually divide within the time scale of our study and acquire cell-cell contacts. Additionally, as opposed to single-cell arrays which are technically quite challenging to robustly form across large areas,

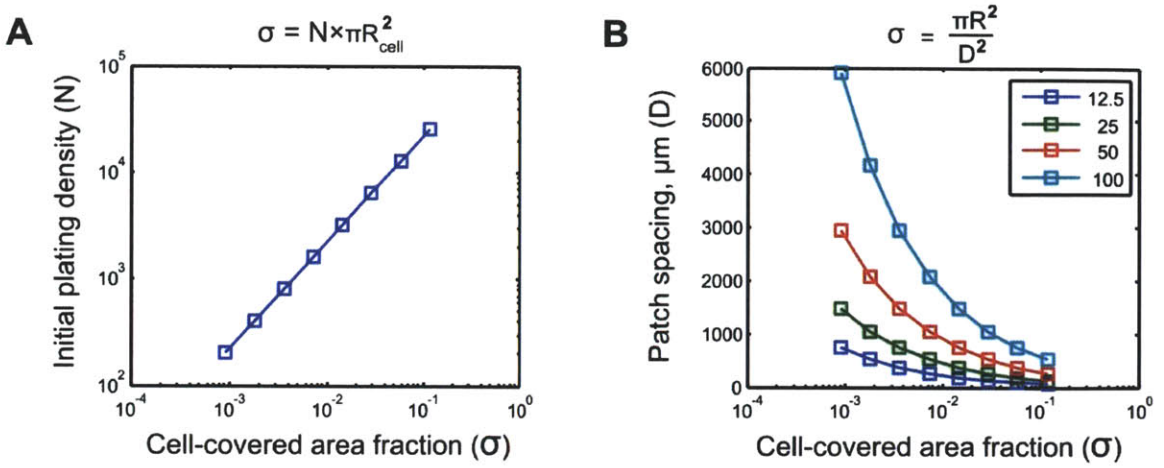

C

R [μm]	Patch spacing(in mm) for varying initial plating densities (N)							
	200	400	800	1600	3200	6400	12800	25600
12.5	0.7366	0.5208	0.3683	0.2604	0.1841	0.1302	0.0921	0.0651
25	1.4731	1.0417	0.7366	0.5208	0.3683	0.2604	0.1841	0.1302
50	2.9463	2.0833	1.4731	1.0417	0.7366	0.5208	0.3683	0.2604
100	5.8926	4.1667	2.9463	2.0833	1.4731	1.0417	0.7366	0.5208

Figure 5-8 The design of uniformly-shaped cell arrays
A) Assuming that cells within each patterned cell patch acquire the same area per cell (a circle with radius of 12 microns), we can convert the equivalent initial cell seeding density to cell-covered area fraction (σ) from $\sigma = N \times \pi R_{cell}^2$. B) Because of the symmetry of our square-latticed cell arrays, we can also determine the appropriate patch spacing for a specific patch size (R) and σ from $\sigma = \pi \times R^2 / D^2$. C) List of the calculated patch spacing for varying patch sizes and different equivalent cell seeding densities.

multi-cell patches can be easily fabricated with stencils. Third, the multiple cells-per-patch design provides an experimental setting that is more similar to the actual tumor microenvironment, where cells always are in close contact with their adjacent neighbors. Finally, our results with E-cadherin blocking antibody (Figure 5-4) demonstrate that A431 cells also need cell-cell contacts, likely to ensure cell survival. Our study used 100 μm radius patches, which corresponds to ~30-70 cells per each patch. Because of the possible discrepancy in cell number among the different patches, we developed an A431 cell line with a nuclear reporter protein (cyan fluorescent protein fused with a nuclear localization signal). This clone enabled us to accurately determine changes in cell number of each cell patch.

Using the developed cell-patterning platform, we examined changes of cell growth with altering array spacing. We found a general increase in cell growth with increasing global cell density (Figure 5-9A). Unlike randomly plated cells, the uniformly-shaped cell arrays did not exhibit growth reduction above the previously identified critical density of 5000 cells/cm^2. To validate the observed growth change, we also examined EdU incorporation. We found that the cell arrays exhibited increases in the EdU$^+$ fractions with increasing global density (Figure 5-9B), consistent with the previously determined increase in EGFR ligand binding (Figure 5-6B). Intriguingly, however, growth reduction could still be observed with increasing number of neighbors at all array spacing (and hence global densities) (Figure 5-9B). These results can be directly observed from the increasing EdU incorporation with increasing global cell density in the raw images (Figure 5-9C). The local density-dependent growth inhibition was not totally unexpected because our patches were specifically designed to incorporate cell-cell contact, which can inhibit growth. Instead, the results illustrate the ability of our cell-patterning platform to better maintain

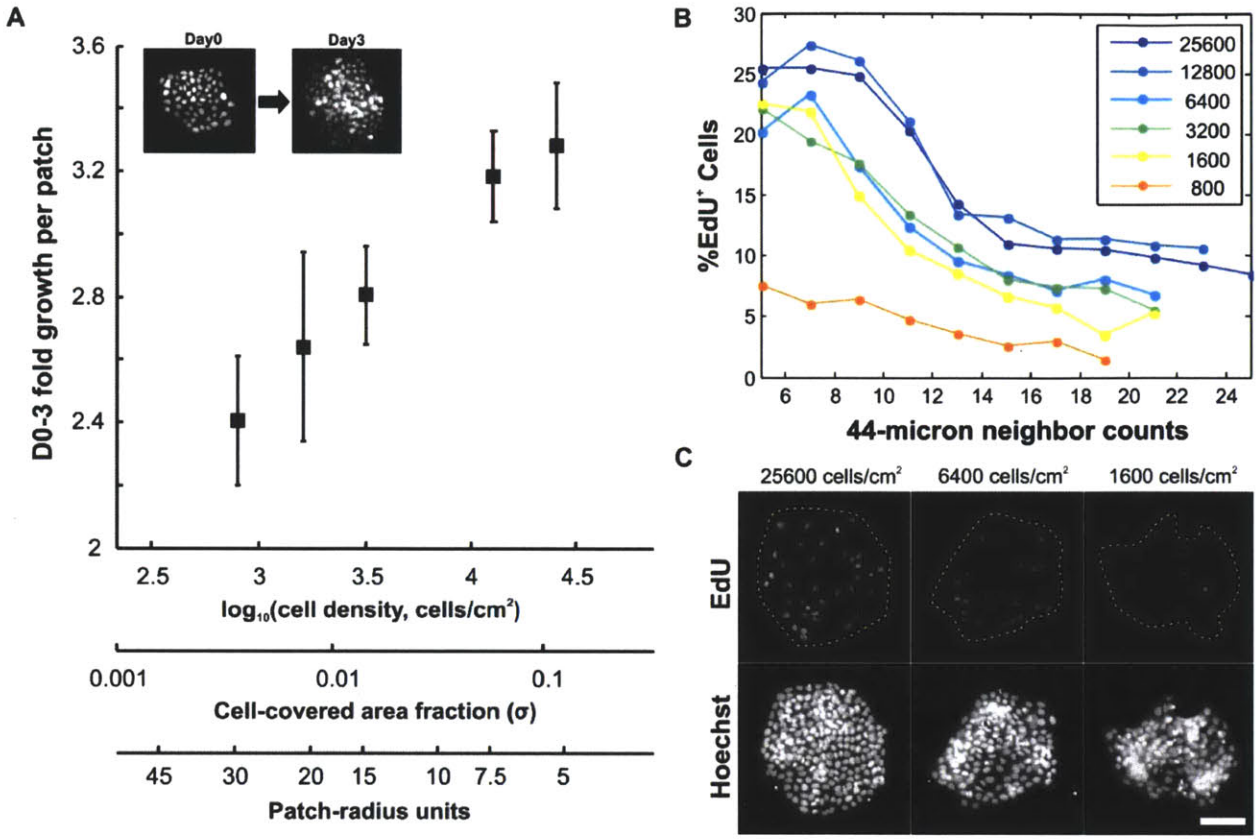

Figure 5-9 Density-dependent growth change of regularly-spaced cell arrays
A) Averaged cell count per patch after 3-day cultivation in serum-free medium at varying global cell densities. Analysis of change in cell count was obtained by direct cell counting from live nuclear reporter (CFP-NLS). The corresponding patch-radius units and the fraction of cell-covered area are also presented. Error bars represent the 95% confidence intervals from at least 30 patches. B) Changes of EdU incorporation with increasing neighbor counts at different initial plating densities (cells/cm^2). Each bin of neighbor counts obtained at least 50 cell members from different patches. C) Original images of EdU incorporation and stained nuclei at three different plating densities. Scale bar, 100 μm.

equal impacts of non-diffusive signaling cues (rather than getting rid of them), enabling growth to be more responsive to the predicted increase of autocrine ligand capture with increasing global cell density. This feature of patterned cell arrays likely stems from their ability to maintain a more homogenous distribution of local density at varying global densities, while randomly-plated cultures exhibit a dramatic discrepancy in local density distribution with increasing plating densities (Figure 5-10) . While we observe similar distributions of neighbor numbers from the two cultivation platforms when using small neighbor radius (22 microns), the distribution of neighbor number with the longer neighbor radius (88 microns) clearly illustrates the ability of cell patterning platform to establish cell culture with more uniform local cell density even with increasing global cell densities. The previous experiments substantiate the use of regularly-shaped cell arrays as an alternative cell cultivation method where the presence and contributions of autocrine loops in promoting cancer growth can be accurately determined without using specific perturbation therapeutics.

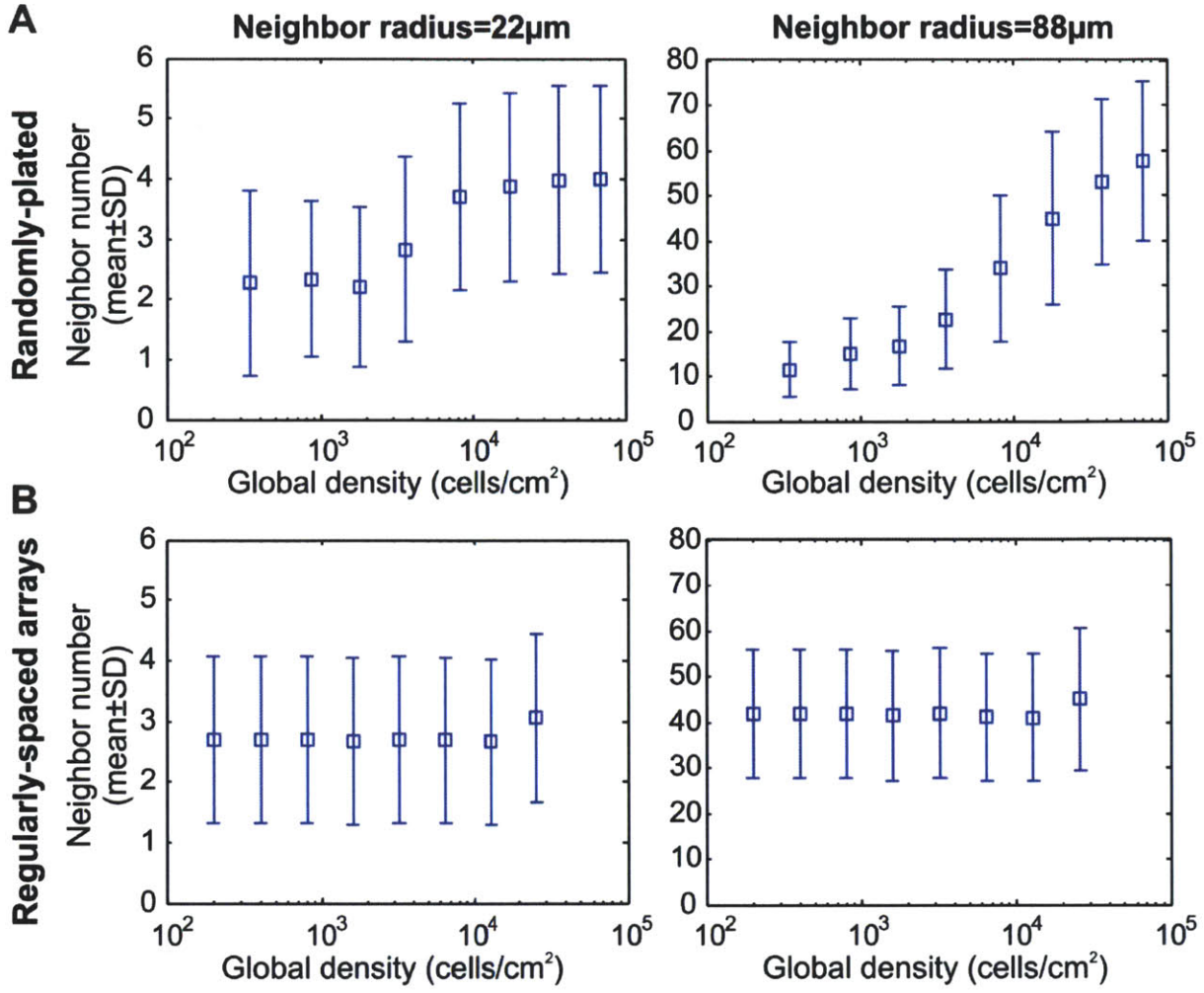

Figure 5-10 Neighbor count distribution of randomly-plated and patterned cell patches
Changes of local cell density with the alteration of global cell density were determined from the histograms of neighbor counts with varying cell plating densities in randomly plated cell culture (A) or equivalent seeding densities in the uniformly-shaped cell patches (B).

Mathematical prediction of autocrine ligand capture for varying cell-positioning configuration

To better understand how modulation of cell arrangement affects the diffusive exchange of secreted ligands in different autocrine systems, we also developed a stochastic model of autocrine signaling that can predict changes in ligand/receptor binding from any input cell-positioning configurations. Using the boundary homogenization technique and the stochastic modeling approach developed by Shvartsman and colleagues (Batsilas, Berezhkovskii et al. 2003; Monine, Berezhkovskii et al. 2005), we can determine changes of ligand/receptor capturing and ligand accumulation in the supernatant for any geometric configurations of our square-latticed arrays of circular patches (described in more detail in Chapter 4).

We used the developed model to examine how autocrine ligand/receptor interactions vary when we systematically modulate the array spacing and the patch radius. With a fixed patch radius but varying array spacing, we observed an exponentially decreasing net ligand secretion per cell with increasing global density (Figure 5-11A). This trend implies an increase in ligand capturing that can be directly observed from the analysis of F_{LC} change with varying global cell densities (Figure 5-11B). An abrupt increase in

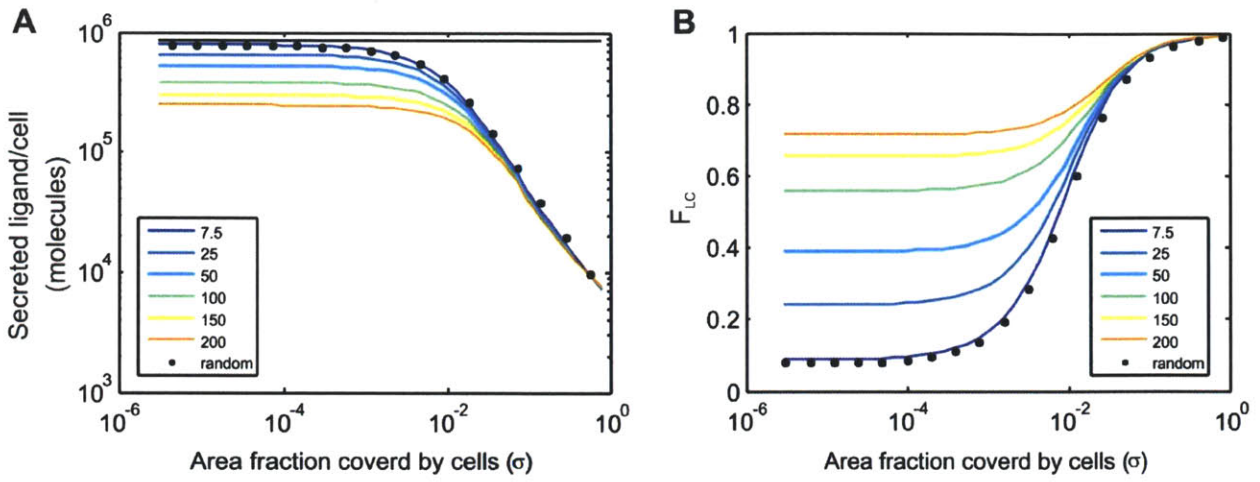

Figure 5-11 Stochastic simulation of paracrine exchange of secreted ligands
A) Simulated changes of net (color lines) and total (black line) ligand secretion per cell with varying global densities in randomly plated culture (black dots) and square-latticed cell arrays of varying patch sizes (patch radii in microns illustrated in legand). B) Using the calculated ligand secretion, we also determine the corresponding fractions of captured ligands (F_{LC}) at varying global densities. Both analyses were simulated results at 72 hours after serum starvation.

complex formation can be seen at the intermediate patch spacing while the generation of complex molecules reaches two different steady-states at both spatial extremes. At higher patch radii, the model predicted an increase in complex formation that becomes more significant with increasing array spacing. In other words, ligand binding was found to be more critically dependent on the patch size when the patterned cells were spaced more broadly from one another. On the other hand, the impact of patch shape on ligand binding becomes less dramatic at high global densities.

To understand the different behaviors of complex formation at the two spatial extremes, we also determine analytically the steady-state solutions of the generated complex molecules (Full details in Chapter 4). With very close array spacing (σ approaches the maximum value of $\pi/4$ for square-latticed circular patches), we found that the boundary condition of cell surface can be treated mathematically as a simple homogenous monolayer of cells. Assuming that the ligand secretion rate did not exceed its consumption rate by cells, the amount of generated complex molecules was found to be equal to the simple ratio of ligand secretion and the rate of complex internalization (Q/k_e). This solution matches well with our predicted value using the stochastic model (red dotted line in Figure 5-12). At the opposite regime when cell patches are positioned very far apart ($\sigma<<1$), we found that the boundary condition of cell arrays can be approximated simply as a flat isolated circular patch on an infinite reflective wall. The steady-state amount of complex formation in this spatial mode was found to be equal to the same ratio of ligand secretion and the rate of complex internalization multiplied by the probability of self-captured ligands ($P_{au} \times Q/k_e$). This solution also matched well with our stochastically-derived numerical prediction (blue dotted lines in Figure 5-12). The simple relationship of complex formations between the two spatial extremes enables us to visualize the increasing ligand capture when we place the patterned cell patches more closely to one another.

Based on the previous simulation analysis, we can abstract the systematic change of ligand capturing with varying cell arrangement as follows (Figure 5-12). In the *isolated* mode, cell patches are too far to communicate to one another diffusively. Binding of secreted ligands therefore depends solely on the local cell density, practically the size and the shape of each cell patch. Complex molecules are generated only from the self-captured ligands, leaving the uncaptured ligands in the surrounding fluid. At the opposite spatial extreme, or in the *communicative* mode, exchange of ligands can occur freely between

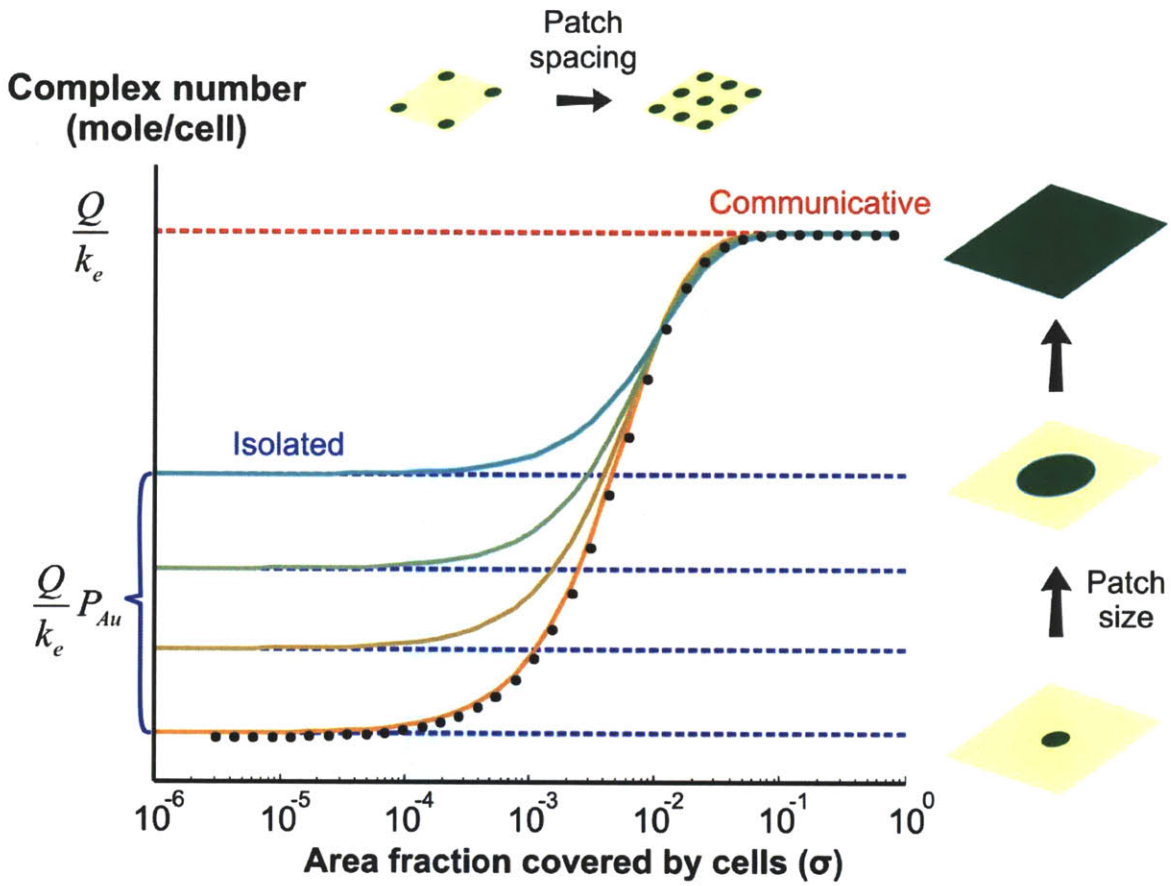

Figure 5-12 Predicted complex formation with changes of cell-patterning configuration
Our stochastic model predicts the number of complex formation using randomly-plated cells (black dots) or regularly-spaced cell arrays with varying patch sizes (colored solid lines). With the decrease in patch spacing or an increase in patch densities, complex formation increases with the amplified diffusive ligand exchange, transitioning from *isolated* to *communicative* modes. Analytical solutions of the complex formation were also superimposed at both spatial regimes.

neighboring patches, independently of the cell positioning geometry. The cell density and the rate at which complex formation transitions from 'isolated' to 'communicative' regimes depend on biochemical natures of the underlying autocrine loops including the diffusivity of ligands, the ligand/receptor affinity and the relative abundance of ligand and receptors (discussed in greater details in Chapter 4).

5.3 Discussion

Our study investigates the use of cell patterning to specifically alter autocrine signaling and thus its impact on cancer cell growth. When trying to modulate the intercellular spacing by simply changing the seeding density of randomly plated A431 cells, we found that the impact of the EGFR autocrine loop cannot be accurately inferred by only monitoring growth change with the altering cell plating densities but instead requires the use of EGFR-blocking antibodies to prove its presence and impacts in promoting A431 growth. While we could not dissect all signaling cues that underlie growth change with altering cell plating densities, we found that E-cadherin-mediated cell adhesion plays a major role in causing growth inhibition at high plating density and can also slightly promote cell growth at low plating densities. Using stencil cell patterning as a method to precisely define cell arrangement, we then illustrated that the uncontrolled changes of non-diffusive signaling cues in randomly-plated culture can be regularized by cultivating cells as uniformly-shaped patches. Unlike randomly plated cells where contact-dependent

growth inhibition plays a more dominating role and gives rise to diminished cell growth at increasing plating densities, we showed that growth of patterned A431 cells increased with increasing global density both by determining the increasing cell number per patch and by analyzing changes of EdU incorporation. These results substantiate the ability of our cell-patterning platform to display the dependency of cancer growth on autocrine loops, by simply altering spacing of the square-latticed arrays of uniformly-shaped paches.

Our results emphasize the complex roles that environmental cues play in regulating cell growth. First, we found that A431 cell growth is controlled by more than two signaling cues. When cultivating the cells with neutralizing antibodies to inhibit both EGFR autocrine loop and E-cadherin-mediated cell adhesion, we still observed the density-dependent growth change, implying that a third (or more) environmental cue exists. Second, we found that different signaling cues exert their growth-affecting roles at different time points. The EGFR autocrine loop was found to promote cell growth as early as one day after serum starvation, whereas the role of E-cadherin-mediated cell-cell contact became more pronounced at later time points. Finally, we found that each cue can exhibit a non-monotonic impact on cell growth. E-cadherin-mediated cell contacts elevate growth at low plating density but reduce growth of densely plated cells. In the case of the EGFR autocrine loop, while our experiments only illustrate the growth-promoting impact due to paracrine exchange of secreted ligands, exogenous supply of EGF ligands can both promote and diminish A431 growth. Specifically, cultivation of A431 cells with picomolar-range EGF was found to increase cell growth while nanomolar-range EGF inhibited growth (Gill and Lazar 1981; Barnes 1982; Bravo, Burckhardt et al. 1985). Considering the complex behavior of each environmental cue as well as their interdependent variations with cell seeding density, it is not surprising that the growth-promoting role of EGFR autocrine loops could not be inferred from changes of cell growth in the randomly plated culture.

The cell-patterning platform provides an experimental technique to diagnose the dependency of cancer growth on possibly existing autocrine loops. Many cancer cells acquire mutations in mitogenic signaling molecules to initiate constitutive mitogenic activation. Recent discoveries emphasize the role of autocrine loops in maintaining cancer growth without mutations of signaling molecules, identifying swapping of autocrine loops as the mechanism to escape targeted cancer therapeutics (Nguyen, Kobayashi et al. 2009; Rexer, Engelman et al. 2009). While genetic mutations can be accurately detected with hybridization or DNA sequencing technology, the investigation of autocrine signaling and its contribution in sustaining tumor growth is much more challenging. Existing methods require the use of perturbation therapeutics (Lauffenburger, Oehrtman et al. 1998; DeWitt, Dong et al. 2001; Joslin, Opresko et al. 2007), making it difficult to study autocrine loops for which inhibitors do not exist. By controlling the changes of non-diffusive signaling cues to be more uniform with increasing global cell density, our cell-patterning platform can illustrate the presence and function of autocrine loops without the need for prior knowledge of underlying ligand-receptor pairs or use of specific inhibitors.

Regardless of its improved specificity to autocrine signaling over the conventional method of seeding density modulation, our platform still may not be able to investigate impacts of some autocrine loops. Depending on the baseline level of receptor occupancy in each cell type, i.e. when the cell is in the *isolated* mode, the increased complex formation with the decreasing intercellular spacing may not give rise to any change in cell growth. First, if the number of secreted ligands is higher than the receptor availability, spatially isolated cells may already acquire functionally saturated receptor occupancy. As an example, engineered cell lines have been generated to secrete varying level of EGF or chimeric EGFR ligand in primary breast cancer cell line (Joslin, Opresko et al. 2007). While changes of cell motility were detected with the modulation of autocrine ligand secretion, these cells did not exhibit any change in cell growth. The observed results are believed to stem from the differing sensitivities between migration and cell proliferation to the input level of EGF. Based on the results we obtained in this study, it is also possible that these engineered cell lines may already acquire 'saturated' receptor occupancy per its relationship with cell proliferation. Second, the range of increased ligand capturing might be too narrow or

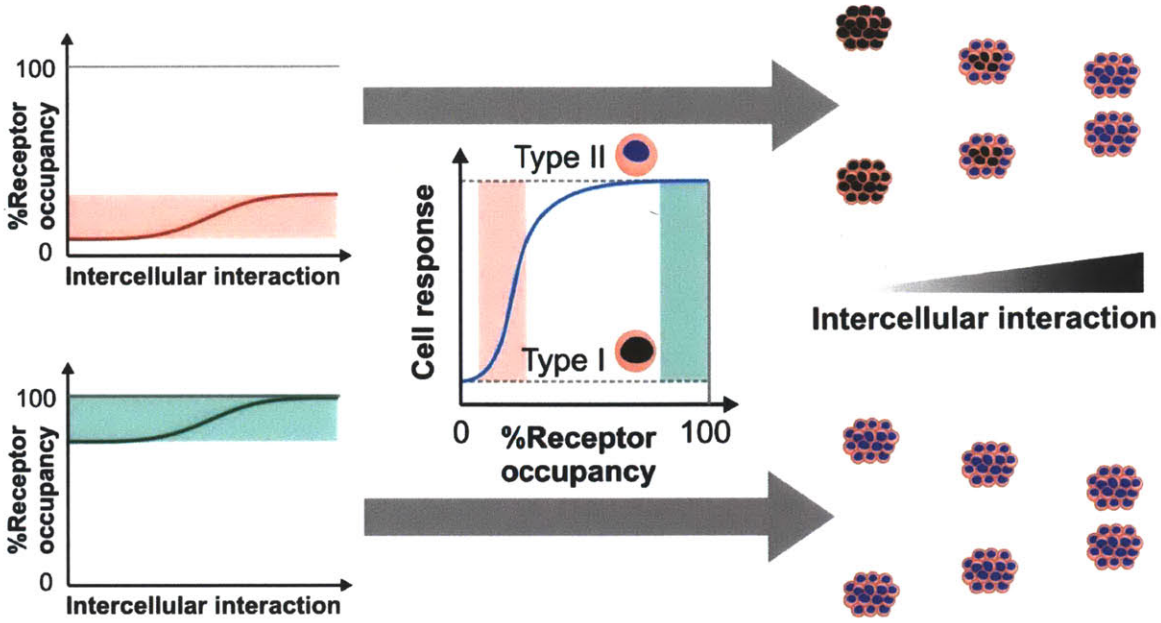

Figure 5-13 Phenotypic changes with altering intercellular spacing of different autocrine loops
Depending on the natures of different autocrine loops, changes of the ultimate phenotype may not be observed with the modulation of intercellular spacing. The above diagram illustrates two different autocrine loops that obtain different receptor occupancy during the isolated mode. If the range of receptor occupancy during the modulation of intercellular spacing does not lie within the critical range of the receptor occupancy-phenotype relationship, that cell line may not exhibit any change of the ultimate phenotype. The parameters that govern the basal level of receptor occupancy for each autocrine loop includes liagnd/receptor occupancy, ligand diffusivity, and the relative production rates of ligand and receptors.

fall within the non-dynamic phenotypic range, resulting in no change in the ultimate cell response. The Amphiregulin/EGFR autocrine loop in A431 cells is a good example of this case. Because we only detected a small change in Amphiregulin capture with increasing plating density, A431 cells would not have exhibited changes in cell growth with varying global densities had they only acquired only the Amphiregulin/EGFR autocrine loop. It is therefore essential to realize that efficacy of our cell-patterning platform relies critically on the characteristics of each underlying autocrine loop, especially on the relationship between its receptor occupancy and the ultimate cell response (Figure 5-13).

Despite the many insights this study has offered, there is still room for future improvement. Regardless of it complex regulation, growth was shown to be a continuous phenotype that increases with the number of generated complexes in EGF-family systems (Starbuck and Lauffenburger 1992). It is possible that, for some other phenotypes and in other cell lines, continuous changes of cell responses may not occur with the altering cell-patterning configuration. Such discrete phenotypic change is commonly observed from ultrasensitive or switch-like activation processes such as self-renewal and differentiation of stem cells (Davey, Onishi et al. 2007). Further characterization must therefore be performed to determine whether our cell-patterning method can in fact be used to exhibit autocrine phenomena in other biological processes. For improving our simulation of autocrine signaling, the connection between autocrine ligand binding to growth and the regulatory processes of other growth-affecting cues could be integrated into the model to enable more detailed prediction of growth change with varying global cell density. We found in our own study that A431 cells already secrete at least two EGFR ligands, TGF-α and Amphiregulin. Even though the role of Amphiregulin on the density-dependent growth change was found to be minimal, it is possible that other autocrine loops could contribute more significantly to the observed density-dependent

growth change. In the case of A431 cells, other tentative autocrine loops include the autocrine loop of IGFI-receptors and IGFII (Guix, Faber et al. 2008) and that of CXCR2 and IL-8/Gro-α (Metzner, Hofmann et al. 1999). To be able to compare contributions among these different autocrine loops, the model must include signaling networks from all of these pathways and should also incorporate their possible cross-interactions. Recent reports have emphasized the need to acknowledge cell-to-cell variability when studying phenotypic regulation (Niepel, Spencer et al. 2009; Snijder, Sacher et al. 2009; Spencer, Gaudet et al. 2009). In our own study, we found that contact-mediated cues gave rise to the variation in cell growth with increasing number of neighbors. For the cell-to-cell variability of autocrine loops, the model must take into account the possible variation in receptor numbers and ligand secretion rates between adjacent neighbors. We could then simulate interactions among these differing cells using, for example, agent-based modeling (Zhang, Wang et al. 2009). By extending the model to include multiple autocrine loops, cell-to-cell variability and different growth-affecting cues, it would be possible to build a mathematical model that could quantitatively predict the role of autocrine signaling, as a positive pressure in selecting for resistive cells during cancer treatment with targeted therapeutics. Finally, to apply the developed mathematical model for clinical applications, we might be able to abstract experimental outcomes from our cell-patterning arrays in terms of self-captured ligands (P_{au}) and ligand secretion rate (Q) and use these parameters for predicting cancer prognosis. For a biological system with a single autocrine loop, P_{au} can be obtained from the ratio between detected complex molecules in the isolated and communicative regimes. The secretion rate of autocrine ligand (Q) can also be obtained by fitting the observed relationship between patch sizes and the generated complex molecules to our simulation. By studying the correlation between these quantitative footprints of autocrine loops and cancer outcome such as survival rate or metastatic index, the model may help define simple quantitative measures for comparing the contributions of autocrine loops in maintaining tumor growth of different cancer tissues.

5.4 Summary

In this chapter, we have demonstrated the complex interplay of growth-affecting cues and the ability of regularly-shaped cell arrays to isolate and exhibit impacts of autocrine signaling. We first illustrate the inaccuracy in inferring the presence of autocrine loop based only on the observed growth change with altering cell plating density. We show the critical impact of E-cadherin mediated signaling and prove that other non-diffusive signaling cues must also play a critical impact in regulating A431 growth. By cultivating cells as square-latticed arrays of circular patches, we show that growth change better correspond with the predicted and measured increasing capturing of EGFR ligands. Specifically, we show that both the fold growth per patch and EdU incorporation increase with the decreasing array spacing (increasing global cell density). These results substantiate the ability to modulate autocrine signaling impact by altering the intercellular spacing, but only when effects of other environmental cues are uniformly maintained. Because cell-patterning platform can illustrate the growth promoting effects of the EGFR autocrine loop without needing the use of EGFR-neutralizing antibody, we believe that the developed platform can be generalized for testing growth dependency on autocrine loops in other cancer tissues. This platform may be adapted to detect the swapping activity of autocrine loops in cancer cells, an important mutation-free mechanism that underlies tumor recurrence.

5.5 Materials and methods

Cell culture

The A431 epidermoid carcinoma cells were cultivated in DMEM/F-12 medium with Glutamax (10565, Gibco) supplemented with 10% bovine calf serum (BCS), (SH20072.03, Hyclone), 100 U/mL penicillin and 100 μg/mL streptomycin (15140122, Invitrogen) at 37°C in 7.5% CO_2. For passaging, cells were trypsinized with 0.25% trypsin/EDTA (25200, Gibco) and subcultured at 20% confluency. For analysis of intercellular interactions, A431 cells were seeded and cultivated overnight in serum-containing medium to ensure uniform cell attachment at all plating densities. After 24-hour serum starvation (DMEM/F12 with Glutamax supplemented with 100 U/mL penicillin and 100 μg/mL streptomycin), we

washed the cells with PBS and cultivated the cells for another 72 hours in serum-free medium. mAb225 was self purified from the supernatant of 225 hybridoma. SHE78-7 was obtained from Invitrogen.

Stencil fabrication

To create stencils, a master wafer was first fabricated to construct microposts on silicon substrate with SU-8 2050 photoresist (Microchem) using standard photolithographic techniques. Stencil membrane was then fabricated by pouring uncured polydimethylsiloxane (PDMS) silicone on the master wafer. The PDMS-covered wafer was then covered with transparency, flat glass plate, and rubber sheet before being pressurized between flat metal plates on a hot plate at 65°C for 2 hours. After the PDMS was cured, an annular ring of PDMS is attached to the stencil membrane for ease in handling using uncured PDMS as adhesives. After being reheated, the stencil can be removed from the wafer.

Patterning cells with stencils

Before the stencil can be exposed to cells, curing agents in the device must be removed via a series of rinsing with solvents, including acetone, isopropanol, 80% ethanol and water, for 12 hours per each solvent. The device was then air-dried and autoclaved for sterility. To pattern cells, we placed the device on the tissue culture substrate that was wetted with a few drops of ethanol to ensure conformal contact. The device in the tissue culture plate was then placed in a vacuum chamber to vaporize ethanol and seal the device on the substrate. After approximately 2 hours, the device was removed from the vacuum chamber and exposed to UV for 15 minutes to ensure sterility. To prevent formation of thin gas film inside the stencil holes while loading cells, cell growth buffer was originally poured into the device in a chamber filled with 100% carbon dioxide. Because carbon dioxide can quickly dissolve into aqueous solution, the carbon dioxide gas within each stencil holes would quickly disappeared (~2 minutes). After carefully rinsing the device with PBS and leaving a thin layer of liquid just enough to cover the whole stencil membrane, cell suspension in growth medium was then loaded to stencil. For A431 cells, the cells were incubated for four hours to promote cell attachment. Stencils were then carefully peeled off while having basic growth medium surrounding the stencil to prevent cell damage.

Quantification of cell growth

For bulk analysis of cell growth, cell numbers per well were determined using Coulter counter (Beckman). For single-cell analysis of cell proliferation, the cells were incubated with BrdU (00-0103, Invitrogen) for three hours before the cells were fixed with 2% paraformaldehyde (15710, Electron Microscopy Sciences). Cell membrane was permeabilized for 20 minutes in methanol. Single-cell analysis of EdU incorporation was performed using the Click-iT EdU cell proliferation assay (C10350, Invitrogen), following the manufacturer's protocols. After the staining of EdU, cells were counter-stained with Hoechst 33342 (H3570, Invitrogen) and whole cell stain blue (8403501, Pierce). To image the stained cells, we use the high-contact screening microscope (CellWorx, Applied Precision). Quantification of fluorescent intensity per cells were then performed with CellProfiler (Carpenter, Jones et al. 2006).

Measurement of net and total ligand secretion

To determine the secreted amount of EGFR ligands, we first collected the supernatant liquid after 3-day cell cultivation. We measured the amount of TGF-α and Amphiregulin in the collected supernatant using the DuoSet ELISA development systems (R&D Systems). The total ligand secretion was obtained by co-cultivating the cells with saturated mAb225 to fully inhibit interactions between EGFR and its cognate ligands. The amount of ligands in the supernatant without mAb225 represents net ligand secretion, taking into account ligand consumption by cells.

Chapter 6

Conclusions

The main objective of this thesis has been the development of a novel experimental platform that enables the examination of autocrine signaling impacts on phenotypic regulation without the need of perturbing molecules or prior knowledge of underlying ligand/receptor pair. This technology will be immediately valuable as a platform for quantifying the dependency of cancer growth on autocrine loops. Ultimately, we can use the developed platform for early detection of tumor recurrence due to the emerging activity of untargeted autocrine loops. The preceding four chapters present the fundamental biology, the underlying cell-patterning and mathematical simulation technology, and our demonstration of the developed method in isolating autocrine signaling from other signaling cues. To recapitulate our major findings, we summarize here the major contributions of this thesis and discuss future directions to further improve and apply our technology for clinical applications.

6.1 Thesis contributions

Development of a novel general method for examining impacts of autocrine signaling

The most important contribution of this thesis is our successful attempt to isolate autocrine signaling from other environmental cues using regularly-shaped cell arrays. Using stencil cell patterning (Chapter 3) and the understanding of ligand capture changes with the modulated geometric configuration of square-latticed cell arrays (Chapter 4), we were able to show that the complex density-dependent growth change of the randomly-plated cells can be experimentally normalized to only exhibit impacts of autocrine signaling, by introducing spatial regularity to cell positioning (Chapter 5). By cultivating cells as uniformly-shaped patches with uniform spacing, we can ensure minimal changes of local cell density while the impact of autocrine signaling can be modulated by altering the array spacing. Because our approach relies only on the adjustment of cell arrangement without using specific inhibitors, our method enables the investigation of autocrine signaling in poorly characterized systems. With the recent discovery of autocrine signaling contribution in causing resistance to cancer therapeutics (Zhou, Peyton et al. 2006; Guix, Faber et al. 2008; Rexer, Engelman et al. 2009), our method also provides the necessary experimental assay for the continual monitoring of combined autocrine activity, a diagnostic tool necessary to detect the swapping roles of autocrine loops and their roles in causing cancer therapeutic resistance.

Demonstration of unique autocrine-signaling characteristics

We have addressed properties of autocrine signaling that underlie the difficulty in investigating autocrine loops and those characteristics that may provide survival benefits to the acquiring cells (Chapter 2). We showed that difference in the spatial distribution of autocrine ligands may complicate the study of autocrine signaling with the medium conditioning assay. Specifically, we show that ligands with high affinity to the corresponding receptors on cell surface may not be dislodged into the surrounding supernatant at high quantity, limiting the using of medium conditioning assay in testing function of only poor-affinity ligands. Therapeutic agents such as the receptor blocking antibody are therefore the only conventional method that can accurately validates the significance of a specific autocrine loop in regulating an interested phenotype. We then showed that a single autocrine system may actually acquire multiple autocrine loops, either by secretion of multiple ligands or expression of multiple receptor types. This result emphasizes the needs for multi-drug cancer treatment, to inhibit activity of all possibly exsisting autocrine loops and to prevent tumor recurrence due to autocrine-loop swapping. Finally, our observation of the gradually rising mitogenic signals due to autocrine signaling in comparison to the fast-rise/slow-decay response due to the exogenous ligand supply emphasizes the ability of autocrine signaling to establish temporally maintained signal activation. Such ability of autocrine systems to create sustained mitogenic activation without needing supports from the integrin signaling may provide survival benefits to

cancer cells and supports the use of autocrine systems as a more physically relevant *in vitro* platform for testing cancer therapeutics.

Development of cell-patterning technologies that can be easily integrated with biological studies

A number of cell-patterning methods have been developed in the past decade but most of these technologies often require specialized expertise that prevents their easy integration with common biological assays. We have illustrated simple modification to the previously reported stencil cell patterning technique, allowing this technique to be fully compatible with both standard and high-throughput biological studies (Chapter 3). Our attempt to introduce spatial regularity to the standard cell culture has led to the development of a novel class of cell-patterning methods, the Stencil-Delineated Electroactive Patterning (S-DEP). S-DEP takes advantages of stencil cell patterning to enable the fabrication of isolated cell plates on a large substrate area and of regular n-DEP to allow complex cell formation within the stencil-defined area. We can use s-DEP to create complex tissue-like constructs for many biological studies such as the characterization of cue-response relationship, the *in vitro* illustration of complex body planning or the determination of the underlying cues of stem cell differentiation.

Description of the cell arrangement impacts on the intercellular communication in autocrine systems

Using the stochastic model and by taking advantage of the unique symmetry of the square-latticed arrays of circular patches (Chapter 4), we were the first to describe how cell arrangement affects intercellular communication in the autocrine system, one of the most ambiguous properties of autocrine systems. Regardless of the commonly observed density-dependent phonotypic change in autocrine systems, different autocrine loops exhibit distinctly different operating range, giving rise to their unique relationship between cell density and the associated cell response. While the "plume" of autocrine ligand has been shown to cause locally-varying self-renewal of embryonic stem cells (Davey and Zandstra 2006; Peerani, Onishi et al. 2009), cell lines that were specifically engineered to differently secret ligands instead exhibit no phenotypic difference (Joslin, Opresko et al. 2007). Using our model, we showed that sharing of ligand between cells varies between the globally uniform environment, what we define as the *communicative* mode, and the more spatially limited environment, or the *isolated* mode. Depending on the relative ligand/receptor production ratios and ligand/receptor affinity, we demonstrated that the significance of cell arrangement on the ligand/receptor binding can vary among the different autocrine systems. To acquire cell-to-cell variation of either the intermediate-early signals or ultimate cell responses, both cell arrangement and the intrinsic properties of the underlying autocrine loop must maintain the intercellular interaction in the *isolated* mode, where local cell density dominates over the global cell densities. Our mathematical model also provides insights and design rules for the study with cell arrays. To prevent communication between the different cell sites and to utilize each cell island as biologically independent replicates, we can determine empirically the array spacing where the intercellular communication is in the *isolated* mode. To take advantage of cell-to-cell communication, possible to sustain a cellular phenotype, we must ensure that the spatial arrangement of cell culture is stably maintained in the *communicative* regime, to prevent cell-to-cell variability due to the impacts of local cell density.

6.2 Future directions and possible challenges

Further exploring changes of phenotypes and signal activation with varying cell-patterning designs

In our study with cell-patterning arrays (Chapter 5), we illustrated changes of fold growth and EdU incorporation with the modified array spacing. While we were able to illustrate changes of cell proliferation that corresponds well with the density-ligand capture trend, both from mathematical prediction as well as our experimental measurement, there is still room for further analysis. First, it would be interesting to investigate changes of the major immediate-early signals, namely ERK and AKT phosphorylation, with varying cell-patterning designs. Based on our observation of nonlinear ERK and AKT phosphorylation change with altering plating densities in randomly-plated cells (Chapter 2), it would be interesting to see how regularity in cell arrangement may affect the spatial variation of these signals.

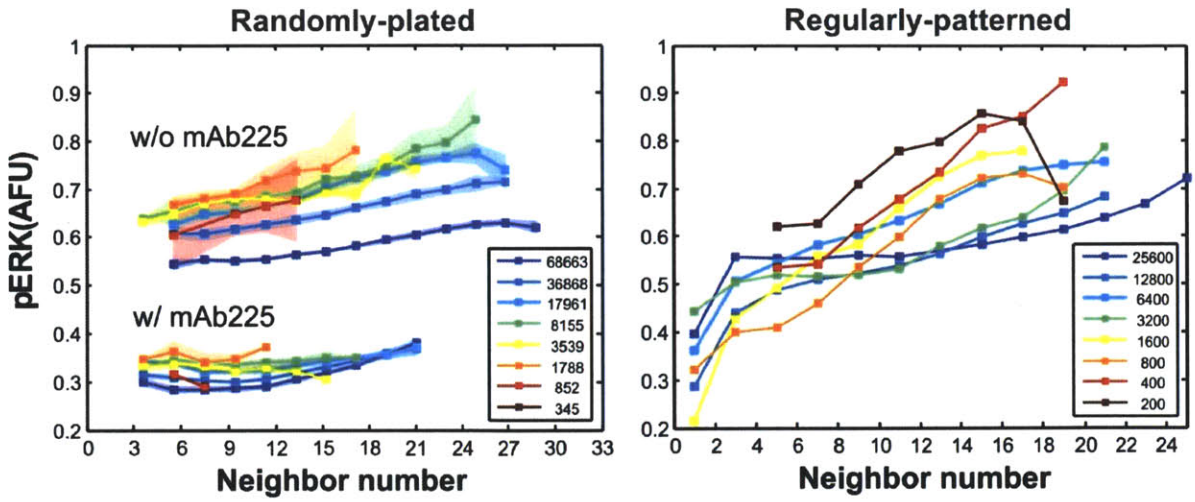

Figure 6-1 Changes of ERK phosphorylation with altering local and global cell densities
Both analyses were performed at 72 hours after serum starvation. Local cell density is determined from the neighbor number, using the neighbor radius of 44 microns. Legends represent initial cell plating density for randomly-plated culture or equivalent cell density for patterned arrays (both shown in the unit of cells/cm^2). The highlighted areas of the randomly-plated plot represent ranges of the 95% confidence interval.

Our preliminary analysis shows that the uniformly-shaped cell arrays and randomly-plated cell culture exhibit a slight variation in ERK phosphorylation with local cell density (Figure 6-1). In cell-patterning arrays, ERK phosphorylation is observed to elevate with increasing local density at low global density, but this spatial variation gradually disappears at higher global density. Randomly-plated cells on the other hand do not exhibit such distinct difference of ERK phosphorylation between low and high global density. We postulate that the observed difference may stem from the ability of the cell-patterning platform to isolate impacts of diffusive signaling from other environmental cues, allowing the dependency on local cell geometry in the *isolated* regime to be revealed. It is still unclear to us why the averaged intensity of ERK phosphorylation in the patterned cells at high global density is lower than the maximal signal intensity of low-density arrays. Based on our previous analysis of ERK phosphorylation in randomly-plated cells, we found that the signal gradually increases within the first 50 hours after serum starvation (Chapter 2). It is possible that ERK phosphorylation may exhibit a non-monotonic change and give rise to the smaller signal intensities in high-global-density cells at 72 hours after serum starvation. To explore this contradiction, we will need to further examine the temporal change of ERK phosphorylation in both randomly-plated cells and patterned cell arrays, with finer time steps.

While we have demonstrated mathematically the distinction between *isolated* and *communicative* modes, we have yet to illustrate this phenomenon experimentally. Specifically, our model postulates that ligand capture in the *isolated* mode will be critically dependent on the patch geometry while ligand binding in the *communicative* mode is predicted to be indifferent of local cell arrangement. We have established cell patterning designs that can experimentally validate this hypothesis (Figure 6-2). To exhibit the dependency on patch geometry, we could examine differences in ligand binding for cell patches with discretely increasing area 7-fold. Using our stochastic model, we can calculate the fraction of ligands with autocrine trajectories (P_{Au}) based on intrinsic properties of autocrine loops and the different patch sizes. Among the tested designs, the composite patches with 50-micron radius gives rise to P_{Au} that can most optimally span across its critical range (Figure 6-2A). Experimentally, two approaches can be conducted to create patches with increasing areas. We either pattern cells as a single patch with increasing radius or

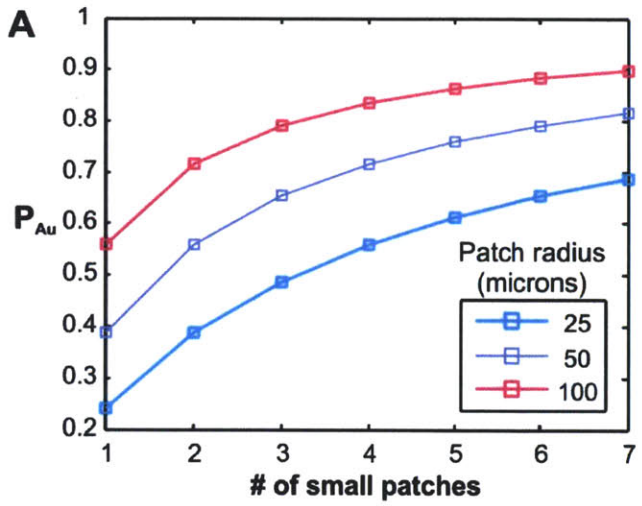

B

# of patch	Combined radius (μm)	R_{cc} (μm)	
		Commu.	Isolated
1	50.0	260.4	2946.3
2	70.7	368.3	4166.7
3	86.6	451.1	5103.1
4	100.0	520.8	5892.6
5	111.8	582.3	6588.1
6	122.5	637.9	7216.9
7	132.3	689.0	7795.1

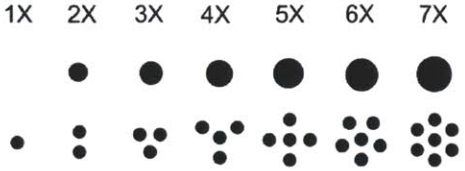

C

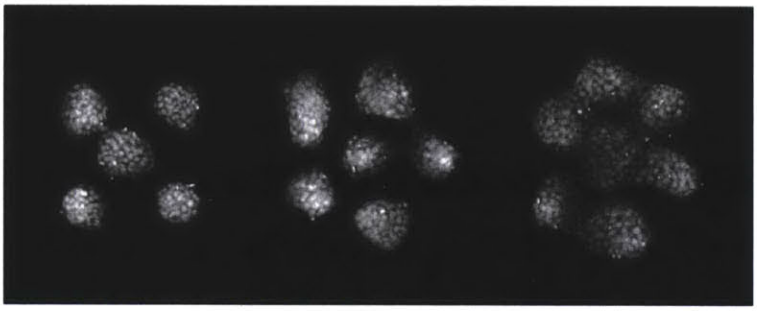

Figure 6-2 Experimental validation of differences between isolated and communication modes
A) Simulated fraction of ligands with autocrine trajectories (P_{Au}) for the different size of baseline patch. B) Calculated array geometry and grouping designs for the different patch area in isolated and communicative regimes. C) Resulted patterned patches for 5x-7x area at 72 hours after serum starvation. Fusion of small patches can be observed in some sites.

simply group multiple small patches together (Figure 6-2B). We can create such cell patches using stencil cell patterning (Figure 6-2C). We believe that the grouping of smaller patches should also help prevent interference from contact-mediated signaling that can also be modulated with increasing patch size. To perform the experiment, we will position these different patch designs to achieve cell-covered area fractions (σ) in *isolated* and *communication* regimes. With the increasing patch area, we expect that the array designs in *communicative* regime will exhibit less spatial variation in cell growth and immediate-early signals than the designs in *isolated* regime. The difference between the one-patch design and the patch-grouping design will also illustrate significance of contact-mediated signaling.

The prediction of cancer prognosis with autocrine activity index

We successfully illustrated the isolation of autocrine signaling impacts from other environmental cues using the cell-patterning platform. For future experiments, it will be interesting to first examine the ability of this method to distinguish autocrine loops with different intrinsic properties. This application has major implications for the detection of autocrine-loop switching, a recently discovered mutation-free mechanism of cancer therapeutic resistance (Rexer, Engelman et al. 2009). Experimentally, we could use the developed cell-patterning platform to determine the density-growth relationship of tumor cells before and after the development of drug resistance. To compare their difference quantitatively, we could define a critical array spacing where fold growth or ligand capturing transitions from the isolated mode to the

communicative mode. We could also compare characteristics of pre- and post-resistant cell populations from fitting parameters such as P_{au} and Q that can be extracted from our experimental results (Chapter 4). Ultimately, when we have studied changes of these quantitative footprints of autocrine loops with cancer prognosis, an autocrine activity index can possibly be established. Similar to the use of body mass index (BMI) for determining the amount of body fat, this autocrine activity index can be used by physicians to determine the appropriate cancer treatment in combination with other cancer-specific biomarkers such as the prostate-specific antigen (PSA) in prostate cancer (Barry 2001) or the HER-2/neu in breast cancer (Slamon, Clark et al. 1987).

Dissecting the role of autocrine signaling as the underlying cause of cell-to-cell variability

With the advancement in biological assay that enables the quantification of both proteins and gene expression down to the single-cell level, we have begun to discover implications of cell-to-cell variability in different biological processes, including the programmed cell death (Spencer, Gaudet et al. 2009) , virus infection (Snijder, Sacher et al. 2009), activation of T cells (Feinerman, Veiga et al. 2008), and responses to cancer therapeutics (Gascoigne and Taylor 2008). While genetic stochasticity (Elowitz, Levine et al. 2002; Colman-Lerner, Gordon et al. 2005) and the non-uniform splitting of proteins during cell division (Spencer, Gaudet et al. 2009) are the currently popular causes of cell-to-cell variability, the variation of

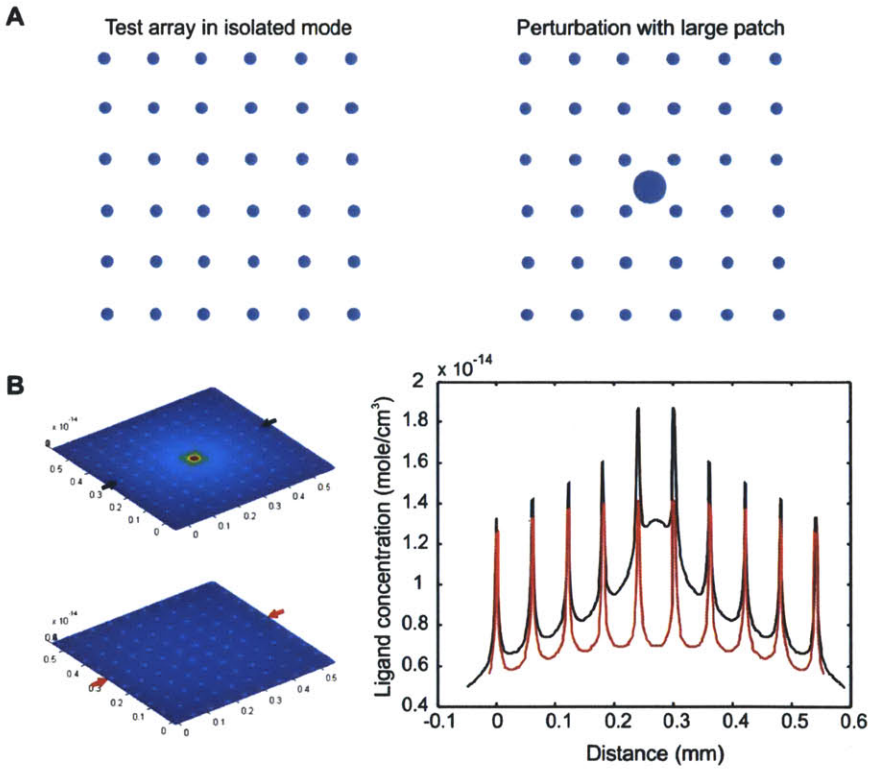

Figure 6-3 Proposed cell patterning design for studying cell-to-cell variability
A) The proposed cell-patterning designs to exhibit quantitative impact of autocrine signaling in causing cell-to-cell variability. The array spacing of the control design is selected to ensure that each cell patch operate in the *isolated* regime. Cell variability is tested by positioning a large cell patch at the center of the test array. B) Simulation of ligand concentration for the testing and control arrays. The plot on the right shows ligand concentration profiles along the lines marked by the arrows (black=testing design, red=control design). Mathematical simulation to generate illustrated ligand concentration profile is contributed by Michael Vahey.

extracellular environment due to morphogen gradient or heterogeneity of cell-cell contacts is certainly a non-negligible factor. To quantify the contribution of autocrine signaling in causing cell-to-cell variability, one can take advantages of our cell-patterning platform. Figure 6-3 illustrates a possible cell-patterning design that can be used to quantify the contribution of autocrine signaling in causing cell-to-cell variability. The central concept of this design is to take advantage of our prior study to establish array of small patches in the isolated regime. Without any diffusive interactions between the different sites, we can use this array of small patches as sensors across the whole substrate. The area of these sensor patches have to be small to ensure that minimal receptor occupancy from self-secreted ligands (autocrine trajectories). To study cell-to-cell variability due to autocrine signaling, we can simply introduce a large patch at the center of the sensor array. The comparison of interested phenotypes between testing design (with the large cell patch) and control design (only small-patch array) can be used to illustrate impact of autocrine signaling on cell-to-cell variability (Figure 6-3B). The gradient of output signal across the whole array enables quantitative comparison between different biological systems.

A microfluidics-based technology for faster measurement of combined autocrine activity

While we have previously demonstrated the ability of cell-patterning-based platform for isolating the impact of autocrine signaling, it is important to note its long time scale, mainly to accumulate enough ligand locally to cause changes of the ultimate cell responses. Microfluidics is another technology that has the capacity to modulate autocrine signaling specifically while also maintaining controlled contribution by other environmental cues. Unlike the conditioned medium that mainly collects secreted ligands with poor ligand/receptor affinity, a microfludic device can be designed to exhibit convection-dominated flow which can compete with ligand binding in autocrine systems.

Figure 6-4 illustrates an example design of the microfluidic device for quantifying combined autocrine activity. The serpentine shape of the device is designed to enable uniform diffusion of collected ligand along the device height. The cross section area of the device is chosen to match the surface area of each cell patch to ensure a 1-to-1 ratio of ligand secretion flux between cell surface and the device cross-section. Fluid velocity should be chosen to enable a slight ligand capturing while mostly enabling ligand collection along with the passing fluid stream. We predict that the increasing ligand concentration along the microfluidic channel will also cause increasing ligand capture in downstream patches. While shear stress can cause changes of phosphorylation signals, its effect can be easily taken care of by including appropriate controls. For a test of specific autocrine loop, we can add receptor or ligand blocking antibodies for the interested ligand/receptor pairs. The parallel fluid conditions can be permanently fabricated by designing multiple fluidic channels that flow in parallel. Alternatively, we might be able to take advantage of the immiscible sheath flow, by flowing liquid such as mineral oils between the different test fluids (Figure 6-4B). Because autocrine loops acquire different intrinsic properties, we expect to observe different patterns of signal activation along the length of the microfluidic device (Figure 6-4D). We believe that the previously described system will enable a fast quantification of combined autocrine activity than cell-patterning platform because the accumulation of ligand occurs rapidly as fluid passes along the microfluidic device.

A major challenge of this system is the fabrication of isolated cell patches along the microfluidic channel. We believe that such cell patterning requirement can be obtained by first patterning a strip of cells on tissue culture substrate. We can then place the serpentine-shaped microfluidic device on top of the cell-aligned substrate. Sealing between the top microfluidic channel and the bottom cell-culture substrate may be achieved by mechanically clamping or by vacuum seal. Another important technical challenge is the selection of cell surface area that can optimally exhibit output signal increase along the fluidic length. An autocrine loop with small ligand secretion rate and/or high total receptor number is expected to require longer channel length before a significant change of signal activation can be visualized. On the opposite end, if we design too large patch size, the gradient of signal change might occur too abruptly, disability our ability to distinguish characteristics of different autocrine loops. By taking advantage of the simple geometry of the device design, we can carefully predict the required device length for a specific set of

transport parameters. Different microfluidic channels can also be designed to cover different parameter ranges. We believe that the proposed microfluidic platform should provide more accurate and flexible measurement tool than our previously developed cell-patterning assay.

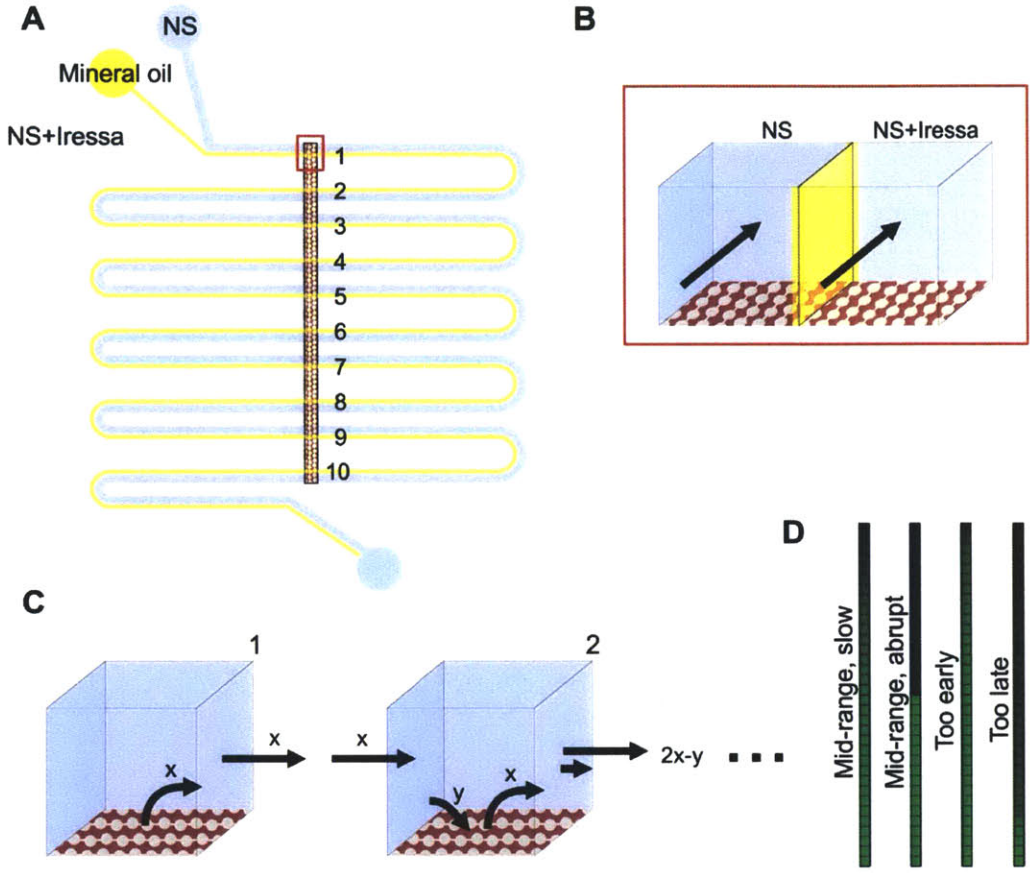

Figure 6-4 Proposed design of microfluidic device to measure combined autocrine activity
A) Top view of the proposed microfluidic device that is composed of two main layers: 1) the top microfluidic channel that is used to manipulate and collect the secreted ligands and 2) the bottom pre-patterned cell surface. B) Cross-sectional view of the microfluidic device. Sheath flow of immiscible liquid such as mineral oil can be used to separate the two different fluid conditions. Alternatively, we can directly design parallel serpentine channels to physically separate the different test flows. C) The cross-sectional area of each fluid condition is designed to match the area of the cell surface to ensure a 1-to-1 ligand secretion flux translation between the two areas. Without addition of growth factors in the fluid, fluid stream will collect secreted ligand from the first cell patch, with ligand secretion flux x. When the fluid stream enters the second cell patch after passing through the first channel loop, concentration of the secreted ligand should already propagate uniformly along the channel height. Some of the entering ligand will be captured by cell surface (capturing flux y which is assumed to be smaller than the input flux x). The net flux after getting through the second cell patch should be greater than flux of the first cell patch. D) Prediction of different output signals from the microfluidic device. Optimal channel length must ensure that the signal does not happen to early or too late and can exhibit a broad range of signal transition to enable comparison between different autocrine loops.

Extending the developed stochastic model for autocrine systems with two ligands

We have discussed the limitation of our stochastic model, being about to predict ligand capture changes of only autocrine systems with one ligand and one receptor (1L1R). To further expand the developed model based on our previous analysis, we illustrate here the steady-state solution of complex formation in the *isolated* regime for autocrine systems with two types of ligand and 1 receptor (2L1R).

The major impact of having more than one ligand types is the shared occupancy of the underlying receptor. We can describe binding of two ligand types to a common receptor as shown in the following reactions.

$$\begin{aligned} L1 + R &\underset{k_{off}^1}{\overset{k_{on}^1}{\rightleftharpoons}} C1 \xrightarrow{k_e^1} \otimes \\ L2 + R &\underset{k_{off}^2}{\overset{k_{on}^2}{\rightleftharpoons}} C2 \xrightarrow{k_e^2} \otimes \end{aligned} \quad [6\text{-}1]$$

Based on these reactions, we can determine the amount of complex formation at steady states from the following equation.

$$\begin{aligned} [C1]+[C2]\big|_{s.s.} &= [R]\left[\left(\frac{k_{on}^1}{k_{off}^1+k_e^1}\right)[L1]+\left(\frac{k_{on}^2}{k_{off}^2+k_e^2}\right)[L2]\right] \\ &= [R]\left[\frac{[L1]}{K_M^1}+\frac{[L2]}{K_M^2}\right] \end{aligned} \quad [6\text{-}2]$$

Assuming the total number of receptor is constant (R_{total}=R+$C1$+$C2$), we can calculate the concentration of unbound receptors and the combined bound receptors from the following equations.

$$[R] = [R_{total}]\frac{1}{\frac{[L1]}{K_M^1}+\frac{[L2]}{K_M^2}+1} \quad [6\text{-}3]$$

$$[C1]+[C2] = [R_{total}]\frac{\frac{[L1]}{K_M^1}+\frac{[L2]}{K_M^2}}{\frac{[L1]}{K_M^1}+\frac{[L2]}{K_M^2}+1} \quad [6\text{-}4]$$

Based on the steady-state solution of ligand concentration that we found in Chapter 4 (Equation [4-23]), we can determine the concentration of both ligand types from:

$$\begin{aligned} [L1]\big|_{s.s.} &= \frac{r_{patch}q^1K_M^1}{\frac{4D}{\pi}K_M^1 + r_{patch}\left([R_{total}]k_e^1 - q^1\right)} \\ [L2]\big|_{s.s.} &= \frac{r_{patch}q^2K_M^2}{\frac{4D}{\pi}K_M^2 + r_{patch}\left([R_{total}]k_e^2 - q^2\right)}. \end{aligned} \quad [6\text{-}5]$$

If we assume that $[R_{total}]k_e^n/q^n >> 1$ like most native autocrine systems with small ligand secretion rate and substitute the above steady-state solutions of ligand concentration into Equation [6-4], we obtain the simplified solution of bound receptors.

$$[C1]+[C2]=[R_{total}]\frac{\frac{P_{Au}^{1}q^{1}}{k_e^{1}}+\frac{P_{Au}^{2}q^{2}}{k_e^{2}}}{1+\frac{P_{Au}^{1}q^{1}}{k_e^{1}}+\frac{P_{Au}^{2}q^{2}}{k_e^{2}}} \quad [6\text{-}6]$$

We can then extend the above solution for autocrine systems with multiple ligand types.

$$\sum_n [C^n]=[R_{total}]\frac{\sum_n \frac{P_{Au}^{n}q^{n}}{k_e^{n}}}{1+\sum_n \frac{P_{Au}^{n}q^{n}}{k_e^{n}}} \quad [6\text{-}7]$$

It is important to remember that this solution is only applicable for autocrine systems with small ligand secretion. Further analysis is still necessary to determine the solution for autocrine systems with multiple receptor types, the important mechanism that underlies development of mutation-free cancer therapeutic resistance.

Bibliography

Adkins, B., A. Leutz, et al. (1984). "Autocrine growth induced by src-related oncogenes in transformed chicken myeloid cells." Cell **39**(3 Pt 2): 439-45.

Albrecht, D. R., R. L. Sah, et al. (2004). "Geometric and material determinants of patterning efficiency by dielectrophoresis." Biophysical Journal **87**(4): 2131-2147.

Anido, J., P. Matar, et al. (2003). "ZD1839, a specific epidermal growth factor receptor (EGFR) tyrosine kinase inhibitor, induces the formation of inactive EGFR/HER2 and EGFR/HER3 heterodimers and prevents heregulin signaling in HER2-overexpressing breast cancer cells." Clin Cancer Res **9**(4): 1274-83.

Ashkin, A., J. M. Dziedzic, et al. (1986). "Observation of a Single-Beam Gradient Force Optical Trap for Dielectric Particles." Optics Letters **11**(5): 288-290.

Balak, M. N., Y. Gong, et al. (2006). "Novel D761Y and common secondary T790M mutations in epidermal growth factor receptor-mutant lung adenocarcinomas with acquired resistance to kinase inhibitors." Clin Cancer Res **12**(21): 6494-501.

Barnes, D. W. (1982). "Epidermal growth factor inhibits growth of A431 human epidermoid carcinoma in serum-free cell culture." J Cell Biol **93**(1): 1-4.

Barry, M. J. (2001). "Clinical practice. Prostate-specific-antigen testing for early diagnosis of prostate cancer." N Engl J Med **344**(18): 1373-7.

Basu, S., Y. Gerchman, et al. (2005). "A synthetic multicellular system for programmed pattern formation." Nature **434**(7037): 1130-4.

Batsilas, L., A. M. Berezhkovskii, et al. (2003). "Stochastic model of autocrine and paracrine signals in cell culture assays." Biophys J **85**(6): 3659-65.

Ben-Shlomo, I., R. Rauch, et al. (2007). "Matching receptome genes with their ligands for surveying paracrine/autocrine signaling systems." Mol Endocrinol **21**(8): 2009-14.

Berezhkovskii, A. M., L. Batsilas, et al. (2004). "Ligand trapping in epithelial layers and cell cultures." Biophys Chem **107**(3): 221-7.

Berezhkovskii, A. M., Y. A. Makhnovskii, et al. (2004). "Boundary homogenization for trapping by patchy surfaces." Journal of Chemical Physics **121**(22): 11390-11394.

Berezhkovskii, A. M., M. I. Monine, et al. (2006). "Homogenization of boundary conditions for surfaces with regular arrays of traps." Journal of Chemical Physics **124**(3): -.

Birner, P., G. Oberhuber, et al. (2001). "Evaluation of the United States Food and Drug Administration-approved scoring and test system of HER-2 protein expression in breast cancer." Clin Cancer Res **7**(6): 1669-75.

Blobel, C. P. (2005). "ADAMs: key components in EGFR signalling and development." Nat Rev Mol Cell Biol **6**(1): 32-43.

Boccardo, E. and L. L. Villa (2007). "Viral origins of human cancer." Curr Med Chem **14**(24): 2526-39.

Bodas, D. and C. Khan-Malek (2006). "Formation of more stable hydrophilic surfaces of PDMS by plasma and chemical treatments." Microelectronic Engineering **83**(4-9): 1277-1279.

Boussiotis, V. A., L. M. Nadler, et al. (1994). "Tumor-Necrosis-Factor-Alpha Is an Autocrine Growth-Factor for Normal Human B-Cells." Proceedings of the National Academy of Sciences of the United States of America **91**(15): 7007-7011.

Bravo, R., J. Burckhardt, et al. (1985). "Stimulation and inhibition of growth by EGF in different A431 cell clones is accompanied by the rapid induction of c-fos and c-myc proto-oncogenes." EMBO J **4**(5): 1193-7.

Bringuier, P. P., R. Umbas, et al. (1993). "Decreased E-cadherin immunoreactivity correlates with poor survival in patients with bladder tumors." Cancer Res **53**(14): 3241-5.

Brown, P. D. (2000). "Ongoing trials with matrix metalloproteinase inhibitors." Expert Opin Investig Drugs **9**(9): 2167-77.

Burke, J. M. (1983). "Cell-cell contact promotes DNA synthesis in retinal glia but not in fibroblasts." Exp Cell Res **146**(1): 204-6.
Cappuzzo, F., F. R. Hirsch, et al. (2005). "Epidermal growth factor receptor gene and protein and gefitinib sensitivity in non-small-cell lung cancer." J Natl Cancer Inst **97**(9): 643-55.
Carpenter, A. E., T. R. Jones, et al. (2006). "CellProfiler: image analysis software for identifying and quantifying cell phenotypes." Genome Biol **7**(10): R100.
Castellano, G., J. F. Reid, et al. (2006). "New potential ligand-receptor signaling loops in ovarian cancer identified in multiple gene expression studies." Cancer Res **66**(22): 10709-19.
Cavallaro, U. and G. Christofori (2004). "Cell adhesion and signalling by cadherins and Ig-CAMs in cancer." Nat Rev Cancer **4**(2): 118-32.
Chang, L. and M. Karin (2001). "Mammalian MAP kinase signalling cascades." Nature **410**(6824): 37-40.
Chen, C. S., M. Mrksich, et al. (1997). "Geometric control of cell life and death." Science **276**(5317): 1425-1428.
Chen, W. W., B. Schoeberl, et al. (2009). "Input-output behavior of ErbB signaling pathways as revealed by a mass action model trained against dynamic data." Mol Syst Biol **5**: 239.
Citri, A., K. B. Skaria, et al. (2003). "The deaf and the dumb: the biology of ErbB-2 and ErbB-3." Exp Cell Res **284**(1): 54-65.
Colman-Lerner, A., A. Gordon, et al. (2005). "Regulated cell-to-cell variation in a cell-fate decision system." Nature **437**(7059): 699-706.
Cook, S. J., N. Aziz, et al. (1999). "The repertoire of fos and jun proteins expressed during the G1 phase of the cell cycle is determined by the duration of mitogen-activated protein kinase activation." Molecular and Cellular Biology **19**(1): 330-41.
Coussens, L. M., B. Fingleton, et al. (2002). "Matrix metalloproteinase inhibitors and cancer: trials and tribulations." Science **295**(5564): 2387-92.
Curto, M., B. K. Cole, et al. (2007). "Contact-dependent inhibition of EGFR signaling by Nf2/Merlin." J Cell Biol **177**(5): 893-903.
Davey, R. E., K. Onishi, et al. (2007). "LIF-mediated control of embryonic stem cell self-renewal emerges due to an autoregulatory loop." Faseb J.
Davey, R. E. and P. W. Zandstra (2006). "Spatial organization of embryonic stem cell responsiveness to autocrine gp130 ligands reveals an autoregulatory stem cell niche." Stem Cells **24**(11): 2538-48.
Dempsey, P. J. and R. J. Coffey (1994). "Basolateral targeting and efficient consumption of transforming growth factor-alpha when expressed in Madin-Darby canine kidney cells." J Biol Chem **269**(24): 16878-89.
Derynck, R. (1988). "Transforming growth factor alpha." Cell **54**(5): 593-5.
Derynck, R., D. V. Goeddel, et al. (1987). "Synthesis of messenger RNAs for transforming growth factors alpha and beta and the epidermal growth factor receptor by human tumors." Cancer Res **47**(3): 707-12.
Desai, S. P. and J. Voldman (2011). "Cell-based sensors for quantifying the physiological impact of microsystems." Integr Biol (Camb) **3**(1): 48-56.
DeWitt, A., T. Iida, et al. (2002). "Affinity regulates spatial range of EGF receptor autocrine ligand binding." Developmental Biology **250**(2): 305-316.
DeWitt, A. E., J. Y. Dong, et al. (2001). "Quantitative analysis of the EGF receptor autocrine system reveals cryptic regulation of cell response by ligand capture." J Cell Sci **114**(Pt 12): 2301-13.
Di Cosimo, S., G. Ferretti, et al. (2004). "[Preclinical and clinical results with the epidermal growth factor receptor inhibitor Gefitinib (ZD1839, Iressa)]." Minerva Med **95**(3): 233-41.
Dong, J., L. K. Opresko, et al. (2005). "The membrane-anchoring domain of epidermal growth factor receptor ligands dictates their ability to operate in juxtacrine mode." Molecular biology of the cell **16**(6): 2984-2998.
Dong, J., L. K. Opresko, et al. (1999). "Metalloprotease-mediated ligand release regulates autocrine signaling through the epidermal growth factor receptor." Proc Natl Acad Sci U S A **96**(11): 6235-40.

Downward, J. (2003). "Targeting RAS signalling pathways in cancer therapy." Nat Rev Cancer **3**(1): 11-22.

Druker, B. J. (2002). "STI571 (Gleevec) as a paradigm for cancer therapy." Trends Mol Med **8**(4 Suppl): S14-8.

Duprez, V., G. Lenoir, et al. (1985). "Autocrine Growth-Stimulation of a Human T-Cell Lymphoma Line by Interleukin-2." Proceedings of the National Academy of Sciences of the United States of America **82**(20): 6932-6936.

Ebner, R. and R. Derynck (1991). "Epidermal growth factor and transforming growth factor-alpha: differential intracellular routing and processing of ligand-receptor complexes." Cell Regul **2**(8): 599-612.

Ellison, D., A. Munden, et al. (2009). "Computational model and microfluidic platform for the investigation of paracrine and autocrine signaling in mouse embryonic stem cells." Mol Biosyst **5**(9): 1004-12.

Elowitz, M. B., A. J. Levine, et al. (2002). "Stochastic gene expression in a single cell." Science **297**(5584): 1183-6.

Engelman, J. A., K. Zejnullahu, et al. (2007). "MET amplification leads to gefitinib resistance in lung cancer by activating ERBB3 signaling." Science **316**(5827): 1039-43.

Fan, Z., J. Baselga, et al. (1993). "Antitumor effect of anti-epidermal growth factor receptor monoclonal antibodies plus cis-diamminedichloroplatinum on well established A431 cell xenografts." Cancer Res **53**(19): 4637-42.

Fan, Z., Y. Lu, et al. (1994). "Antibody-induced epidermal growth factor receptor dimerization mediates inhibition of autocrine proliferation of A431 squamous carcinoma cells." J Biol Chem **269**(44): 27595-602.

Fan, Z., B. Y. Shang, et al. (1997). "Reciprocal changes in p27(Kip1) and p21(Cip1) in growth inhibition mediated by blockade or overstimulation of epidermal growth factor receptors." Clinical Cancer Research **3**(11): 1943-1948.

Feinerman, O., J. Veiga, et al. (2008). "Variability and robustness in T cell activation from regulated heterogeneity in protein levels." Science **321**(5892): 1081-4.

Fischer, O. M., S. Hart, et al. (2003). "EGFR signal transactivation in cancer cells." Biochem Soc Trans **31**(Pt 6): 1203-8.

Folch, A., B. H. Jo, et al. (2000). "Microfabricated elastomeric stencils for micropatterning cell cultures." J Biomed Mater Res **52**(2): 346-53.

Folch, A. and M. Toner (2000). "Microengineering of cellular interactions." Annu Rev Biomed Eng **2**: 227-56.

Forsten, K. E. and D. A. Lauffenburger (1994). "The Role of Low-Affinity Interleukin-2 Receptors in Autocrine Ligand-Binding - Alternative Mechanisms for Enhanced Binding Effect." Molecular Immunology **31**(10): 739-751.

Francis, K. and B. O. Palsson (1997). "Effective intercellular communication distances are determined by the relative time constants for cyto/chemokine secretion and diffusion." Proc Natl Acad Sci U S A **94**(23): 12258-62.

Freeman, M. (2000). "Feedback control of intercellular signalling in development." Nature **408**(6810): 313-9.

French, A. R., G. P. Sudlow, et al. (1994). "Postendocytic Trafficking of Epidermal Growth Factor-Receptor Complexes Is Mediated through Saturable and Specific Endosomal Interactions." Journal of Biological Chemistry **269**(22): 15749-15755.

French, A. R., D. K. Tadaki, et al. (1995). "Intracellular trafficking of epidermal growth factor family ligands is directly influenced by the pH sensitivity of the receptor/ligand interaction." J Biol Chem **270**(9): 4334-40.

Fridman, J. S., E. Caulder, et al. (2007). "Selective inhibition of ADAM metalloproteases as a novel approach for modulating ErbB pathways in cancer." Clin Cancer Res **13**(6): 1892-902.

Fuchs, E., T. Tumbar, et al. (2004). "Socializing with the neighbors: Stem cells and their niche." Cell **116**(6): 769-778.
Gascoigne, K. E. and S. S. Taylor (2008). "Cancer cells display intra- and interline variation profound following prolonged exposure to antimitotic drugs." Cancer Cell **14**(2): 111-122.
Gill, G. N. and C. S. Lazar (1981). "Increased phosphotyrosine content and inhibition of proliferation in EGF-treated A431 cells." Nature **293**(5830): 305-7.
Glisson, B. S. (2010). "Targeting an autocrine loop in small-cell lung cancer: irrelevant target or ineffective drug?" Clin Lung Cancer **11**(4): 222.
Goishi, K., S. Higashiyama, et al. (1995). "Phorbol ester induces the rapid processing of cell surface heparin-binding EGF-like growth factor: conversion from juxtacrine to paracrine growth factor activity." Mol Biol Cell **6**(8): 967-80.
Graeber, T. G. and D. Eisenberg (2001). "Bioinformatic identification of potential autocrine signaling loops in cancers from gene expression profiles." Nat Genet **29**(3): 295-300.
Grier, D. G. (2003). "A revolution in optical manipulation." Nature **424**(6950): 810-816.
Gschwind, A., S. Hart, et al. (2003). "TACE cleavage of proamphiregulin regulates GPCR-induced proliferation and motility of cancer cells." EMBO J **22**(10): 2411-21.
Guix, M., A. C. Faber, et al. (2008). "Acquired resistance to EGFR tyrosine kinase inhibitors in cancer cells is mediated by loss of IGF-binding proteins." J Clin Invest **118**(7): 2609-19.
Hanahan, D. and R. A. Weinberg (2000). "The hallmarks of cancer." Cell **100**(1): 57-70.
Harris, R. C., E. Chung, et al. (2003). "EGF receptor ligands." Experimental cell research **284**(1): 2-13.
Henson, E. S., J. B. Johnston, et al. (2007). "Clinical activities of the epidermal growth factor receptor family inhibitors in breast cancer." Biologics **1**(3): 229-39.
Herbst, J. J., L. K. Opresko, et al. (1994). "Regulation of postendocytic trafficking of the epidermal growth factor receptor through endosomal retention." J Biol Chem **269**(17): 12865-73.
Hilbert, D. (1999). Geometry and the imagination. Providence, R.I., AMS Chelsea Pub.
Horiuchi, K., S. Le Gall, et al. (2007). "Substrate selectivity of epidermal growth factor-receptor ligand sheddases and their regulation by phorbol esters and calcium influx." Mol Biol Cell **18**(1): 176-88.
Hui, E. E. and S. N. Bhatia (2007). "Micromechanical control of cell-cell interactions." Proc Natl Acad Sci U S A **104**(14): 5722-6.
Hynes, N. E. and G. MacDonald (2009). "ErbB receptors and signaling pathways in cancer." Curr Opin Cell Biol **21**(2): 177-84.
Hynes, R. O. (2009). "The extracellular matrix: not just pretty fibrils." Science **326**(5957): 1216-9.
Hynes, R. O. and Q. Zhao (2000). "The evolution of cell adhesion." J Cell Biol **150**(2): F89-96.
Inui, S., S. Higashiyama, et al. (1997). "Possible role of coexpression of CD9 with membrane-anchored heparin-binding EGF-like growth factor and amphiregulin in cultured human keratinocyte growth." J Cell Physiol **171**(3): 291-8.
Jemal, A., R. Siegel, et al. (2010). "Cancer statistics, 2010." CA Cancer J Clin **60**(5): 277-300.
Jones, G. J., N. S. Heiss, et al. (1993). "Amplification and expression of the TGF-alpha, EGF receptor and c-myc genes in four human oesophageal squamous cell carcinoma lines." Biosci Rep **13**(5): 303-12.
Joslin, E. J., L. K. Opresko, et al. (2007). "EGF-receptor-mediated mammary epithelial cell migration is driven by sustained ERK signaling from autocrine stimulation." J Cell Sci **120**(Pt 20): 3688-99.
Juliano, R. L., P. Reddig, et al. (2004). "Integrin regulation of cell signalling and motility." Biochem Soc Trans **32**(Pt3): 443-6.
Kim, J. H., K. Kushiro, et al. (2009). "Tunable interplay between epidermal growth factor and cell-cell contact governs the spatial dynamics of epithelial growth." Proceedings of the National Academy of Sciences of the United States of America **106**(27): 11149-11153.
King, N. (2004). "The unicellular ancestry of animal development." Dev Cell **7**(3): 313-25.
King, N., C. T. Hittinger, et al. (2003). "Evolution of key cell signaling and adhesion protein families predates animal origins." Science **301**(5631): 361-3.

Kiyota, A., S. Shintani, et al. (2002). "Anti-epidermal growth factor receptor monoclonal antibody 225 upregulates p27(KIP1) and p15(INK4B) and induces G1 arrest in oral squamous carcinoma cell lines." Oncology **63**(1): 92-8.

Klagsbrun, M. and A. Baird (1991). "A dual receptor system is required for basic fibroblast growth factor activity." Cell **67**(2): 229-31.

Kobayashi, S., T. J. Boggon, et al. (2005). "EGFR mutation and resistance of non-small-cell lung cancer to gefitinib." N Engl J Med **352**(8): 786-92.

Kojic, N., M. Kojic, et al. (2006). "Computational modeling of extracellular mechanotransduction." Biophys J **90**(11): 4261-70.

Krupp, M. N., D. T. Connolly, et al. (1982). "Synthesis, turnover, and down-regulation of epidermal growth factor receptors in human A431 epidermoid carcinoma cells and skin fibroblasts." J Biol Chem **257**(19): 11489-96.

Lal, A., C. A. Glazer, et al. (2002). "Mutant epidermal growth factor receptor up-regulates molecular effectors of tumor invasion." Cancer Res **62**(12): 3335-9.

Lauffenburger, D. and C. Cozens (1989). "Regulation of Mammalian-Cell Growth by Autocrine Growth-Factors - Analysis of Consequences for Inoculum Cell-Density Effects." Biotechnology and Bioengineering **33**(11): 1365-1378.

Lauffenburger, D. A., G. T. Oehrtman, et al. (1998). "Real-time quantitative measurement of autocrine ligand binding indicates that autocrine loops are spatially localized." Proceedings of the National Academy of Sciences of the United States of America **95**(26): 15368-15373.

Lemjabbar, H., D. Li, et al. (2003). "Tobacco smoke-induced lung cell proliferation mediated by tumor necrosis factor alpha-converting enzyme and amphiregulin." J Biol Chem **278**(28): 26202-7.

Li, S., K. R. Schmitz, et al. (2005). "Structural basis for inhibition of the epidermal growth factor receptor by cetuximab." Cancer Cell **7**(4): 301-11.

Li, S. W., G. D. Plowman, et al. (1992). "Heparin Inhibition of Autonomous Growth Implicates Amphiregulin as an Autocrine Growth-Factor for Normal Human Mammary Epithelial-Cells." Journal of cellular physiology **153**(1): 103-111.

Lichtner, R. B. and V. Schirrmacher (1990). "Cellular distribution and biological activity of epidermal growth factor receptors in A431 cells are influenced by cell-cell contact." J Cell Physiol **144**(2): 303-12.

Lim, J. Y. and H. J. Donahue (2007). "Cell sensing and response to micro- and nanostructured surfaces produced by chemical and topographic patterning." Tissue Eng **13**(8): 1879-91.

Liu, V. A., W. E. Jastromb, et al. (2002). "Engineering protein and cell adhesivity using PEO-terminated triblock polymers." Journal of Biomedical Materials Research **60**(1): 126-134.

Liu, X., J. S. Fridman, et al. (2006). "Selective inhibition of ADAM metalloproteases blocks HER-2 extracellular domain (ECD) cleavage and potentiates the anti-tumor effects of trastuzumab." Cancer Biol Ther **5**(6): 648-56.

Luk, Y. Y., M. Kato, et al. (2000). "Self-assembled monolayers of alkanethiolates presenting mannitol groups are inert to protein adsorption and cell attachment." Langmuir **16**(24): 9604-9608.

Luppi, F., A. M. Longo, et al. (2007). "Interleukin-8 stimulates cell proliferation in non-small cell lung cancer through epidermal growth factor receptor transactivation." Lung Cancer **56**(1): 25-33.

Lysiak, J. J., G. R. Johnson, et al. (1995). "Localization of amphiregulin in the human placenta and decidua throughout gestation: role in trophoblast growth." Placenta **16**(4): 359-66.

Maretzky, T., K. Reiss, et al. (2005). "ADAM10 mediates E-cadherin shedding and regulates epithelial cell-cell adhesion, migration, and beta-catenin translocation." Proc Natl Acad Sci U S A **102**(26): 9182-7.

Markowitz, S. D., K. Molkentin, et al. (1990). "Growth stimulation by coexpression of transforming growth factor-alpha and epidermal growth factor-receptor in normal and adenomatous human colon epithelium." J Clin Invest **86**(1): 356-62.

Masui, H., T. Kawamoto, et al. (1984). "Growth inhibition of human tumor cells in athymic mice by anti-epidermal growth factor receptor monoclonal antibodies." Cancer Res **44**(3): 1002-7.

Matar, P., F. Rojo, et al. (2004). "Combined epidermal growth factor receptor targeting with the tyrosine kinase inhibitor gefitinib (ZD1839) and the monoclonal antibody cetuximab (IMC-C225): superiority over single-agent receptor targeting." Clin Cancer Res **10**(19): 6487-501.

McCole, D. F., S. J. Keely, et al. (2002). "Transactivation of the epidermal growth factor receptor in colonic epithelial cells by carbachol requires extracellular release of transforming growth factor-alpha." J Biol Chem **277**(45): 42603-12.

Meloche, S. and J. Pouyssegur (2007). "The ERK1/2 mitogen-activated protein kinase pathway as a master regulator of the G1- to S-phase transition." Oncogene **26**(22): 3227-3239.

Mendelsohn, J. (1997). "Epidermal growth factor receptor inhibition by a monoclonal antibody as anticancer therapy." Clinical Cancer Research **3**(12): 2703-2707.

Mendelsohn, J. and J. Baselga (2003). "Status of epidermal growth factor receptor antagonists in the biology and treatment of cancer." J Clin Oncol **21**(14): 2787-99.

Mendelsohn, J. and J. Baselga (2006). "Epidermal growth factor receptor targeting in cancer." Semin Oncol **33**(4): 369-85.

Mendelsohn, J., H. Masui, et al. (1987). "Anti-epidermal growth factor receptor monoclonal antibodies may inhibit A431 tumor cell proliferation by blocking an autocrine pathway." Trans Assoc Am Physicians **100**: 173-8.

Metzner, B., C. Hofmann, et al. (1999). "Overexpression of CXC-chemokines and CXC-chemokine receptor type II constitute an autocrine growth mechanism in the epidermoid carcinoma cells KB and A431." Oncol Rep **6**(6): 1405-10.

Mittal, N., A. Rosenthal, et al. (2007). "nDEP microwells for single-cell patterning in physiological media." Lab Chip **7**(9): 1146-53.

Mittal, N. and J. Voldman "Nonmitogenic survival-enhancing autocrine factors including cyclophilin A contribute to density-dependent mouse embryonic stem cell growth." Stem Cell Res **6**(2): 168-76.

Moasser, M. M., A. Basso, et al. (2001). "The tyrosine kinase inhibitor ZD1839 ("Iressa") inhibits HER2-driven signaling and suppresses the growth of HER2-overexpressing tumor cells." Cancer Res **61**(19): 7184-8.

Monine, M. I., A. M. Berezhkovskii, et al. (2005). "Ligand accumulation in autocrine cell cultures." Biophysical Journal **88**(4): 2384-2390.

Morra, M. and C. Cassineli (1999). "Non-fouling properties of polysaccharide-coated surfaces." Journal of Biomaterials Science-Polymer Edition **10**(10): 1107-1124.

Mrksich, M., L. E. Dike, et al. (1997). "Using microcontact printing to pattern the attachment of mammalian cells to self-assembled monolayers of alkanethiolates on transparent films of gold and silver." Experimental Cell Research **235**(2): 305-313.

Nakamura, K., R. Iwamoto, et al. (1995). "Membrane-anchored heparin-binding EGF-like growth factor (HB-EGF) and diphtheria toxin receptor-associated protein (DRAP27)/CD9 form a complex with integrin alpha 3 beta 1 at cell-cell contact sites." J Cell Biol **129**(6): 1691-705.

Nelson, C. M. and C. S. Chen (2002). "Cell-cell signaling by direct contact increases cell proliferation via a PI3K-dependent signal." Febs Letters **514**(2-3): 238-242.

Nelson, C. M., S. Raghavan, et al. (2003). "Degradation of micropatterned surfaces by cell-dependent and -independent processes." Langmuir **19**(5): 1493-1499.

Nelson, C. M., M. M. Vanduijn, et al. (2006). "Tissue geometry determines sites of mammary branching morphogenesis in organotypic cultures." Science **314**(5797): 298-300.

Nguyen, K. S., S. Kobayashi, et al. (2009). "Acquired resistance to epidermal growth factor receptor tyrosine kinase inhibitors in non-small-cell lung cancers dependent on the epidermal growth factor receptor pathway." Clin Lung Cancer **10**(4): 281-9.

Niepel, M., S. L. Spencer, et al. (2009). "Non-genetic cell-to-cell variability and the consequences for pharmacology." Curr Opin Chem Biol **13**(5-6): 556-61.

Normanno, N., C. Bianco, et al. (2003). "Target-based agents against ErbB receptors and their ligands: a novel approach to cancer treatment." Endocr Relat Cancer **10**(1): 1-21.

Oehrtman, G. T., H. S. Wiley, et al. (1998). "Escape of autocrine ligands into extracellular medium: Experimental test of theoretical model predictions." Biotechnology and Bioengineering **57**(5): 571-582.

Okegawa, T., R. C. Pong, et al. (2004). "The role of cell adhesion molecule in cancer progression and its application in cancer therapy." Acta Biochim Pol **51**(2): 445-57.

Ono, M., A. Hirata, et al. (2004). "Sensitivity to gefitinib (Iressa, ZD1839) in non-small cell lung cancer cell lines correlates with dependence on the epidermal growth factor (EGF) receptor/extracellular signal-regulated kinase 1/2 and EGF receptor/Akt pathway for proliferation." Mol Cancer Ther **3**(4): 465-72.

Ostuni, E., R. Kane, et al. (2000). "Patterning mammalian cells using elastomeric membranes." Langmuir **16**(20): 7811-7819.

Paez, J. G., P. A. Janne, et al. (2004). "EGFR mutations in lung cancer: correlation with clinical response to gefitinib therapy." Science **304**(5676): 1497-500.

Pao, W., V. A. Miller, et al. (2005). "Acquired resistance of lung adenocarcinomas to gefitinib or erlotinib is associated with a second mutation in the EGFR kinase domain." PLoS Med **2**(3): e73.

Peerani, R., K. Onishi, et al. (2009). "Manipulation of signaling thresholds in "engineered stem cell niches" identifies design criteria for pluripotent stem cell screens." PLoS One **4**(7): e6438.

Peng, D., Z. Fan, et al. (1996). "Anti-epidermal growth factor receptor monoclonal antibody 225 up-regulates p27KIP1 and induces G1 arrest in prostatic cancer cell line DU145." Cancer Res **56**(16): 3666-9.

Perrais, M., X. Chen, et al. (2007). "E-cadherin homophilic ligation inhibits cell growth and epidermal growth factor receptor signaling independently of other cell interactions." Mol Biol Cell **18**(6): 2013-25.

Piepkorn, M., C. Lo, et al. (1994). "Amphiregulin-dependent proliferation of cultured human keratinocytes: autocrine growth, the effects of exogenous recombinant cytokine, and apparent requirement for heparin-like glycosaminoglycans." J Cell Physiol **159**(1): 114-20.

Piepkorn, M., M. R. Pittelkow, et al. (1998). "Autocrine regulation of keratinocytes: the emerging role of heparin-binding, epidermal growth factor-related growth factors." J Invest Dermatol **111**(5): 715-21.

Pires-daSilva, A. and R. J. Sommer (2003). "The evolution of signalling pathways in animal development." Nat Rev Genet **4**(1): 39-49.

Pouliot, N. and A. W. Burgess (2000). "Multiple autocrine factors including an extracellular matrix protein are required for the proliferation and spreading of human colon carcinoma cells in vitro." Growth Factors **18**(1): 31-49.

Prenzel, N., E. Zwick, et al. (1999). "EGF receptor transactivation by G-protein-coupled receptors requires metalloproteinase cleavage of proHB-EGF." Nature **402**(6764): 884-8.

Raab, G., K. Kover, et al. (1996). "Mouse preimplantation blastocysts adhere to cells expressing the transmembrane form of heparin-binding EGF-like growth factor." Development **122**(2): 637-45.

Rana, B. K. and P. A. Insel (2005). "Receptor databases and computational websites for ligand binding." Methods Mol Biol **306**: 1-15.

Rein, A. and H. Rubin (1968). "Effects of local cell concentrations upon the growth of chick embryo cells in tissue culture." Experimental cell research **49**(3): 666-678.

Reiss, M., E. B. Stash, et al. (1991). "Activation of the autocrine transforming growth factor alpha pathway in human squamous carcinoma cells." Cancer Res **51**(23 Pt 1): 6254-62.

Rettig, J. R. and A. Folch (2005). "Large-scale single-cell trapping and imaging using microwell arrays." Analytical Chemistry **77**(17): 5628-5634.

Rexer, B. N., J. A. Engelman, et al. (2009). "Overcoming resistance to tyrosine kinase inhibitors: lessons learned from cancer cells treated with EGFR antagonists." Cell Cycle **8**(1): 18-22.

Roovers, K. and R. K. Assoian (2000). "Integrating the MAP kinase signal into the G1 phase cell cycle machinery." Bioessays **22**(9): 818-826.

Roovers, K. and R. K. Assoian (2000). "Integrating the MAP kinase signal into the G1 phase cell cycle machinery." Bioessays **22**(9): 818-26.
Roovers, K., G. Davey, et al. (1999). "Alpha5beta1 integrin controls cyclin D1 expression by sustaining mitogen-activated protein kinase activity in growth factor-treated cells." Mol Biol Cell **10**(10): 3197-204.
Rosenthal, A. and J. Voldman (2005). "Dielectrophoretic traps for single-particle patterning." Biophys J **88**(3): 2193-205.
Rosenthal, A. and J. Voldman (2005). "Dielectrophoretic traps for single-particle patterning." Biophysical Journal **88**(3): 2193-2205.
Rubin, H. (1966). "A substance in conditioned medium which enhances the growth of small numbers of chick embryo cells." Experimental cell research **41**(1): 138-148.
Rubin, H. (1966). "A substance in conditioned medium which enhances the growth of small numbers of chick embryo cells." Exp Cell Res **41**(1): 138-48.
Schafer, B., B. Marg, et al. (2004). "Distinct ADAM metalloproteinases regulate G protein-coupled receptor-induced cell proliferation and survival." J Biol Chem **279**(46): 47929-38.
Schoeberl, B., E. A. Pace, et al. (2009). "Therapeutically targeting ErbB3: a key node in ligand-induced activation of the ErbB receptor-PI3K axis." Sci Signal **2**(77): ra31.
Shoyab, M., G. D. Plowman, et al. (1989). "Structure and function of human amphiregulin: a member of the epidermal growth factor family." Science **243**(4894 Pt 1): 1074-6.
Shvartsman, S. Y., H. S. Wiley, et al. (2001). "Spatial range of autocrine signaling: modeling and computational analysis." Biophysical journal **81**(4): 1854-1867.
Singh, A. B. and R. C. Harris (2005). "Autocrine, paracrine and juxtacrine signaling by EGFR ligands." Cell Signal **17**(10): 1183-93.
Slamon, D. J., G. M. Clark, et al. (1987). "Human breast cancer: correlation of relapse and survival with amplification of the HER-2/neu oncogene." Science **235**(4785): 177-82.
Snijder, B., R. Sacher, et al. (2009). "Population context determines cell-to-cell variability in endocytosis and virus infection." Nature **461**(7263): 520-3.
Spangler, J. B., J. R. Neil, et al. (2010). "Combination antibody treatment down-regulates epidermal growth factor receptor by inhibiting endosomal recycling." Proc Natl Acad Sci U S A **107**(30): 13252-7.
Spencer, S. L., S. Gaudet, et al. (2009). "Non-genetic origins of cell-to-cell variability in TRAIL-induced apoptosis." Nature **459**(7245): 428-32.
Sporn, M. B. and A. B. Roberts (1985). "Autocrine growth factors and cancer." Nature **313**(6005): 745-7.
Sporn, M. B. and A. B. Roberts (1992). "Autocrine secretion--10 years later." Ann Intern Med **117**(5): 408-14.
Sporn, M. B. and G. J. Todaro (1980). "Autocrine secretion and malignant transformation of cells." N Engl J Med **303**(15): 878-80.
St Croix, B., C. Sheehan, et al. (1998). "E-Cadherin-dependent growth suppression is mediated by the cyclin-dependent kinase inhibitor p27(KIP1)." J Cell Biol **142**(2): 557-71.
Starbuck, C. and D. A. Lauffenburger (1992). "Mathematical model for the effects of epidermal growth factor receptor trafficking dynamics on fibroblast proliferation responses." Biotechnol Prog **8**(2): 132-43.
Stoka, A. M. (1999). "Phylogeny and evolution of chemical communication: an endocrine approach." J Mol Endocrinol **22**(3): 207-25.
Tada, H., R. Sasada, et al. (1999). "Processing and juxtacrine activity of membrane-anchored betacellulin." J Cell Biochem **72**(3): 423-34.
Taff, B. M. and J. Voldman (2005). "A scalable addressable positive-dielectrophoretic cell-sorting array." Analytical Chemistry **77**(24): 7976-83.
Tan, J. L., J. Tien, et al. (2002). "Microcontact printing of proteins on mixed self-assembled monolayers." Langmuir **18**(2): 519-523.

Thienelt, C. D., P. A. Bunn, Jr., et al. (2005). "Multicenter phase I/II study of cetuximab with paclitaxel and carboplatin in untreated patients with stage IV non-small-cell lung cancer." J Clin Oncol **23**(34): 8786-93.

Thomas, C. H., J. B. Lhoest, et al. (1999). "Surfaces designed to control the projected area and shape of individual cells." Journal of Biomechanical Engineering-Transactions of the Asme **121**(1): 40-48.

Thornley, A. L. and G. J. Jones (1992). "In vitro secretion of transforming growth factor alpha (TGF-alpha): a comparison of the A431 cell line with three human oesophageal squamous cell carcinoma lines." Biosci Rep **12**(4): 293-302.

Umekita, Y., Y. Ohi, et al. (2000). "Co-expression of epidermal growth factor receptor and transforming growth factor-alpha predicts worse prognosis in breast-cancer patients." Int J Cancer **89**(6): 484-7.

Vallesi, A., G. Giuli, et al. (1995). "Autocrine mitogenic activity of pheromones produced by the protozoan ciliate Euplotes raikovi." Nature **376**(6540): 522-4.

Van de Vijver, M. J., R. Kumar, et al. (1991). "Ligand-induced activation of A431 cell epidermal growth factor receptors occurs primarily by an autocrine pathway that acts upon receptors on the surface rather than intracellularly." J Biol Chem **266**(12): 7503-8.

Wang, Q. and M. I. Greene (2008). "Mechanisms of resistance to ErbB-targeted cancer therapeutics." J Clin Invest **118**(7): 2389-92.

Wasserman, J. D. and M. Freeman (1998). "An autoregulatory cascade of EGF receptor signaling patterns the Drosophila egg." Cell **95**(3): 355-64.

Weber, J. D., D. M. Raben, et al. (1997). "Sustained activation of extracellular-signal-regulated kinase 1 (ERK1) is required for the continued expression of cyclin D1 in G(1) phase." Biochemical Journal **326**: 61-68.

Wheeler, D. L., S. Huang, et al. (2008). "Mechanisms of acquired resistance to cetuximab: role of HER (ErbB) family members." Oncogene **27**(28): 3944-56.

Wiley, H. S., J. J. Herbst, et al. (1991). "The role of tyrosine kinase activity in endocytosis, compartmentation, and down-regulation of the epidermal growth factor receptor." J Biol Chem **266**(17): 11083-94.

Wiley, H. S., S. Y. Shvartsman, et al. (2003). "Computational modeling of the EGF-receptor system: a paradigm for systems biology." Trends in cell biology **13**(1): 43-50.

Yamamoto, T., M. Ebisuya, et al. (2006). "Continuous ERK activation downregulates antiproliferative genes throughout G1 phase to allow cell-cycle progression." Curr Biol **16**(12): 1171-82.

Yamanaka, Y., H. Friess, et al. (1993). "Coexpression of Epidermal Growth-Factor Receptor and Ligands in Human Pancreatic-Cancer Is Associated with Enhanced Tumor Aggressiveness." Anticancer Research **13**(3): 565-570.

Yan, Y., K. Shirakabe, et al. (2002). "The metalloprotease Kuzbanian (ADAM10) mediates the transactivation of EGF receptor by G protein-coupled receptors." J Cell Biol **158**(2): 221-6.

Yayon, A., M. Klagsbrun, et al. (1991). "Cell surface, heparin-like molecules are required for binding of basic fibroblast growth factor to its high affinity receptor." Cell **64**(4): 841-8.

Yonesaka, K., K. Zejnullahu, et al. (2008). "Autocrine production of amphiregulin predicts sensitivity to both gefitinib and cetuximab in EGFR wild-type cancers." Clin Cancer Res **14**(21): 6963-73.

Zhang, J., K. Iwanaga, et al. (2008). "Intratumoral epiregulin is a marker of advanced disease in non-small cell lung cancer patients and confers invasive properties on EGFR-mutant cells." Cancer Prev Res (Phila) **1**(3): 201-7.

Zhang, L., Z. Wang, et al. (2009). "Multiscale agent-based cancer modeling." J Math Biol **58**(4-5): 545-59.

Zhang, X. P., G. Zheng, et al. (2008). "Notch activation promotes cell proliferation and the formation of neural stem cell-like colonies in human glioma cells." Mol Cell Biochem **307**(1-2): 101-8.

Zhou, B. B., M. Peyton, et al. (2006). "Targeting ADAM-mediated ligand cleavage to inhibit HER3 and EGFR pathways in non-small cell lung cancer." Cancer Cell **10**(1): 39-50.